FUNDAMENTAL ASPECTS OF SELECTED RHODIUM COMPLEXES IN HOMOGENEOUS CATALYTIC ACETIC ACID PRODUCTION

A thesis submitted to meet the requirements for the degree of

Philosophiae Doctor

in the

Department of Chemistry
Faculty of Natural and Agricultural Sciences

at the

University of the Free State

by

Llewellyn Joseph Damoense

Promotor
Prof. A. Roodt

Co-promotor
Prof. W. Purcell

November 2000

Voorwoord

Hiermee wens ek my opregte dank en waardering uit te spreek teenoor Prof. A. Roodt vir sy uitsonderlike leiding tydens hierdie studie. Dit was vir my 'n voorrreg om deur 'n wetenskaplike van hierdie formaat opgelei te word. Vervolgens wil ek ook my dank uitspreek aan Prof. W. Purcell, verál vir sy waardevolle bydrae aan die begin van hierdie studie. Ek wil ook my dank en waardering uitspreek teenoor die departementele hoof, Prof. S.S. Basson vir sy belangstelling en morele ondersteuning tydens my studiejare. Vervolgens 'n spesiale woord van dank aan my eggenote Lorna vir haar aanmoediging en ondersteuning tydens die afhandeling van hierdie proefskrif. Laastens wil ek my ouers bedank vir hulle aanmoediging en opoffering gedurende my studiejare en dra dan ook hierdie proefskrif as 'n geringe blyk van waardering aan hulle op.

Llewellyn Damoense

Contents

Chapter Four

Synthesis and characterization of Rh(I)-complexes

Chapter Five

X-Ray Structural determinations of Rh(I) and Rh(III) complexes

Chapter Six

Kinetics of iodomethane oxidative addition to [Rh(aminovinylketonato)(CO)(PR_3)] complexes

List of Publications resulting from this study

1. Damoense, L.J., Purcell, W., Roodt, A., and Leipoldt, J.G., 1994, *Rhodium Ex.*, **5**, 10; The Crystal Structure of (2-Aminovinyl-4-pentanonato- O, N)-carbonyl-triphenylphosphinerhodium (I).

2. Damoense, L.J., Purcell, W., and Roodt, A., 1995, *Rhodium Ex.*, **5**, 10; The Crystal Structure of Acyl[methyl(2-Aminovinyl-4-pentanonato)-κO,κN]iodo)carbonyltriphenylphosphine-rhodium(III).

3. Damoense, L.J., Roodt, A., and Purcell, W., *J. of the Chem. Soc., Dalton Transactions* (in preparation); Oxidative Addition of Iodomethane to β-aminovinylketonatocarbonyltriphenyl-phosphinerhodium(I) complexes: Stepwise X-ray Crystallographic, $^{31}P/^{13}C$ NMR and Kinetic study of formation of alkyl and acyl species,.

4. Damoense, L.J., Roodt, A., and Purcell, W., *Acta Cryst.* (in preparation); The Crystal Structure of (2-Aminovinyl-4-pentanonato- O, N)-carbonyl-triphenylarsinerhodium(I).

Abbreviations and Symbols

Abbreviations

acac	acetylacetone/-acetonato
anmeth	4-methoxy-*N*-methylbenzothiohydroxamate
avk	aminovinylketone
ba	benzylacetone/-acetonato
(-)-BINAP	2,2'-Bis(diphenylphosphino)-1,1'-binaphthyl
(-)-BINAS	(bis[disulfonatophenylphosphinomethyl])-tetrasulfonatobinaphthene
cacsm	methyl(2-cyclohexylamino-1-cyclopentene-1)-dithiocarboxylato
cod	1,5-cyclooctadiene
Cp	cyclopentadiene
Cy	cyclohexyl
cupf	*N*-hydroxy-*N*-nitrosobenzeneamine
dbbtu	N,N-dibenzyl-N'-benxoylthiourea
dmavk	2-Aminovinyl-4-pentanonato
DMF	dimethylformamide
$PFcPh_2$	Diphenyl ferocenyl phosphine
hacsm	methyl(2-amino-1-cyclopentene-1-dithiocarboxylato)
hpt	1-hydroxy-2-piridinethione
macsm	2-methyl-amino-1-cyclopentene-1-dithiocarboxylato
macsh	2-methyl-amino-1-cyclopentene-1-dithiocarboxylato
ox	8-hydroxyquinoline
pbtu	N-benzoyl-N'-phenylthiorea
pic	2-picolinic acid
quin	2-carboxyquinoline
sacac	thioacetylacetone/-acetonato

stsc	salicylaldehydethiosemicarbazone
salnr	N-*o*-tolylsalicylaldimine
tavk	2-Aminovinyl-5,5,5-trifluro-4-pentanonato
trop	tropolone
tfba	trifluorobenzoylacetone
tfaa	1,1,1-trifluoro-2,4-pentanedione
tta	2-thenoyltrifluoroacetone

Symbols

δ	chemical shift in parts per million
^1J	coupling constant Hz
D_N	solvent donocity
$\Delta H^{\#}$	enthalpy of activation
$\Delta S^{\#}$	entropy of activation
k_{obsd}	observed pseudo-first-order rate constant
υ_{CO}	carbonyl stretching frequency
pK_a	$-Log[H^+]$, K_a = acid dissociation constant
θ	Tolman cone angle

CHAPTER 1

General introduction and Aim of study

1.1 ORGANOMETALLIC CHEMISTRY AND HOMOGENEOUS CATALYSIS[1,2,3,4]

The first organometallic compound "liqueur fumante de l' arsenique" was synthesized by Cadet de Gassicourt in 1760. This discovery was followed by the synthesis of the first metal olefin complex, $K[(C_2H_4)PtCl_3]$, by W.C. Zeise in 1827 of which the structure was determined by X-ray diffraction only during the 1950s. The technical and commercial importance of organometallic compounds was however first recognised with the development of successful homogeneous catalyzed industrial processes.

During 1938 Roelen and Reppe did important work in the field of the development of catalysts which involved the reaction of synthesis gas with different olefins (hydroformylation), with water (hydrocarboxylation), etc., resulting in the synthesis of useful products such as organic acids, alcohols, esters, etc. Further important milestones were achieved by Ziegler, Natta, and others (See Fig. 1.1). Thus, organometallic chemistry probably would not have been that prominent today if it were not for its important industrial applications. On the other hand, many chemical industries would not have existed since the introduction of organometallic compounds allowed the synthesis of certain chemicals at profitable levels. This synergic effect between the chemical industry on the one side and basic research in the laboratory on the other side lead especially, since the 1950s, to the development of new and better chemical processes. Today homogeneous catalysis is an established field of organometallic chemistry and it has become a central feature within the chemical sciences.

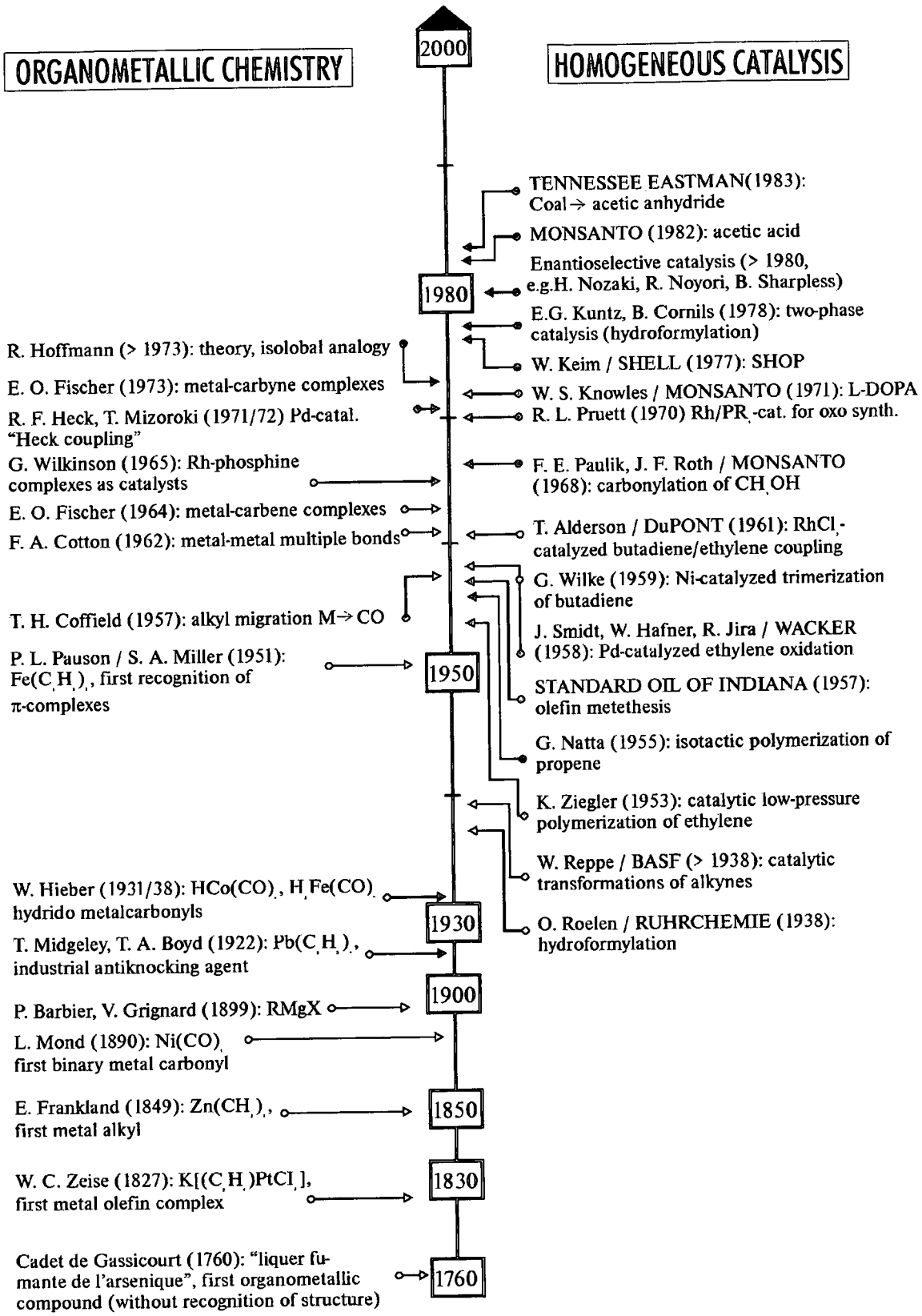

Fig. 1.1 Synoptic presentation of the development of organometallic chemistry and homogeneous catalysis

Some of the best known catalytic processes involving organometallic compounds are[5]:

- ⇛ hydrogenation of olefins in the presence of compounds of low-valent metals such as rhodium [e.g., $RhCl(PPh_3)_3$, **Wilkinson's catalyst**];
- ⇛ hydroformylation of olefins using a cobalt or rhodium catalyst (**Oxo process**);
- ⇛ oxidation of olefins to aldehydes and ketones (**Wacker process**);
- ⇛ polymerization of propylene using an organoaluminium-titanium catalyst (**Ziegler-Natta** catalyst) to give stereoregular polymers;
- ⇛ cyclooligomerization of acetylenes using nickel catalysts (**Reppe's or Wilke's** catalysts);
- ⇛ olefin isomerization using nickel catalysts.

Another important and commercially essential example proving the variability of homogeneous catalysis is the synthesis of acetic acid from methanol in the Monsanto process [Scheme 1.1]

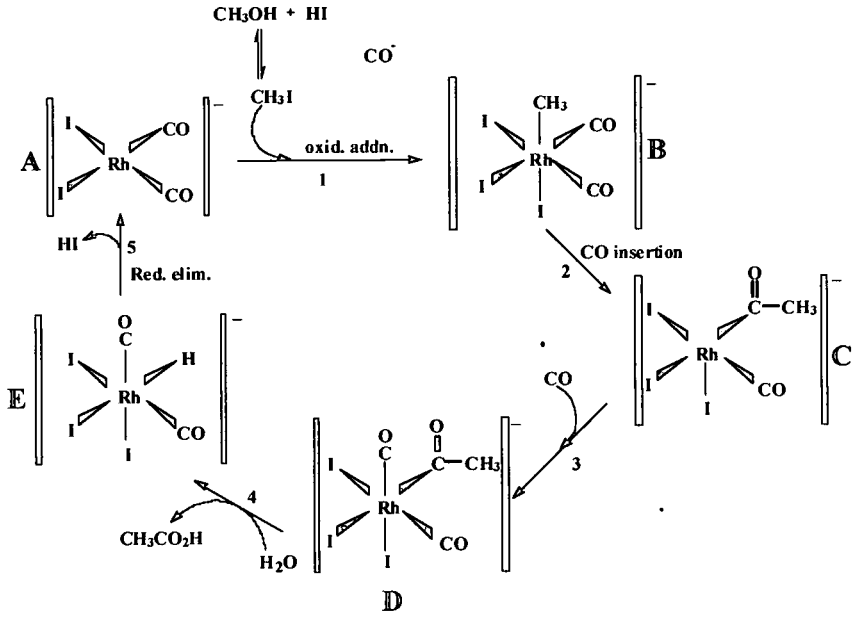

Scheme 1.1 Carbonylation of methanol in the Monsanto process

In the Monsanto process iodomethane undergoes oxidative addition to the square planar Rh(I)-complex 𝔸 yielding an octahedral Rh(III)-complex 𝔹. Subsequent CO-insertion into the *cis* CH_3-Rh bond gives a five-coordinate acetyl complex ℂ that forms a six-coordinate species 𝔻 after addition of another CO molecule. In the presence of H_2O, CH_3CO_2H is liberated, forming complex 𝔼 which undergoes reductive elimination of HI to regenerate the initial catalyst. The HI that is eliminated reacts with the next methanol molecule to form iodomethane and the cycle restarts. This cycle has been separated and each step individually investigated by Maitlis *et al.*[6,7] applying techniques such as FTIR and isotopic labeling (mainly with ^{13}C). The rate-determining step in the rhodium-iodide catalyzed reaction is the oxidative addition of methyl iodide to $[Rh(CO)_2I_2]^-$ (𝔸); the product of this reaction, the reactive intermediate $[MeRh(CO)_2I_3]^-$ (𝔹) has been detected and fully characterized spectroscopically, while the rates, as well as activation parameters, for several of these steps have been measured[8]. If the rhodium is replaced by iridium, contrasting results for a similar catalytic cycle is obtained e.g., the reaction of $[MeIr(CO)_2I_3]^-$ (𝔹) with CO to give $[(MeCO)Ir(CO)_2I_3]^-$ (𝔻) is rate determining. Model studies show that while k_{Rh}/k_{Ir} is *ca.* 1:150 for the oxidative addition step, it is *ca.* 10^5-10^6:1 for CO insertion. The migratory insertion for iridium can be substantially accelerated by adding either methanol or a Lewis Acid (SnI_2). Recently BP announced the introduction of an iridium-catalyzed process of methanol carbonylation[8], i.e., the Cativa technology.

Previous research[9] done in this laboratory was mainly focused upon the mechanistic behavior of β-diketonato and its analogues in complexes of Rh(I) towards oxidative addition and CO-insertion; reactions which are closely related to those found in the Monsanto process, see Eq. 1.1,

$$[Rh(L,L'\text{-}BID)(CO)(PR_3)] + CH_3I \underset{k_{-1}}{\overset{k_1}{\rightleftharpoons}} [Rh(L,L'BID)(I)(CH_3)(CO)(PPh_3)] \quad \text{(alkyl)}$$

$$\downarrow k_2$$

$$[Rh(L,L'\text{-}BID)(I)(COCH_3)(PR_3)] \quad \text{(acyl)} \qquad \text{1.1}$$

where L,L'-BID = bidentate ligand, PR_3 = tertiary phosphine[10] or phosphite[11], k_1 = rate of oxidative addition, k_{-1} = rate of reductive elimination and k_2 = rate of CO-insertion.

An initial driving force for this research originated from the possibility to support these complexes on a polymer like polystyrene, thus heterogenizing the potential homogeneous catalysts. The bidentate ligands that were studied mainly included monoanionic ligands with donor atom combinations O,O, O,S, N,S and N,O, also varying the size of the chelate ring (five- and six-membered rings). It was found that the above factors are important in terms of the reactivity of the transition metal complexes. The oxidative addition kinetic data of some selected [Rh(LL'-BID)(CO)(PPh_3)] complexes (where L,L' = donor atoms and BID = bidentate ligand) with iodomethane studied in this laboratory are given in Table 1.1.

Table 1.1 Kinetic data for some selected [Rh(LL'-BID)(CO)(PPh_3)] complexes; Oxidative addition with CH_3I at 25 °C in chloroform[12]

Ligand	L	L'	Ringsize	Rate constants[a]	
				alkyl/$M^{-1}s^{-1}$ (k_1)	acyl/s^{-1} (k_2)
cupf	O	O	5	0.0050(1)	0.0012(1)
acac	O	O	6	0.0065(4)	0.0016(1)
pic	O	N	5	0.010	-
sacac	O	S	6	-	>0.01
hpt	O	S	5	0.0083	0.01
macsm	N	S	6	0.034(1)	0.0078(4)
macsh	N	S	6	0.56(1)	0.0072(2)

a) See Eq. 1.1

The data in Table 1.1 indicate that in general, for the same donor atoms L and L', an increase in the rate of oxidative addition with an increase in size of the chelate ring is observed. The increase in the rate for the donor atoms of the bidentate ligand was found to be in the order O,O < O,S < O,N < N,S, while no meaningful correlation was found for the rate of acylation.

From the above discussion, it is clear that bidentate ligands of the β-diketonato type and its analogues play an important role in the activation of the Rh(I) metal center in complexes with possible catalytic application.

1.2 AIM OF THIS STUDY

With the above in mind, the oxidative addition of iodomethane to [Rh(L,L'-BID)(CO)(PR_3)] complexes is extended by the inclusion of bidentate ligands with the ß-aminovinylketonato (avk) backbone, containing nitrogen and oxygen as donor atoms. Some of these ligands are easy to synthesize and in general they form relatively stable Rh(I)- and Rh(III)-complexes, whereas most of specifically the Rh(III)-complexes in a range of the other systems previously studied are not well characterized. Furthermore, the nitrogen atom, if required, allows the functionalization of the N-group by introducing electronic and steric groups close to the metal center; an effect which should influence the reactivity of the metal center in reactions such as e.g. oxidative addition[12]. The presence of carbonyl - and phosphorous ligands also allow the utilization of experimental techniques such as IR- (for CO-ligands only) and NMR spectroscopy (both for CO- and phosphorous ligands) in the study of these complexes.

The aim of this study is summarized in the following paragraphs:

1. ***To synthesize and characterize the following complexes:***
   [Rh(dmavk)(CO)(PPh_3)], [Rh(dmavk)(CO)(*p*-Cl-Ph)$_3$P], [Rh(dmavk)(CO)($AsPh_3$)], [Rh(tavk)(CO)(PPh_3)], [Rh(tavk)(CO)(*p*-OMe-Ph)$_3$P] and [Rh(tavk)(CO)($AsPh_3$)].

2. ***Chemical kinetics***:
   (i) To investigate the influence of the substituents R_1 and R_2 of the N,O-BID ligand on the reaction between iodomethane and [Rh(N,O-BID)(CO)(PPh_3)].

(ii) To investigate the electronic influence of different tertiary phosphines for the reaction between iodomethane and [Rh(avk)(CO)(PR_3)] (avk = β-aminovinylketonato type ligands; including all substituents on the bidentate ligands).

(iii) To investigate the relative electronic and steric influence of PPh_3 *vs.* $AsPh_3$ for the reaction between iodomethane and [Rh(avk)(CO)(XPh_3)] (X = P or As).

(iv) To determine the influence of the reaction medium on iodomethane oxidative addition to [Rh(dmavk)(CO)(PPh_3)] in a range of solvents with different properties.

3. ***Structure and stereochemistry***

The characterization by single crystal X-ray methods of selected Rh(I) starting, alkyl intermediate and acyl final products to accurately determine bonding distances, –modes and coordination geometry.

4. ***Comparative study***

(i) To investigate isomer formation of [Rh(dmavk)(CO)(PPh_3)], [Rh(dmavk)(I)(CH_3)(CO)(PPh_3)] and [Rh(dmavk)(I)(CH_3CO)(PPh_3)] in acetone solution utilizing ^{31}P-NMR spectrometry and correlate the coupling constants ^{1}J(PRh) and ^{1}J(CRh) as well as the Rh-P bond distance with other related [Rh(BID)(CO)(PPh_3)] complexes.

(ii) To determine the mechanism of oxidative addition of [Rh(avk)(CO)(XR_3)] type of complexes (X = P or As; R = unfunctionalized and functionalized phenyl groups) with iodomethane from the kinetic and structural data.

REFERENCES

1. Cornils, B., and Hermann, W.A. 1996, *Applied Homogeneous Catalysis with Organometallic Compounds*, VCH. Weinheim.
2. Halpern, J. 1981, *Inorg. Chim. Acta*, **50**, 11.
3. Butler, I.S., and Harrod, J.F. 1989, *Inorganic Chemistry: Principles and Applications*, Benjamin Cummings Publ. Co., Redwood City, California.
4. Collman, J.P., and Hegedus, L.S. 1980, *Principles and Applications of Organotransition Metal Chemistry*, University Science Books, Mill Valley, California.
5. Roelen, O. 1977, *ChED Chem. Exp. Didakt.*, **3**, 119.
6. Fulford, A., Hickey, C.E.,and Maitlis, P.M. 1990, *J. Organomet. Chem.*, **398**, 311.
7. Haynes, A., Mann, B.E., Gulliver, D.J., Morris, G.E., and Maitlis, P.M. 1991, *J. Am. Chem. Soc.*, **113**, 8567.

   Haynes, A., Mann, B.E., Gulliver, D.J., Morris, G.E., and Maitlis, P.M. 1993, *J. Am. Chem. Soc.*, **115**, 4093.
8. Maitlis, P.M., Haynes, A., Sunley, G.J., and Howard, M.J. 1996, *J. Chem. Soc., Dalton Trans.*, 2187.
9. Basson, S.S., Leipoldt, J.G., and Nel, J.T. 1984, *Inorg. Chim. Acta*, **86**, 167; Basson, S.S., Leipoldt, J.G., Roodt, A., Venter, J.A., and van der Walt, T.J., 1986, *ibid.*, **119**, 35; Basson, S.S., Leipoldt, J.G., Roodt, A., and Venter, J.A. 1987, *ibid.*, **128**, 31; Leipoldt, J.G., Basson, S.S. and Botha, L.J. 1990, *ibid.*, **168**, 215; Leipoldt, J.G., Steynberg, E.C., and van Eldik, R. 1987, *Inorg. Chem.*, **26**, 3068; Van Zyl, G.J., Lamprecht, G.J., Leipoldt, J.G., and Swaddle, T.W. 1988, *Inorg. Chim. Acta*, **143**, 223; Leipoldt, J.G., Lamprecht, G.J., and van Zyl, G.J., 1985, *ibid.*, **96**, L31; van Zyl, G.J., Lamprecht, G.J., and Leipoldt, J.G. 1985, *ibid.*, **102**, L1; Lamprecht, G.J., Leipoldt, J.G., and van Zyl, G.J. 1985, *ibid.*, **97**, 31.
10. Basson, S.S., Leipoldt, J.G., and Nel, J.T. 1984, *Inorg. Chim. Acta*, **86**, 167;

Basson, S.S., Leipoldt, J.G., Roodt, A., Venter, J.A., and van der Walt, T.J., 1986, *ibid.*, **119**, 35; Basson, S.S., Leipoldt, J.G., Roodt, A., and Venter, J.A. 1987, *ibid.*, **128**, 31; Leipoldt, J.G., Basson, S.S. and Botha, L.J. 1990, *ibid.*, **168**, 215; Leipoldt, J.G., Steynberg, E.C., and van Eldik, R. 1987, *Inorg. Chem.*, **26**, 3068;

11. Van Zyl, G.J., Lamprecht, G.J., Leipoldt, J.G., and Swaddle, T.W. 1988, *Inorg. Chim. Acta*, **143**, 223; Leipoldt, J.G., Lamprecht, G.J., and van Zyl, G.J., 1985, *ibid.*, **96**, L31; van Zyl, G.J., Lamprecht, G.J., and Leipoldt, J.G. 1985, *ibid.*, **102**, L1; Lamprecht, G.J., Leipoldt, J.G., and van Zyl, G.J. 1985, *ibid.*, **97**, 31.

12. Steyn, G.J.J., Roodt, A., and Leipoldt, J.G. 1993, *Rhodium Ex.*, **1**, 25.

CHAPTER 2

Electronic and stereochemical aspects of selected ligands in rhodium(I) substrates

2.1 INTRODUCTION

New knowledge regarding the structure and reactivity of organometallic compounds has created new catalytic processes in industry or has improved reaction conditions, e.g. higher yields, lower temperatures and pressures to enhance the economic viability of known processes[1]. An important example includes the replacement of cobalt by rhodium in a number of industrially otherwise less favourable processes such as methanol carbonylation or commonly known as the Monsanto process. In addition, ligand modification around the catalytic transition metal is of paramount importance, which is typically demonstrated by the development of hydroformylation. The first process employing $[HCo(CO)_4]$ as catalyst (O. Roelen) was followed by those with ligand-modified cobalt carbonyls (Shell process with alkylphosphines, 1966 onwards); the latter was again succeeded by Union Carbide's LPO process with $[HRh(CO)(PPh_3)_3]$. The Ruhrchemie-Rhône-Poulenc oxo process with rhodium catalysts and water-soluble phosphines landmarked yet another improvement. All process variants were linked with increased selectivity and yield, more specific product distribution (Shell process), milder reaction conditions, facile catalyst-product separation, and simplified process technology (new Ruhrchemie-Rhône-Poulenc process since 1988). Thus, a great challenge to obtain optimum conditions for any homogeneous process involves firstly the understanding of the catalytic cycle, followed then by the introduction of ligands with specific characteristics (electronic; steric) to enhance reaction rates, and eliminating reactions leading to the formation of side-products, etc.

As mentioned above, ancillary (non-labile) ligands have been used in a multitude of modes and forms to modify and manipulate the metal center which it is coordinated to.

Thus many forms of mono- and bidentate ligands are known to induce different effects also in potential homogeneous catalysts, and specifically that of rhodium. These ligands include many p-block elements as donor atoms, of which carbon (as in e.g. in cylcooctadiene (cod))[2,3], nitrogen (NO)[3,4], phosphorous (PPh_3)[3], arsine ($AsPh_3$)[3,5,6], stibine ($SbPh_3$)[3,5,6,7], etc. Many also induces chirality (-)-BINAP and (-)-BINAS[8] to the metal center and are applied to produce enantiomeric enriched forms of substrates. In this regard mono-, bi- and multidentate phosphorous ligands play a particularly important role. Since only monodentate ligands with phosphorous as donor atom were utilized in this study, only this group of phosphorous ligands will be discussed in more detail. Furthermore, combinations of the p-block elements enable different additional aspects in the form of unsymmetrical systems to be employed. This results in further manipulations possible of the metal center, a few aspects in this regard are thus also discussed below. This chapter deals with theoretical background on some aspects and of selected ligands which are also employed in this study.

2.2 PHOSPHOROUS LIGANDS

Ligands such as CO, RNC, PR_3, POR_3 (R= Ph, Et, Cy, etc.), NO, arenes and various molecules with delocalized π orbitals (pyridine, 2,2'-bipyridine, 1,10-phenantroline etc.) are commonly referred to as π-acids due to the availability of orbitals with the correct symmetry to form π-bonds with transition metals[9]. In many of these complexes, the metal atoms are in low-positive, zero or negative formal oxidation state. It is a characteristic of these ligands that they can stabilize low metal oxidation states *via* back donation of electron density from the filled metal d-orbitals to the π^*-orbitals of the ligand. The metal-ligand bond strength is determined by both the synergic δ-donor ability and π-acceptor ability of the ligand. Thus, the introduction of strong π-acid ligands to a metal coordination sphere normally has the tendency to decrease the electron

density on the metal center, which will have an effect on the reactivity of such complexes. Most phosphines are good δ-donors but not good π-acceptors.

The two main aspects involved in the bonding of tertiary phosphines to transition metals is the electronic and steric properties of phosphorous ligands. Both these properties are dependent on the bonded substituents on the phosphorous atoms and are briefly discussed below.

2.2.1 Electronic influence of tertiary phosphines

The electronic effect is the result of electron density transmission *via* chemical bonds and variation in electron donating or withdrawing substituents on the phosphorous atom, thus having an effect on the basicity of the tertiary phosphine. The most widely quoted parameter to indicate Lewis basicity of tertiary phosphines is $pK_a(H_2O)$, which is a measure of Brϕnsted basicity. In general, the pK_a of the phosphine is increased by the introduction of substituents (R in PR_3) with better electron donating ability. This can be related to other parameters e.g. reactivity of Rh(I) square planar complexes towards oxidative addition and the CO-bond strengths of complexes containing both phosphine and CO ligands. The replacement of, for example the electron donating methoxy group in P(*p*-OMe-Ph)$_3$ by the electron withdrawing chloride group in P(*p*-Cl-Ph)$_3$ resulted in a decrease in the rate of oxidative addition of iodomethane on [Rh(cacsm)(CO)(PR_3)] complexes[10].

The electronic effect of tertiary phosphines on a metal center can thus be well described by the carbonyl stretching frequencies *trans* to the tertiary phosphine in [Ni(CO)$_3$(PR_3)] type square planar complexes[11], i.e. the so-called Tolman electronic parameter. Comparison of the υ_{CO} will give an indication of the influence of PR_3 and thus of R on the reactivity of the complex; typical values for this for a series of [Ni(CO)$_3$(PR_3)] complexes are given in Table 2.1. The results showed that as the electron donating capability of the substituents on the tertiary phosphine decreases (decrease in pK_a), there

is an increase in the CO stretching frequencies. The empirical implication is an inclination towards B away from A in Eq. 2.1.

$$\underset{\mathbf{A}}{M{=}C{=}O} \rightleftharpoons \underset{\mathbf{B}}{M^{\delta-}{-}C{\equiv}O^{\delta+}} \qquad \textbf{2.1}$$

This implies that an increase in υ_{CO} means less π-bond stabilization in the M-C moiety, caused by the decrease in metal-ligand $d \rightarrow \pi^*$ back donation due to the decrease in electron density on the metal center.

Table 2.1 pK_a–values for tertiary phosphines and υ_{CO} in $[Ni(CO)_3(PR_3)]$[11]

Tertiary Phosphine	pK_a	$\upsilon_{CO}(cm^{-1})$
P(*t*-Bu)$_3$	11.40	2056.1
PCy$_3$	9.65	2056.4
P(*p*-OMe-Ph)$_3$	4.57	2066.1
P(*p*-Me-Ph)$_3$	3.84	2066.7
PPh$_3$	2.73	2068.9
P(*p*-F-Ph)$_3$	1.97	2071.3
P(*p*-Cl-Ph)$_3$	1.03	2072.8

2.2.2 Steric influence of tertiary phosphines

The steric requirement of a tertiary phosphine, PR_3, is usually expressed by Tolman's cone angle, θ. The cone angle[12] (θ) is defined as the apex angle of a cylindrical cone, centered 2.28 Å from the center of the phosphorous atom, which just touches the Van der Waals radii of the outermost atoms in the phosphine model (see Fig. 2.1)

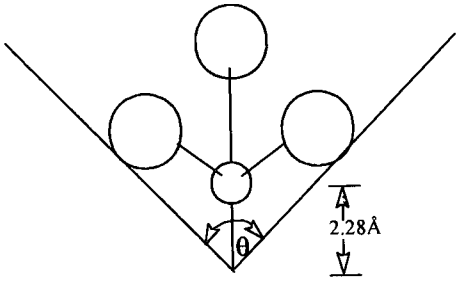

Fig. 2.1 The cone angle (θ) for a monodentate tertiary phosphine

Vaska *et al.*[13] illustrated, e.g., the steric influence of phosphine ligands on the rate of oxidative addition of H_2 to *trans*-[IrCl(CO)L_2] according to the following reaction:

$$\textit{trans}\text{-}[IrCl(CO)(PR_3)_2] + H_2 \underset{}{\overset{k}{\rightleftharpoons}} [IrCl(H)_2(CO)(PR_3)_2] \qquad 2.2$$

A decrease in the rate constant k was observed by increasing the cone angle of the coordinated phosphine (rate decreases in the order where L = PPh_3 ≈ P(*p*-Me-Ph)$_3$ > P(*m*-Me-Ph)$_3$ > PCy_3 > P(*o*-Me-Ph)$_3$), see Table 2.2. Further evidence for the steric influence is the significant decrease in the rate of oxidative addition for PCy_3 despite its large basicity.

Table 2.2 Rate and equilibrium constants in chlorobenzene at 30 °C for reaction 2.2

L	pK_a	θ (°)	k ($M^{-1}s^{-1}$)
PPh_3	2.73	145	1.2
P(*p*-Me-Ph)$_3$	3.84	145	1.7
P(*m*-Me-Ph)$_3$	3.30	>145, <194	0.69
PCy_3	9.65	170	0.0066
P(*o*-Me-Ph)$_3$	3.08	194	No reaction in 3h

2.3 SELECTED MONOCHARGED BIDENTATE LIGANDS

Utilization of bidentate ligand systems in Rh(I) chemistry has been done for the past two decades in this laboratory[14]. Complexes of the form with monoanionic bidentate ligands including acetylacetonato, trifluoroacetylacetonato, hexafluoroacetylacetonato, 4-methoxy-*N*-methylbenzothiohydroxamato, *N*-hydroxy-*N*-nitrosobenzeneamato, 8-hydroxyquinolinato, etc. and related systems were employed to evaluate the effect of the donor atoms on the reactivity and mechanisms of these Rh(I) complexes. A short overview of aspects of this research is therefore given in this paragraph.

The title complexes are normally prepared in these studies by the stoichiometric addition of the selected phosphine to the dicarbonyl starting compound, [Rh(L,L'-BID)$(CO)_2$]. Bonati and Wilkinson[15] showed that in these substitution reactions only one carbonyl group can be substituted by triphenyl phosphine, while in the case of asymmetric bidentate ligands, the product can be one of two possible isomers. This fact made it possible to study the relative *trans*-influence of the bonding atoms in the bidentate ligands, since it may be assumed that the carbonyl group *trans* to the donor atom with the largest *trans*-influence will be substituted by the phosphine.

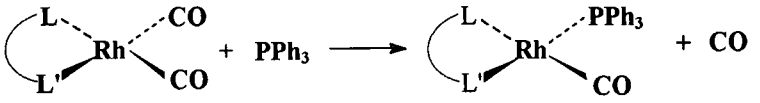

2.3

The X-ray structural results, in general, indicated that the most electronegative atom (or in the case of β-diketones, the oxygen atom nearest to the strongest electron withdrawing substituent like CF_3) has the smallest *trans*-influence[16]. This is in agreement with the polarization theory and the δ-*trans* effect, since the oxygen atom nearest to the more electron-attracting CF_3 group will be least polarizable and a weaker δ-donor, as a result of the greater electron withdrawing power of the CF_3 group. A similar result was

concluded for the structure determination of 1,1,1-trifluoro-2,4-pentanedionatocarbonyl-tri-*p*-chlorophosphinerhodium(I)[17].

Previous X-ray structural studies[18,19,20] showed that for asymmetric bidentate ligands with different donor atoms, the *trans*-influence or structural *trans*-effect for oxygen, nitrogen and sulfur follows the reverse electronegativity range, i.e. S > N > O. It is however known[19,21] that it is not necessarily always the thermodynamically stable isomer that crystallizes since the crystallization energy of a specific isomer will determine the solid state structure, specifically in labile Rh(I) systems. Poletaeva *et al.*[22] showed by means of ^{13}C and ^{31}P-NMR, that two isomers exist for [Rh(tta)(CO)(PPh_3)] in a 53%:47% ratio in solution, although only the predicted isomer (according to the δ-*trans* effect) crystallized out as was previously determined by Leipoldt *et al.*[16]. The two isomers seem to co-exist in dynamic equilibrium, with the isomer ratio dependent on the solvent. Steyn *et al.*[23,10] also found that the pattern of substitution is not always electronically controlled in complexes with ligands such as cacsmH, macsmH and hacsmH, i.e. the methyl esters of the 2-amino-1-cyclopentene-2-dithiocarboxylate backbone, functionalized at the amino nitrogen with hydrogen, methyl and cyclohexyl (see Figures 2.2). It was observed from structural determinations that the expected isomer for the [Rh(hacsm)(CO)(PPh_3)][19] (Fig. 2.2 C) complex crystallizes out from solution (PPh_3 *trans* to S). The introduction of the bulkier methyl or cyclohexyl groups on the N atom of the same bidentate ligand backbone resulted in the unexpected substitution pattern for the [Rh(macsm)(CO)(PPh_3)][23] (Fig. 2.2 A) and [Rh(cacsm)(CO)(PPh_3)][10] (Fig. 2.2 B) complexes in the solid state structures, i.e. the CO ligand *trans* to the nitrogen atom in the dicarbonyl complexes [Rh(L,L'-BID)($CO)_2$] was substituted. This unexpected substitution mode was attributed to the much larger steric demand of the methyl and cyclohexyl groups on the nitrogen atom in the macsm and cacsm ligands.

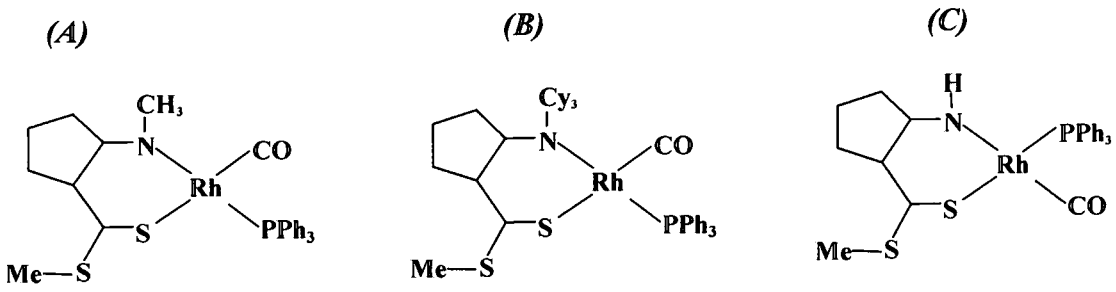

Figures 2.2 ***(A,B,C)*** Structural representation of for [Rh(macsm)(CO)(PPh_3)] *(A)*, [Rh(cacsm)(CO)(PPh_3)] *(B)* and [Rh(hacsm)(CO)(PPh_3)] *(C)*

Another aspect of importance of the L,L'-BID type ligands to be considered is the bite angle formed with the metal center (the L-Metal-L' angle), which is dependent on the ring size. The average bite angle of five-membered chelate ring are 78.4°[18], while the similar average angle for six-membered chelate rings are 88.2°. Table 2.3 briefly summarizes the Rh-P bond distance for complexes of the type [Rh(L,L'-BID)(CO)(PPh_3)] with different donor atoms L,L' and varying ring size.

Table 2.3 Average Rh-P bond distances in complexes of the type [Rh(L,L'-BID)(CO)(PPh_3)][18]

	Rh-P bond distance (Å)	
Donor atom (L)	Five-membered	Six-membered
(L' = O)	Chelate ring	Chelate ring
O	2.232(2)	2.243(2)
N	2.260(2)	2.278(2)
S	2.278(1)	2.300(2)

[a] The phosphorous atom is *trans* to atom L.

A definite lengthening of the Rh-P bond is observed from five- to six-membered chelate rings for all three different donor atom entries, see Table 2.3. The smaller bite angle of five-membered chelate rings decreases the *trans*-influence of the donor atom in the ring relative to the same donor atom in a six-membered chelate ring. The explanation for the lengthening of the Rh-P bond lies in the effective overlap of the relevant σ-orbitals of the L,L'-BID ligand with the dsp^2-hybrid orbitals of the metal. Theoretically, a bite angle of 90° will allow for the most effective overlap of the σ-orbital of the L,L'-BID ligand. Any

deviation from a 90° bite angle will inhibit the electron donating power of the donor atom to the metal, decreasing it's effective *trans*-influence.

Further correlations between Rh-P bond distance and ^{31}P NMR parameters [$\delta(^{31}P)$; $^{1}J(PRh)$] for five- and six-membered chelate Rh(I) complexes forms part of this current investigation and will be discussed in more detail in Chapter 5.

Finally it is also worth noting the effect of ring size of bidentate ligands on the [Rh(L,L'-BID)(CO)(PPh_3)] type complexes formed upon addition of PPh_3 to [Rh(L,L'-BID)$(CO)_2$]. As mentioned earlier, only one carbonyl will be substituted during such an addition. X-ray crystal structure determinations of Rh(I) complexes containing five-membered chelates such as [Rh(cupf)$(CO)(PPh_3)_2$][24] and [Rh(trop)$(CO)\{P(FcPh_2)_3\}_2$][25] showed that although one carbonyl is substituted by a phosphine, an additional phosphine can be added to the Rh-center resulting in a five coordinated complex. An explanation for this phenomena is that due to the relative weak electron donating ability of five-, compared to six-membered chelates as discussed earlier, the metal center is electron deficient enough to accept additional electron density of another incoming phosphine ligand. Further more, due to the larger bite angle of six-membered chelates compared to five-membered chelates of similar type, the latter is sterically less hindered to accommodate an additional ligand, thus favouring the formation of bis phosphine complexes.

In general, it is thus clear that the characteristics of the Rh(I) metal center can be manipulated conveniently by bidentate ligands containing group 15 and 16 donor atoms. Steric and electronic aspects can be tuned, and specifically by using the N,O-BID ligands described in this study, interesting effects were observed which will be addressed in the following chapters.

REFERENCES

1. Cornils, B., and Hermann, W.A. 1996, Applied Homogeneous Catalysis with Organometallic Compounds, VCH. Weinheim.
2. M. Theron, MSc. Thesis, University of the Orange Free State, 1994.
3. Wilkinson, G., Gallard, R.D., and Mcleverty, J.A. 1987, Comprehensive Coordination Chemistry, Pergamon Press.
4. Hieber, H., and Heinickey, K 1962, *Z. Anorg. Allg. Chem.*, **316**, 321.
5. Mague, J.T., and Wilkinson, G. 1966, *J. Chem. Soc.* (A), 1736.
6. Lawson, D.N., Osborne, J.A., and Wilkinson, G. 1966, *J. Chem. Soc.* (A), 1233.
7. Garrow, P.E., and Harkwell, G.E., 1975, *Inorg. Chem.*, **14**, 194.
8. Hermann, W.A., and Cornils, B. 1977, *Angew. Chem. Int. Ed. Engl.*, **36**, 1048.
9. Cotton, F.A., and Wilkinson, G. 1988, Advanced Inorganic Chemistry; Fifth Ed., John Wiley and Sons Inc., New York.
10. Steyn, G.J.J. 1994, PhD-Thesis, University of the Orange Free State, Bloemfontein, South Africa.
11. Tolman, C.A. 1980, *J. Am. Chem. Soc.*, **92**, 2953.
12. Tolman, C.A. 1977, *Chem. Rev.*, **77**, 313.
13. Brady, R., DeCamp, W.H., Flynn, B.R., Schneider, M.L., Scott, J.D., Vaska, L., and Werneke, M.F. 1975, *Inorg. Chem.*, **14**, 2669.
14. Basson, S.S., Leipoldt, J.G., and Nel, J.T. 1984, *Inorg. Chim. Acta*, **86**, 167; Basson, S.S., Leipoldt, J.G., Roodt, A., Venter, J.A., and van der Walt, T.J., 1986, *ibid.*, **119**, 35; Basson, S.S., Leipoldt, J.G., Roodt, A., and Venter, J.A. 1987, *ibid.*, **128**, 31; Leipoldt, J.G., Basson, S.S. and Botha, L.J. 1990, *ibid.*, **168**, 215; Leipoldt, J.G., Steynberg, E.C., and van Eldik, R. 1987, *Inorg. Chem.*, **26**, 3068; Van Zyl, G.J., Lamprecht, G.J., Leipoldt, J.G., and Swaddle, T.W. 1988, *Inorg. Chim. Acta*, **143**, 223; Leipoldt, J.G., Lamprecht, G.J., and van Zyl, G.J., 1985, *ibid.*, **96**, L31; van Zyl, G.J., Lamprecht, G.J., and Leipoldt, J.G. 1985, *ibid.*, **102**, L1; Lamprecht, G.J., Leipoldt, J.G., and van Zyl, G.J. 1985, *ibid.*, **97**, 31.
15. Bonati, F., and Wilkinson, G. 1964, *J. Chem. Soc.*, 3156.
16. Leipoldt, J.G., Bok, L.D.C., van Vollenhoven, J.S., and Pieterse, A.I. 1978, *J.*

Inorg. Nucl. Chem., 40, 61.

17. Steynberg, E.C., Lamprecht, G.J., and Leipoldt, J.G. 1987, *Inorg. Chim. Acta*, 133, 33.
18. Graham, D.E., Lamprecht, G.J., Potgieter, I.M., Roodt, A., and Leipoldt, J.G. 1991, *Transition Met. Chem.*, 16, 193.
19. Steyn, G.J.J., Roodt, A., Poletaeva, I., and Varshavsky, Y.S. 1997, *J. Organomet. Chem.*, **536/537**, 797.
20. Botha, L.J., Basson, S.S., and Leipoldt, J.G. 1987, *Inorg. Chim. Acta.*, 126, 25.
21. Langford, C.H., and Gray, H.B. 1965, Ligand Substitution Processes, Benjamin. New York.
22. Poletaeva, I.A., Cherkasova, T.G., T.G., Osetrova, L.V., Varshavsky, Y.S., Roodt, A., and Leipoldt, J.G. 1994, *Rhodium Ex.*, 3, 21.
23. Steyn, G.J.J., Roodt, A., and Leipoldt, J.G. 1992, *Inorg. Chem.*, 31, 3477.
24. Basson, S.S., Leipoldt, J.G., and Venter, J.A. 1990, *Acta Cryst.*, C46, 1324.
25. Steyl, G., and Roodt, A., Unpublished Results.

CHAPTER 3

Some important reactions in homogeneous catalysis

3.1 INTRODUCTION

Reactions such as substitution, oxidative addition, carbonyl insertion and reductive elimination are important steps in catalytic processes and it is common that one or more of these reaction steps occur during the catalytic cycle of organic substrate functionalization. A study of the factors which influences the mechanisms and rates of these reactions is therefor of vital importance. Oxidative addition reactions have received a great deal of attention since 1968 both from the point of view as interesting reactions for organometallic compounds as well as important steps in homogeneous catalytic processes. Ugo[1] and Vaska[2] did pioneering work aimed at a better understanding of the reactivity of transition metal complexes toward oxidative addition. These properties are largely determined by the characteristics (electronic; steric) of the ligand bonded to the transition metal. This chapter deals with selected reactions of these type which are important for this study.

3.2 OXIDATIVE ADDITION

3.2.1 Introduction

The discovery in 1962 by Vaska and Diluzio[3] of the reversible binding of H_2 (and other molecules) to an iridium(I) complex to give the iridium(III) dihydride (Eq. 3.1) was significant in that it led to the reaction classification of oxidative addition to square planar complexes. Similarly, this and the reverse reductive elimination from octahedral

complexes, are now clearly recognized as being critical in hydrogenation and homogeneous catalytic reactions in general.

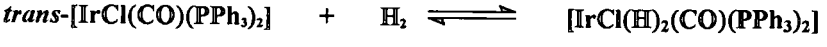

3.1

In general oxidative addition reactions may be defined as the addition of neutral molecules to coordinatively unsaturated d^8 or d^{10} transition metal complexes where the metal complex simultaneously acts as Lewis acid (acceptor of an electron pair) and Lewis base (donor of an electron pair). The increase in formal oxidation state of the metal center by two units is compensated for by the same increase in coordination number. Three basic conditions must be satisfied before oxidative addition can take place: firstly, the availability of non-bonding electron density on the metal center; secondly, the existence of two vacant coordination positions for the incoming ligands; and finally, the metal oxidation state should be two units lower than the most stable oxidation state.

3.2.2 Stereochemistry of oxidative addition

The stereochemistry of oxidative addition reactions is important in formulating possible transition states occuring during the course of the reaction. Although the stereochemistry of the final oxidative addition product is usually complicated by ligand exchange and isomerization reactions, the thermodynamic most stable isomer or isomer mixture can in many cases be isolated and characterised[4].

The mode of addition of a non-polar molecule (X-Y) to a metal complex can take place by either *cis*- or *trans*-addition of the addend molecule as illustrated in Eq. 3.2.

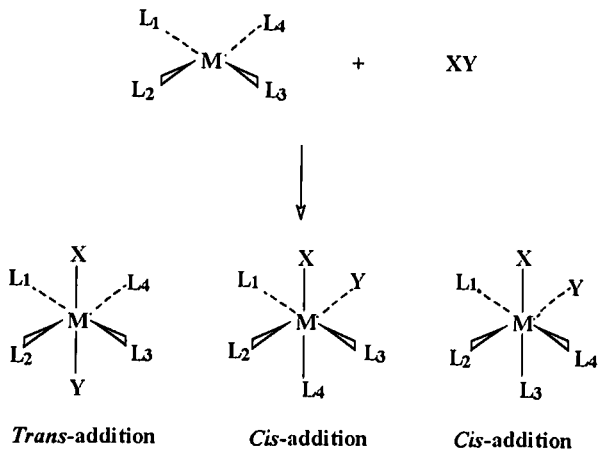

3.2

In general, non-polar substances such as H_2, O_2 and C_2H_4 add in a *cis* fashion[5,6]. These additions are believed to proceed *via* a three-centered intermediate as shown by the following illustration.

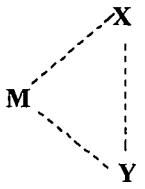

Non-polar three-center transition state

Alkyl halide addition has been reported to yield both *cis*- and *trans*-products[7], but mainly *trans*. There are however cases where *cis*-addition of polar molecules took place, as is illustrated by the oxidative addition product (see Eq. 3.3) of iodomethane and $[Rh(cupf)(CO)(PPh_3)]$[8] which was isolated and characterized by X-ray crystallography.

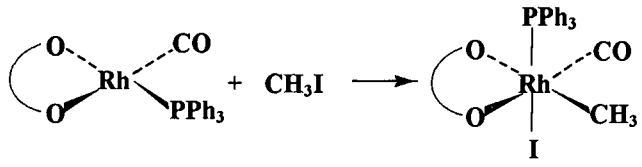

3.3

Another example where *cis*-products were obtained include the addition of alkyl halides to $[Ir(Cl)(CO)(PMe_2Ph)_2]$[9].

An example of *trans*-addition is found in the oxidative addition of CH_3I to $[Rh(tfba)(P(OPh)_3)_2]$[10] as shown in Eq. 3.4.

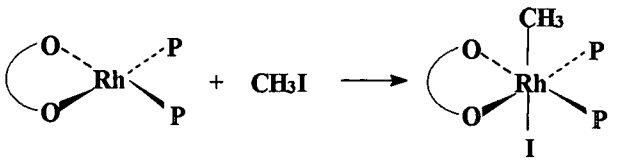

3.4

P=P(OPh)3

It was accepted that this reaction proceeds *via* a linear transition state as illustrated in Eq. 3.5.

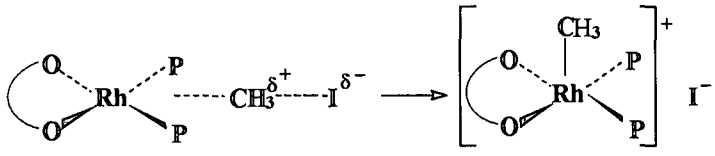

3.5

Literature studies show that the stereochemistry of oxidative addition may be influenced by factors such as solvent, temperature, pressure, etc.[11] The reaction of CH_3I or CH_3Br with *trans*-[Ir(Cl)(CO)(PPhMe)$_2$)][9] for example, yielded the *trans*-product in benzene medium and both *cis*- and *trans*-products in methanol as solvent. It is also important to note that any conclusions in terms of the mode of addition of the addendum molecule by analyzing the final product should be approached with caution. There are known examples where isomerization of ionic intermediates takes place yielding products in which the fragments of the addendum molecule are *cis* to one another after coordination of the anion[12]. Thus a *cis*-product does not necessarily indicate a three-centered intermediate. Furthermore, examples are known where the *trans*-product isomerizes to the *cis*-product, as was found in the case of the *trans*-oxidative addition product for the reaction between CH_3Cl and [Ir(Br)(CO)(PPh$_2$Me)$_2$][13]. When the *trans*-product is refluxed in a methanol/benzene mixture, the *cis*-product is obtained.

From a mechanistic point of view it is important to know whether the addition is *cis* or *trans*. *Cis*-addition should stereochemically favour reductive elimination rather than *trans*-addition since the X;Y fragments (see Eq. 3.2) are in close proximity for interactions to take place.

3.2.3 Mechanism of oxidative addition reactions

There is still uncertainty regarding the mechanistic pathway of oxidative addition reactions, in particular with respect to the existence and nature of a formal transition state which is usually impossible to isolate and characterize. Reaction mechanisms most

commonly proposed include the concerted three-centered process, S_N2, free radical and ionic mechanisms, which are briefly discussed below.

3.2.3.1 The concerted three-center mechanism

The addition of non-polar molecules such as H_2, O_2, Cl_2, C_2H_2, etc. in non-polar solvents normally takes place *via* this mechanism[14] and only *cis*-addition is possible, since *trans*-addition is a symmetry forbidden process[15]. The mechanism is often described in terms of the overlap of a filled d_{xy} or d_{yz} orbital of the metal and an empty σ^* orbital of the addend molecule, see Fig. 3.1. Overlapping of the filled σ-orbital of the addend molecule with an empty metal orbital leading to electron flow to the metal, also plays an important role[16]. Both interactions weaken the Y-Z bond and strengthen the M-Y and the M-Z bonds.

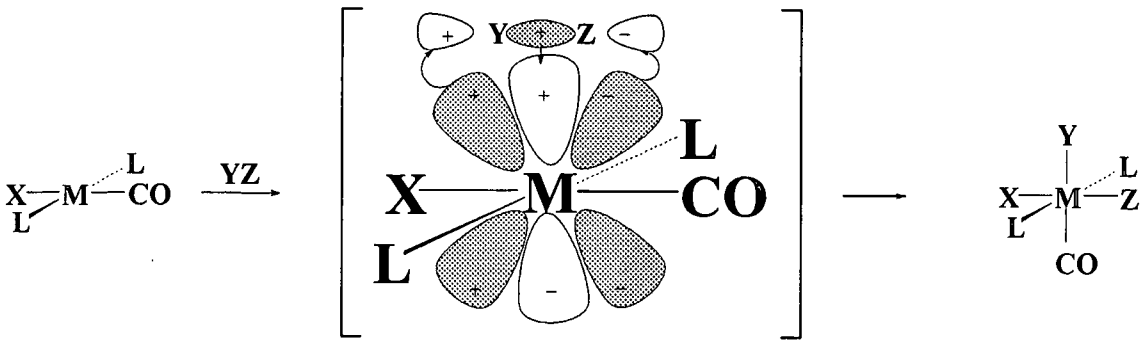

Fig. 3.1 A concerted mechanism for the oxidative addition of YZ to *trans*-$[MX(CO)L_2]$

3.2.3.2 The S_N2 two-step mechanism

This process is based upon nucleophilic attack of the metal center on the α-carbon of polar addend molecules such as alkyl halides (methyl, benzyl or allyl halides) and subsequent formation of a polar, five coordinated transition state[14]. This mechanism is

expected to yield a *trans*-product (Fig. 3.2) in terms of the proposed linear transition state *via* the formation of an ionic intermediate; i.e., if no isomerization of the ionic intermediate takes place.

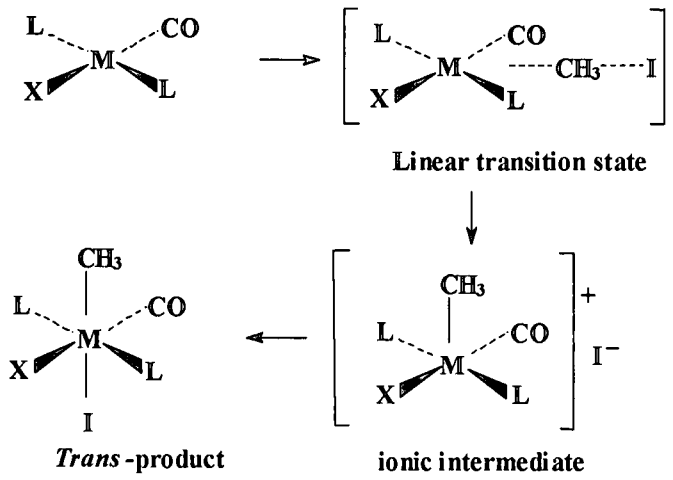

Fig. 3.2 The S_N2 mechanism for the oxidative addition of CH_3I to *trans*-$[MX(CO)L_2]$

In terms of orbital interactions the linear transition state may be visualized as the overlap of a donor metal orbital (presumably the filled d_z^2-orbital) with an σ^*-orbital of the addend molecule (Y-Z) as depicted in Fig. 3.3 below. Although only *trans*-addition is favoured according to molecular considerations, isomerization may lead to the formation of *cis*-adducts.

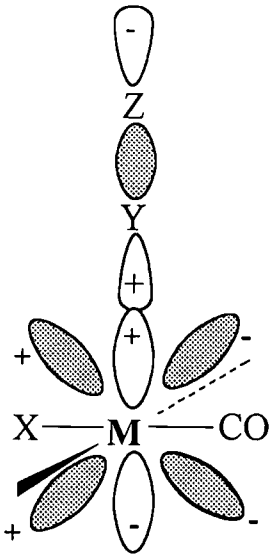

Fig. 3.3 The linear transition state in terms of orbital interactions.

3.2.3.3 Free radical mechanism

A few oxidative addition reactions proceed *via* a free radical mechanism[17] initiated by the presence of trace amounts of impurities or by molecular oxygen, benzoylperoxide or even light. All steps in this mechanism involve single electron processes. Alkyl halides, vinyl and aryl halides as well as α-halo esters undergo oxidative addition to Vaska complexes by a radical chain mechanism.

3.2.3.4 The ionic mechanism[11]

In polar solvents, addend molecules such as HCl and HBr will dissociate to a larger or smaller extent. Protonation of a square planar complex, like *trans*-$[MX(CO)L_2]$, first produces a five-coordinate intermediate (Fig. 3.4), which then proceeds to form the final products.

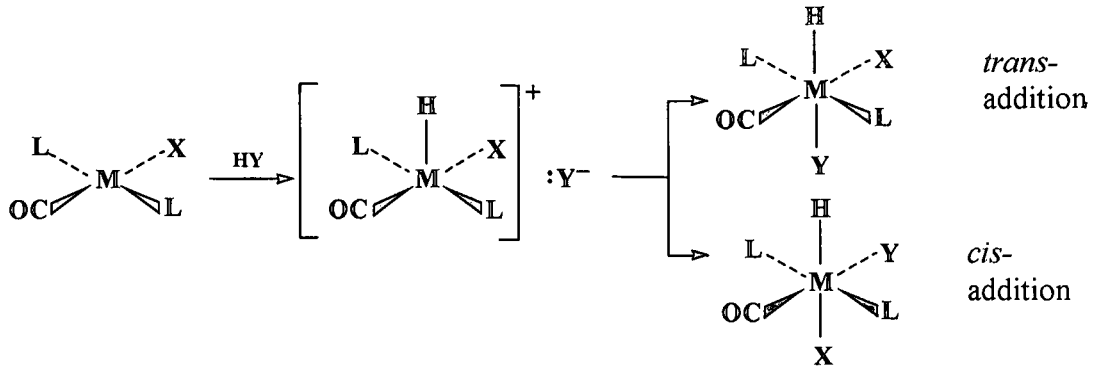

Fig. 3.4 Ionic reaction mechanism for oxidative addition

3.2.4 Factors influencing the rate of oxidative addition

During oxidative addition the metal center can be considered to act as a nucleophile, therefor any factors influencing the nucleophilicity of the metal, will affect the course of the reaction (rate and products). Since the coordination number of the metal complex increases, steric factors will also play a role (see Section 2.2.2). A few important factors influencing oxidative addition, will be briefly discussed below.

3.2.4.1 The metal center

Fig. 3.5 summarizes the general tendency for d^8 complexes to undergo oxidative addition. According to these results, larger metal centers in lower oxidation states (though not without exception) are more reactive towards oxidative addition. The ease of oxidation of a metal center provides further indication of the reactivity towards oxidative addition.

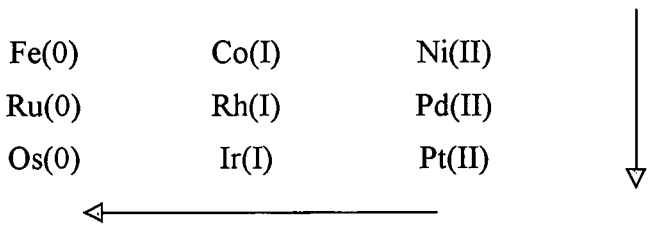

Fig. 3.5 Reactivity of d^8 metal centers towards oxidative addition. Arrows indicate increased reactivity.

3.2.4.2 *Coordinated (non-labile) ligands*

The σ- and π-bonding properties of bonded ligands largely influence the electron density and thus the nucleophilicity of the metal center. Ligands with good σ-donating properties enhance oxidative addition while good π-accepting ligands inhibit reactivity[18].

3.2.4.3 *The reaction medium*

The influence of the solvent on the rate of oxidative addition reactions of square planar complexes has been extensively investigated[19,20,21]. The dielectric constant (ε) and donocity (D_n) is a good indicator of the polarity and donor ability of a solvent. Basson *et al.*[8] for example observed a marked effect of solvent polarity and donocity on the rate of the oxidative addition reaction of CH_3I with [Rh(cupf)(CO)(PPh_3)]. The formation of a polar transition complex, accompanied by considerable charge separation, was postulated.

3.2.4.4 *Nucleophilic catalysis*

The existence of ions in solution can lead to the enhancement of the rate of oxidative addition by means of coordination to the substrate, making it more reactive to electrophilic centers. An example of this type of catalysis is the coordination of I^- to $[RhI_2(CO)_2]^-$, which enhances the oxidative addition of CH_3I[22] (see Fig. 3.6).

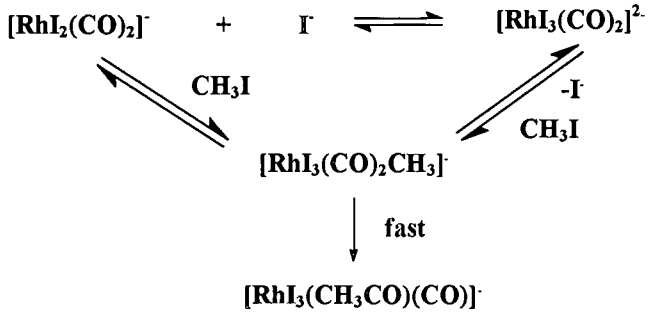

Fig. 3.6 Iodide catalysis in the oxidative addition of CH_3I to $[RhI_2(CO)_2]^-$

3.3 REDUCTIVE ELIMINATION

Frequently, but not generally, oxidative addition is reversible. The term reductive elimination is used to describe the reverse reaction (Eq. 3.2) in which both the coordination number and formal oxidation state of the complex decreases. Just as oxidative addition is an important method to activate small molecules by attachment to the metal center, reductive elimination is equally important for removing organic moieties from a complex. Since reductive elimination is not a significant part of this study, it will only be briefly discussed. Four common reductive elimination reactions are shown below (Eq. 3.6-3.9), where R is an alkyl or aryl group.

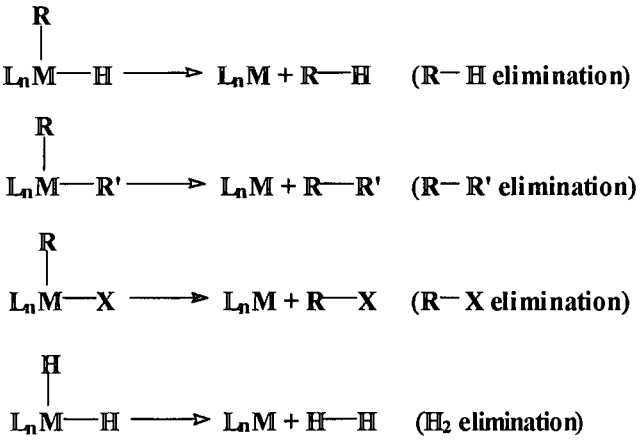

3.6

3.7

3.8

3.9

As in the case of oxidative addition and CO-insertion, some factors are significantly influencing reductive elimination reactions. Factors important[23] in effecting intramolecular, mononuclear reductive eliminations include a *cis* orientation between the two ligands being eliminated. Furthermore, bulky ancillary ligands contributes a thermodynamic driving force toward the elimination process since the coordination number of the complex decreases by two units upon elimination, affording a product with considerable less intramolecular steric repulsion. Similarly, relative high formal charge on the metal center favours reductive elimination, while for general reductive elimination reactions, illustrated in reactions (Eq. 3.6-3.9), the electrostatic stability of the product, L_nM, is critical. If the resulting complex is quite stable, reductive elimination is favoured.

3.4 CARBONYL INSERTION

Carbonyl insertion is generally regarded as the insertion of CO between the metal and R group to form the acyl species as shown in Eq 3.10[24].

$$[MR(CO)L_2] \xrightarrow{CO} [M-\overset{\overset{O}{\|}}{C}-R(CO)L_2] \qquad \text{3.10}$$

acyl

The question of whether CO insertion takes place, or the R group migrates, was mechanistically investigated for complexes of the type $[CH_3Mn(CO)_5]$[25]. By using ^{13}CO as incoming ligand (and thus the driving force to facilitate the process), the following observations were made:

(i) The CO molecule that finally becomes the acyl carbonyl, is not derived from external CO but is one already coordinated to the metal atom.

(ii) The incoming ligand is added *cis* to the acyl group and the alkyl of the complex migrates to a *cis*-bonded CO.

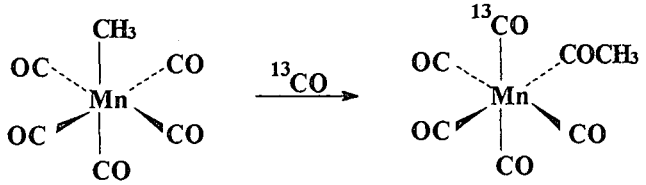

3.11

(iii) The conversion of the alkyl group into an acyl group can be effected by addition of ligands other that CO, see Eq. 3.12.

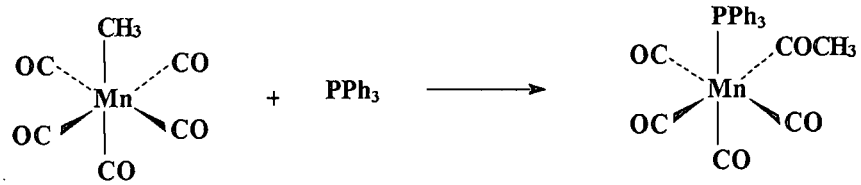

3.12

In general, the CO-insertion mechanism thus basically concerns a 1,2-migration of an alkyl group to a *cis*-located carbonyl group *via* a three-center transition state, as depicted in Eq. 3.13[24].

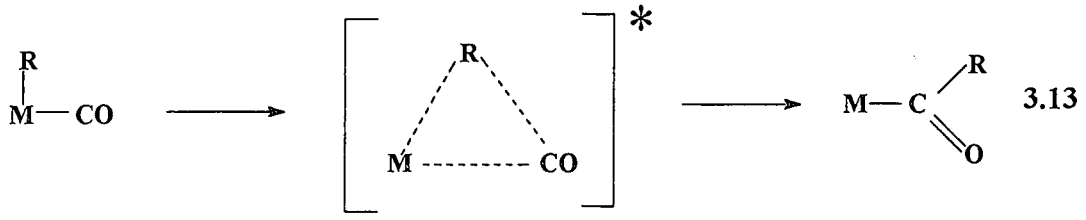

3.13

Carbonyl insertion (not indicating any specific mechanism) can also proceed without external addition of another ligand, which is illustrated for example by the oxidative addition reaction of iodomethane and subsequent insertion of CO into the metal-methyl bond in [Rh(Cl)(CO)L_2)], Eq. 3.14[26].

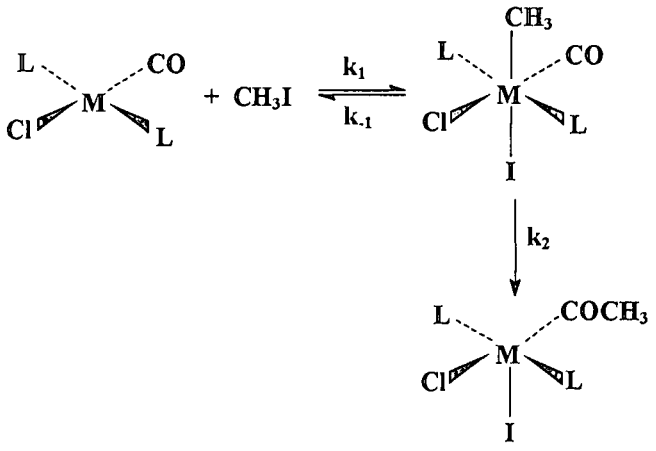

3.14

3.4.1 Some important factors influencing CO-insertion reactions

3.4.1.1 The metal center

Carbonyl insertion reactions have been observed for a range of organometallic compounds, and from these studies, it appears that the reactivity towards CO-insertion is given as 3d- > 4d- > 5d-transition metals. This tendency is illustrated in Eq. 3.14 where the k_{-1} and k_2 steps are absent for Ir(5d)[26], while in the case of Rh(4d)[27] the complete reaction model holds. These observations can be explained in terms of stronger metal-

carbon bonds for 5d-transition metals, thus retarding the rate of migration. Recently, iridium was successfully employed in place of rhodium in the production of acetic acid (Monsanto technology) in the so-called "Cativa" process[28]. Model studies showed that the rate of oxidative addition is enhanced with the introduction of iridium, however, the rate of carbonyl insertion was retarded. The migratory insertion reaction for iridium was substantially accelerated by addition of a Lewis acid (SnI_2) or a polar solvent (methanol). The effect of the metal center is thus clearly illustrated.

3.4.1.2 The migrating group (R)

The reaction given in Eq. 3.15 was studied by Maitlis *et al.*[29] as a model for the migration step in rhodium catalysed carbonylation reactions. The R group was varied in terms of phenyl and *para* substituted phenyls.

$$\underset{\textit{alkyl}}{[RhI(C_5Me_5)(CO)R]} + PPh_3 \longrightarrow \underset{\textit{acyl}}{[RhI(C_5Me_5)(COR)(PPh_3)]} \qquad 3.15$$

R = *p*-X-Ph, with X = H, Me, Cl, CHO, CN and NO_2

The order of reactivity in toluene at 25 °C was found to be: R = Ph > *p*-Cl-Ph > *p*-CHO-Ph > *p*-CN-Ph > *p*-NO_2-Ph, with the electron donating ability of the R group decreasing in the same order. It is thus clear that the nature of the migrating group is important in these type of reactions.

3.4.1.3 Solvent effects

Migratory CO-insertion can be dependent on solvent effects, which in some cases are quite large[30,31,32]. Bibler and co-workers[33] found proof of the solvent effect during the reaction of $[Fe(Cp)(CO)_2(CH_3)]$ with PPh_3. This reaction proceeds to completeness in tetrahydrofurane (THF) to form the acyl product $[Fe(Cp)(CO)(COCH_3)(PPh_3)]$ while no

reaction was observed in hexane. The observation was explained in terms of solvent coordination, which provides a pathway for the insertion process.

A question that might be asked is how solvent interaction takes place. There are two conflicting explanations[34] for this type of solvent effects on carbonyl insertion reactions: (1) the solvent (especially a polar one) may stabilize the transition state during carbonyl insertion by solvation or (2) direct attack on the metal center by the solvent (solvents with high donocity) will increase the electron density on the metal center and subsequently lead to a decrease in Rh-R bond strength thus increasing the migratory ability of the coordinated R-group to the carbonyl. Evidence for the coordinating ability of solvents was found by Wax en Bergman[30] who studied carbonyl insertion of $[Mo(Cp)(CO)_3CH_3]$ in a range of THF derivatives as solvents (THF, 2-Me-THF and 2,5-Me_2-THF). It can be assumed that the donocity of these solvents will differ but not the polarities. The results indicated that, in spite of the higher Lewis basicity of 2,5-Me_2-THF (compared to THF), the conversion to the acyl complex still proceeded more rapidly in THF. This observation was explained in terms of the larger steric demand of 2,5-Me_2-THF in an associative step. The steric hindrance of the solvent thus leads to a retardation in the formation of the solvent coordinated intermediate, prior to the migration of the methyl group.

3.4.1.4 The ancillary ligands

Anderson and Cross[35] synthesized three geometrical isomers of $[PtCl(CO)(Ph)(PMePh_2)]$ and observed that only the isomer *trans* with respect to $PMePh_2$ (isomer I) undergoes carbonyl insertion to form the halide bridged acyl complex, see Fig. 3.7. For isomer (I) with the migrating group (Ph) *trans* to the ligand PR_3, it was found that phosphines with better electron donating power (thus a high *trans*-influence) favour the formation of the halogen bridged acyl dimer[36]. In isomer (III) the phenyl group is *trans* to Cl and is thus

not labilized. In isomer (II) the migrating group (Ph) and CO are *trans* to one another making methyl migration impossible, since a *cis* configuration is needed.

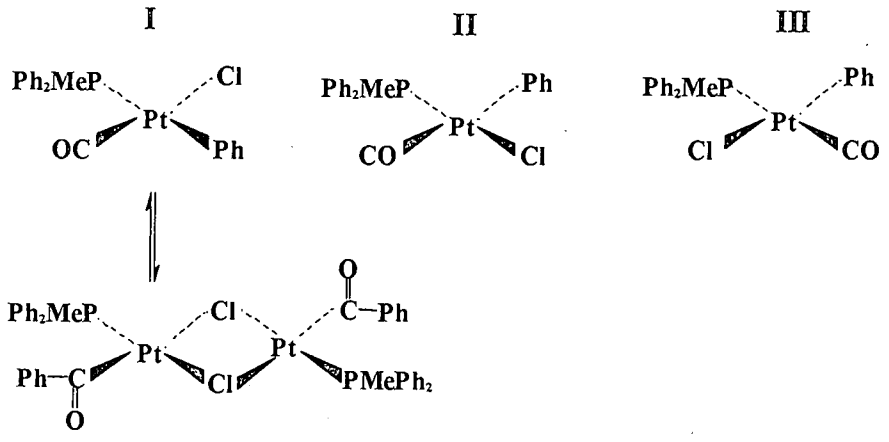

Fig. 3.7 Selected formation of acyl complex in different isomers of $[PtCl(CO)(Ph)(PMePh_2)$

3.4.1.5 Lewis acids

Rate increases of orders of magnitude can be obtained by addition of Lewis acids[29,37] like BF_3 or $AlCl_3$ that interacts with the carbonyl group and thus drive the reaction probably *via* steps of the type as shown in Fig. 3.8.

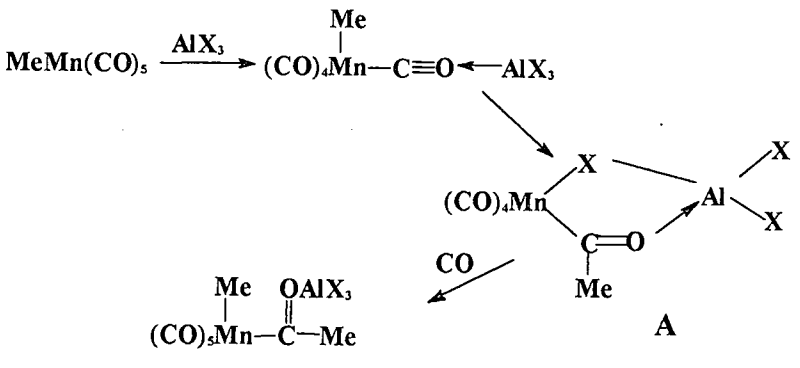

Fig. 3.8 Possible interaction of Lewis acids with coordinated carbonyl to increase migratory insertion of the methyl group.

Intermediate **A** has been characterized for $AlBr_3$ but other intermediates has also been proposed[38,39].

3.4.2 Carbonyl insertion in M-H-bonds

The CO-insertion step in M-R-bonds is comparable to the insertion of CO in M–H bonds leading to acyl and formyl formation respectively. The latter reaction has been previously thoroughly investigated as a potential first step in the Fischer-Tropsch reduction[40] of CO by H_2 , see for example Eq. 3.16.

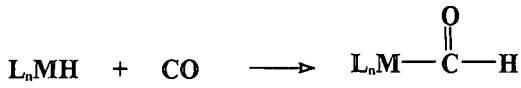

3.16

The reaction (MH + CO) is mainly endothermic for the early transition metals, whereas the reaction between MR and CO is exothermic. This difference can be attributed to the significantly stronger M-H bond compared to the M-C bond (the bond energy is approximately 30 kcal mol^{-1} higher for the M-H bond)[41]. The difference in bond energy between M-H and M-C for the actinides is only ± 15 kcal mol^{-1} and due to this reason the formyl, as in the case of the acyl exhibit carbenic character in actinides[42] (Eq. 3.17).

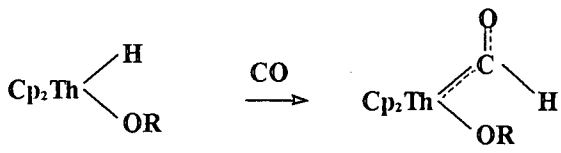

3.17

CO-insertion in M-H bonds for d-block elements is not as well documented as in the case of insertion into M–C bonds[40,43,44,45]. Kinetic studies of $[XM(CO)_n]$ type of compounds[46] showed that when X = H, the rate of CO substitution is much faster compared to when X = Cl or CH_3. This indicates a definite kinetic significant amount of formyl intermediate (see Eq. 3.18) formed during the reaction

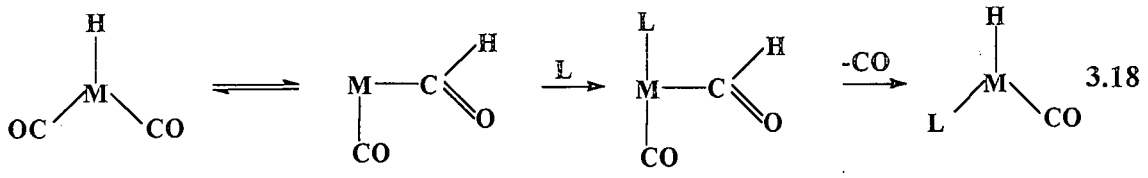

3.18

Attempts to increase the rate of H-migration by the introduction of Lewis acids, which were found to be effective for methyl migration, however did not result in the formation of formyls, but rather led to the reaction in Eq. 3.19[47]:

$$[(CO)_5MnH] + BCl_3 \rightleftharpoons [(CO)_5Mn\cdots H\cdots BCl_3] \qquad 3.19$$

REFERENCES

1. Ugo, R., and Carrá, S. 1967, *Inorg. Chim. Acta Rev.*, **1**, 49.
2. Vaska, L. 1971, Inorg. Chim. Acta 5; 295; Vaska, L., 1968, *Acc. Chem. Res.*, **1**, 335; Vaska, L., and Chen, L.S. 1971, *J. Chem. Soc. Chem. Comm.*, 1080.
3. Vaska, L., and Diluzio, J.W., 1962, *J. Am. Chem. Soc.*, **84**, 679.
4. Dickson, R.S., 1983, Organometallic Chemistry of Rhodium and Iridium, Academic Press, London, 71.
5. Natta, G., and Farina, M., 1972, Stereochemistry, William Clowes&Sons, London
6. Cornils, B, Hermann, W.A., Rasch, M., 1994, *Angew. Chem.*, **106**, 2219; Cornils, B., Hermann, W.A., and Rasch, M., 1994, *Angew. Chem., Int. Ed. Engl.*, **33**, 2144.
7. Natta, G., 1955, *Brennst. Chem.*, **36**, 176.
8. Basson, S.S., Leipoldt, J.G., Roodt, A., Venter, J.A., 1987, *Inorg. Chim. Acta*, **128**, 31.
9. Deeming, A.J., Shaw, B.L. 1969, *J. Chem. Soc.*, **A**, 1562.
10. Van Zyl, G.J., Lamprecht, G.J., Leipoldt, J.G., and Swaddle, T.W. 1988, *Inorg. Chim. Acta*, **143**, 223.
11. Cotton, F.A., and Wilkinson, G., 1976, Basic Inorganic Chemistry, John Wiley and Sons Inc., New York.
12. Meaken, P., Schunn, R.A., and Jesson, J.P. 1974, *J. Am. Chem. Soc.*, **96**, 277. English, A.D., Meaken, P., and Jesson, J.P. 1976, *J. Am. Chem. Soc.*, **98**, 422.
13. Collmann, J.P., and Sears, C.T. 1968, J. *Inorg. Chem.*, 7, 27.
14. Cross, R.J. 1985, *Chem. Soc. Rev.*, **14**, 197.
15. Pearson, R.G. 1976, Symmetry Rules for Chemical Reactions, Wiley Interscience.
16. Saillard, P.S., Hoffmann, R. 1984, *J. Am. Chem. Soc.*, **106**, 2006.
17. Davidson, L.J. 1965, *Inorganic Reaction Mechanisms*, **6**, 414.
18. Leipoldt, J.G., Basson, S.S., and Botha, L.J. 1990, *Inorg. Chim. Acta*, **168**, 215.
19. Basson, S.S., Leipoldt, J.G., and Nel, J.T. 1984, *Inorg. Chim. Acta*, **84**, 167.
20. Hart-Davis, A.S., and Graham, W.A.G. 1970, *Inorg. Chem.*, **9**, 2658.

21. Kubota, M., Kiefer, G.W., Ishikawa, R.M., and Bencala, K.E. 1973, *Inorg. Chim. Acta*, 7, 195.

22. Hickey, C.E., and Maitlis, P.M., 1984, *J.C.S. Chem. Commun.*, 1609.

23. Deutsch, P.P., and Eisenberg, R., 1988, *Chem. Rev.*, **88**, 1147.

24. Cotton, F.A., and Wilkinson, G. 1988, Advanced Inorganic Chemistry; Fith Ed., Wiley.

25. Noack, K., and Calderazzo, F., 1967, *J. Organomet. Chem.*, **10**, 101.

26. Chock, P.B., and Halpern, J. 1966, *J. Am. Chem. Soc.*, **88**, 3511.

27. Douek, I.C., and Wilkinson, G. 1969, *J. Chem. Soc.*, **A**, 2604.

28. Maitlis, P.M., Haynes, A., Sunley, G.J., and Howards, M.J. 1996, *J. Chem. Soc. Dalton Trans.*, 2187.

29. Sunley, G.J., Fanizzi, F.P., and Maitlis, P.M. 1990, *J. Chem. Soc. Dalton Trans.*, 1799.

30. Wax, M.J., and Bergman, R.G. 1981, *J. Am. Chem. Soc.*, **103**, 7028.

31. Webb, S.L., Giandomenico, C.M., and Halpern, J. 1986, *J. Am. Chem. Soc.*, **108**, 345.

32. Martin, B.D, Warner, K.E., and Norton, J.R. 1986, *J. Am. Chem. Soc.*, **108**, 33.

33. Bibler, J.P., and Wojciki, A. 1966, *Inorg. Chem.*, **5**, 889.

34. Flood, T.C., Jensen, J.E., and Statler, J.A. 1981, *J. Am. Chem. Soc.*, **103**, 4410.

35. Anderson, G.K., and Cross, R.J. 1979, *J. Chem. Soc., Dalton Trans.*, 1246.

36. Anderson, G.K., and Cross, R.J. 1984, *Acc. Chem. Res.*, **17**, 67.

37. Calderazzo, F. 1977, *Angew. Chem. Int. Ed. Engl.*, **16**, 299.

38. Cotton, J.D., and Markwell, R.D. 1985, *Organometallics*, **4**, 937.

39. Norton, J.R. 1986, *J. Am. Chem. Soc.*, **108**, 33.

40. Cornils, B., and Hermann, W.A. 1996, Applied Homogeneous Catalysis with Organometallic Compounds, VCH. Weinheim.

41. Herrmann, W.A. 1982, *Angew. Chem., Int. Ed. Engl.*, **21**, 117.

42. Moloy, K.G., and Marks, T.J. 1984, *J. Am. Chem. Soc.*, **106**, 7051.

43. Cheng, C.-H, and Eisenberg, R.J. 1977, *J. Am. Chem. Soc.*, **99**, 3003.

44. Wilkinson, G., Gordon, F., Stone, A., and Abel, E.W. 1982, *Comprehensive Organometallic Chemistry*, Pergamon Press.

45. Steyn, G.J.J., Roodt, A., and Leipoldt, J.G. 1993. *Rhodium Ex.*, **0**, 11.

46. Pearson, R.G. 1981, *Inorg. Chem.*, **20**, 2741.

47. Shriver, D.F. 1982, *Organometallics*, **1**, 1624.

CHAPTER 4

Synthesis and characterization of Rh(I)-complexes

4.1 INTRODUCTION

The synthesis and characterization of ligands and starting Rh(I)-complexes relevant to this study is described. Characterization techniques include IR, ^{1}H NMR, and ^{31}P NMR. The rhodium(I) complexes prepared are of the type [Rh(N,O-BID)(CO)(PR_3)] and [Rh(N,O-BID)(CO)($AsPh_3$)], with N,O-BID = mono anionic bidentate ligand, with coordinating atoms nitrogen and oxygen (six membered chelates); PR_3 = tertiary phosphine with R = Ph, *p*-Cl-Ph and *p*-OMe-Ph.

4.1.1 Apparatus

IR spectra were recorded in KBr disks on a Hitachi 270-50 spectrophotometer in the range 4000-250 cm^{-1}. Both ^{1}H NMR and ^{31} P NMR spectra were recorded on a Bruker AM 300 spectrophotometer.

4.1.2 Reagents and solvents

Unless otherwise stated, all reagents were recrystallised and all solvents distilled prior to use. $[Rh(CO)_2Cl]_2$ (Strem Chemicals Inc.) was used as received for the preparation of all relevant [Rh(β-diketonato)$(CO)_2$][1] complexes or were prepared *in situ* in DMF from $RhCl_3 3H_2O$. The N,O-BID ligands were obtained from Varshavsky[2] and used as received. One of these ligands (dmavk) was however also prepared in this laboratory. Triphenylphosphine (PPh_3), triphenylarsine ($AsPh_3$), tri(*p*-chlorophenyl)phosphine (P(*p*-

Cl-Ph)$_3$ and tri(*p*-methoxyphenyl)phosphine (P(*p*-MeO-Ph)$_3$ are commercially available and were used without further purification.

4.2 PREPARATION OF Rh(I)-COMPLEXES

The synthetic route for the preparation of the Rh(I)-complexes is described in Scheme 4.1.

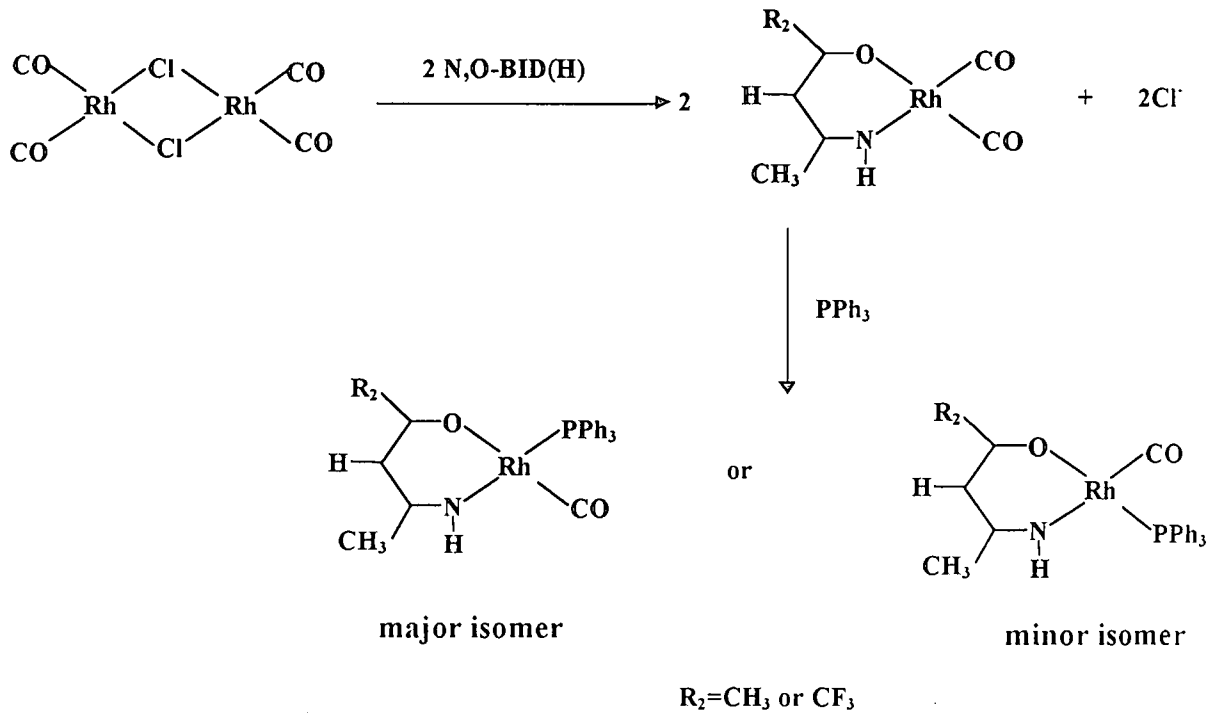

Scheme 4.1 General synthetic route

The products formed during the synthetic route exhibit different IR spectra in terms of the stretching frequency for the C≡O moieties in each. The dicarbonylrhodium(I) species gives an infrared spectrum with two distinct singlet peaks present between 1995 and 2074 cm^{-1}. Substitution of one of the carbonyl ligands by a tertiary phosphine yields a Rh(I)monocarbonylphosphine species, resulting in the disappearance of both dicarbonyl

peaks and the appearance of a carbonyl peak absorbing in the range absorbing between 1950-1970 cm^{-1}.

4.2.1 Experimental procedures

4.2.1.1 dmavkH (2-Aminovinyl-4-pentanone)

To 5.00 g Acetylacetone (50 mmol) in a beaker, 3.50 g NH_4OH (100mmol) was added and the solution slightly heated (40 °C) for 1 hour while stirring. The solution was allowed to stand overnight to allow evaporation of the excess NH_4OH. The solution changed colour from light yellow to dark yellow.

4.2.1.2 [Rh(dmavk)$(CO)_2$] (2-Aminovinyl-4-pentanonato-κO,κN)-dicarbonyl rhodium(I)

$[RhCl(CO)_2]_2$ was prepared in situ by refluxing ca. 300 mg (1.14 mmol) of $RhCl_3 3H_2O$ in 10 ml of DMF for ca. 30 minutes. The [Rh(dmavk)$(CO)_2$] complex was prepared by addition of 0.13 g (1.3 mmol) of the dmavkH ligand to the cooled DMF solution of $[RhCl(CO)_2]_2$. After precipitation by ice-water and centrifuge, a microcrystalline purple product was obtained (200 mg, yield ≈68 %). **IR(KBr, cm^{-1})**: (C≡O) 2058 (s) , 1995 (s). **^{1}H-NMR (C_3D_6O):** 2.16; 2.01 (s, 3 H, CH_3); 5.32 (s, 1 H, CH); 9.0-8.8 (m, 1 H, NH) ppm

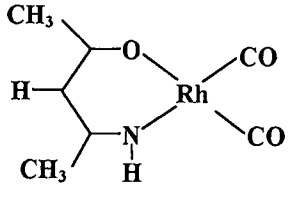

4.2.1.3 [Rh(dmavk)(CO)(PPh_3)] (2-Aminovinyl-4-pentanonato-κO,κN)-carbonyl(triphenylphosphine) rhodium(I)

To 5 ml of heptane solution containing 30 mg (0.12 mmol) of [Rh(dmavk)$(CO)_2$] was added 31 mg (0.12 mmol) of PPh_3, resulting in the immediate evolution of gas. Evaporation produced yellow crystals [Rh(dmavk)(CO)(PPh_3)], suitable for X-ray structure determination (49 mg, yield 83%). **IR(KBr, cm^{-1})**: (C≡O) 1960 (s)

^{1}H-NMR (C_3D_6O): 2.12; 1.65 (s, 2x3 H, CH_3); 5.07 (d, 1 H, CH); 7.85 (NH) ppm

^{31}P-NMR (C_3D_6O): major isomer- 41,45 ppm (d, 1x1P); $^1J_{RhP}$ = 149.72 Hz;

minor isomer – 54.91 ppm (d, 1x1P); $^1J_{RhP}$ = 172.03 Hz;

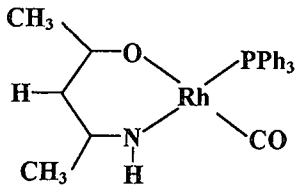

4.2.1.4 [Rh(dmavk)(CO)(*p*-Cl-Cl-Ph)$_3$P] (2-Aminovinyl-4-pentanonato-κO,κN)-carbonyl(tri(*p*-chlorophenylphosphine) rhodium(I)

To 5 ml of acetone solution containing 30 mg (0.12 mmol) of [Rh(dmavk)$(CO)_2$] was added 44 mg (0.12 mmol) of $(p\text{-}ClC_6H_4)_3P$ resulting in the immediate evolution of gas. Five drops of water was and after slow vaporation produced yellow microcrystalline product [Rh(dmavk)(CO)$(p\text{-}ClC_6H_4)_3P$)]. (58 mg, yield 81%). **IR(KBr, cm^{-1})**: (C≡O) 1960 (s)

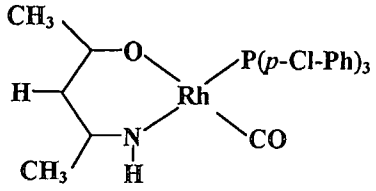

4.2.1.5 [Rh(dmavk)(CO)(AsPh$_3$] (2-Aminovinyl-4-pentanonato-κO,κN)-carbonyl triphenylarsine rhodium(I)

To 5 ml of heptane solution containing 30 mg (0.12 mmol) of [Rh(dmavk)(CO)$_2$] was added 37 mg (0.12 mmol) of AsPh$_3$, resulting in the immediate evolution of gas. Evaporation produced yellow crystals [Rh(dmavk)(CO)(AsPh$_3$)], suitable for X-ray structure determination (55 mg, yield 85%).

%). **IR(KBr, cm^{-1})**: (C≡O) 1956 (s)

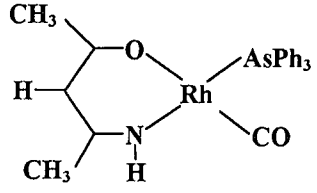

4.2.1.6 [Rh(tavk)(CO)(PPh$_3$)] (2-Aminovinyl-5,5,5-trifluro 4-pentanonato-κO,κN)-carbonyl(triphenylphosphine) rhodium(I)

To 5 ml of heptane solution containing 30 mg (0.097 mmol) of [Rh(tavk)(CO)$_2$] was added 26 mg (0.097 mmol) of PPh$_3$, resulting in the immediate evolution of gas. Evaporation produced yellow crystals [Rh(tavk)(CO)(PPh$_3$ (45 mg, yield 85%). **IR(KBr, cm^{-1})**: (C≡O) 1974 (s)

^{1}H-NMR (C_3D_6O): 2.22 (s, 1x3 H, CH_3); 5.56 (d, 1 H, CH) ppm

^{31}P-NMR (C_3D_6O): 39.9 ppm (d, 1x1P); $^1J_{RhP}$=149.5 Hz

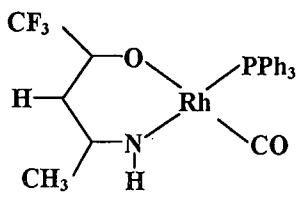

4.2.1.7 [Rh(tavk)(CO)($AsPh_3$)] (2-Aminovinyl-5,5,5-trifluro 4-pentanonato-κO,κN)-carbonyl(triphenylarsine) rhodium(I)

To 5 ml of a heptane solution containing 30 mg (0.097 mmol) of [Rh(tavk)$(CO)_2$] was added 30 mg (0.097 mmol) of $AsPh_3$, resulting in the immediate evolution of gas. Evaporation produced yellow crystalline [Rh(tavk)(CO)($AsPh_3$] (51 mg, yield 90%). **IR(KBr, cm^{-1})**: (C≡O) 1965 (s)

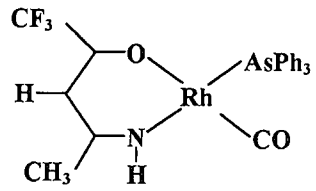

4.2.1.8 [Rh(tavk)(CO)((p-MeO-Ph)$_3$P)] (2-Aminovinyl-5,5,5-trifluro 4-pentanonato-κO,κN)-carbonyl(tri(p-methoxyphenyl)phosphine rhodium(I)

To 5 ml of acetone solution containing 30 mg (0.097 mmol) of [Rh(tavk)$(CO)_2$] was added 35 mg (0.097 mmol) of P(p-MeO-Ph)$_3$, resulting in the immediate evolution of gas. Addition of five drops of water and slow evaporation produced yellow microcrystalline product [Rh(tavk)(CO)(P(p-MeO-Ph)$_3$] (49 mg, yield 80%). **IR(KBr, cm^{-1})**: (C≡O) 1960 (s)

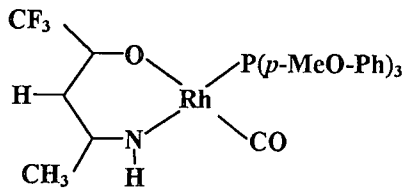

4.2.1.9 [Rh(dmavk)(I)(CH_3)(CO)(PPh_3)] (2-Aminovinyl-4-pentanonato-κO,κN)-idodo methyl carbonyl(triphenylphosphine) rhodium(I)

50 mg [Rh(dmavk)(CO)(PPh_3)] was dissolved in *n*-pentane (1.5 ml) and diethyl ether (1.5 ml). 0.57 g MeI was added to this solution. The solution was covered with parafilm and was left overnight in a fridge at -15 °C. Good quality crystals, suitable for x-ray crystallography was obtained. The I.R. spectrum exhibits a single carbonyl stretching frequency at 2070 cm^{-1} indicative of an alkyl complex.

^{1}H-NMR (C_3D_6O): 2.07, 1.92 (s, 2x3 H, CH_3); 4.94 (d, 1 H, CH); 7.0 (b, 1H, NH); 1.19 (t, 3xH, Rh-CH_3) ppm

^{31}P-NMR (C_3D_6O): 21.35 ppm (d, 1x1P); $^1J_{RhP}$=107.4 Hz

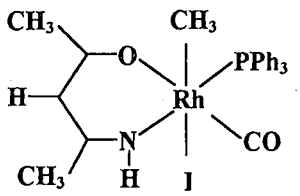

4.2.1.10 [Rh(dmavk)(I)($COCH_3$)(PPh_3)] (2-Aminovinyl-4-pentanonato-κO,κN)-idodo methyl acyl(triphenylphosphine) rhodium(I)

The starting compound, [Rh(dmavk)(CO)(PPh_3)], was synthesized from the reaction between [Rh(dmavk)($CO)_2$] and one equivalent of PPh_3 as described earlier. [Rh(dmavk)(CO)(PPh_3)] (5 mg, 0.0102 mmol) was dissolved in a mixture of 1.5 ml diethyl ether and 1.5 ml cyclohexane at 0 °C. An excess of iodomethane (0.57 g, 40 mmol) was added to this solution. The reaction mixture was covered with parafilm and left on ice. After 4 hrs yellow needles, characterized by infrared spectroscopy (KBr pellets) as the alkyl complex ($\upsilon_{(CO)}$ = 2070 cm^{-1}), crystallized. The solution was filtered, covered and left overnight on ice. Red crystals ($\upsilon_{(CO)}$ = 1716 cm^{-1}), suitable for X-ray crystallography, were obtained after 12 hrs.

^{1}H-NMR (C_3D_6O): 2.21, 1.58 (s, 2x3 H, CH_3); 5.04 (d, 1 H, CH); 5.25 (m, NH); 2.92 (3xH, $COCH_3$) ppm

^{31}P-NMR (C_3D_6O): 41.25 ppm (d, 1x1P); $^1J_{RhP}$=152.2 Hz

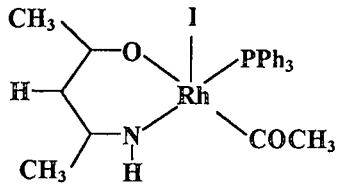

REFERENCES

1. Bonati, F., and Wilkinson, G. 1964, *J. Chem. Soc.*, 3156.
2. Varshavsky, Yu. S., Lebedev National Rubber Research Institute, 1 Gapsalskaya str., 198035, St. Petersburg, Russia.

CHAPTER 5

X-Ray Structural determinations of Rh(I) and Rh(III) complexes

5.1 INTRODUCTION

In general, replacement of one CO ligand in square planar complexes of the type $[Rh(L,L'\text{-BID})(CO)_2]$ (L,L'-BID = monoanionic bidentate ligand with donor atoms L and L') by PPh_3 may lead to the formation of two isomeric monocarbonyl complexes A and B as shown below. Crystallographic studies on different $[Rh(L,L'\text{-BID})(CO)(PPh_3)]$ complexes specifically revealed that in most cases, only one isomer crystallizes from solution[1]. The unique case where two isomers of the $[Rh(ba)(CO)(PPh_3)]$ complex (ba = benzoylacetonato) crystallized in the same unit cell, was however also noted[2]. From the structural data, the order of preference for carbonyl substitution by phosphine if the LL'-BID ligand contains donor atoms O,N or O,S, is *trans* to either the nitrogen or sulfur atom respectively[1]. These results can be explained in terms of the stronger *trans*-influence of the N and S atoms compared to that of the O atom. If the donor capabilities of L and L' are similar, isomers A and B are formed in comparable ratios. If the difference in the donor/acceptor properties of the donor atoms L and L' is large enough (e.g. N and O atoms), NMR studies of reaction mixtures revealed high selectivity of the carbonyl group replacement. For example, two isomers with well pronounced dominance of one of them for β-aminovinylketonate ligands are formed[3,4].

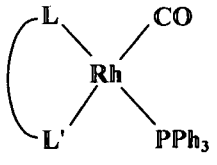

A

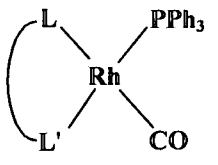

B

These results are clearly not in contrast with the structural data reported earlier for five membered chelates with L,L' = N,O like [Rh(ox)(CO)(PPh_3)][5] and [Rh(quin)(CO)(PPh_3)][1] and rather account for the fact that in most cases only one isomer, the most abundant in solution, crystallizes in the solid state.

In this chapter, the crystal structures of two of the monocarbonyl tertiary group 15 complexes, used as starting materials for subsequent oxidative addition reactions, are reported. These are the solid state substitution products [Rh(dmavk)(CO)(PPh_3)] and [Rh(dmavk)(CO)($AsPh_3$)], obtained from the reaction between [Rh(dmavk)($CO)_2$] and PPh_3 and $AsPh_3$ respectively. It was important for this study to determine the solid state structure of the [Rh(dmavk)(CO)(PPh_3)] complex, thus confirming the coordination mode, and for interpretation of kinetic results and mechanistic behaviour (see Chapter 6). A further motivation for this solid state study was the extended correlation of the solution coupling constants $^1J(^{103}Rh\text{-}^{31}P)$ and chemical shifts $\delta(^{31}P)$ with the Rh-P bond distances for the aminovinyl ketonato type of ligands. Furthermore, the crystal structure of [Rh(dmavk)(CO)($AsPh_3$)] was done since not many structures of the Rh(I)-bidentate ligand systems of the type [Rh(L,L'-BID)(CO)($AsPh_3$)] are known. However, more important was the fact that bond distances in this group 15 donor ligand were therefor obtained for comparison with the corresponding PPh_3 complex. An attempt was made to quantify kinetic and equilibrium data in terms of structural parameters, i.e. how the varying bond lengths can influence the reactivity in these compounds in [Rh(dmavk)(CO)(PPh_3)] and [Rh(dmavk)(CO)($AsPh_3$)] (see Chapter 6).

Previous crystallographic and kinetic studies concerning the oxidative addition of iodomethane to [Rh(L,L'-BID)(CO)(PR_3)] complexes have illustrated the different products that can be obtained from these reactions[6,7,8,9,10]. These studies confirmed that both *cis*-and *trans*-addition of iodomethane to the Rh(I) center can occur, thus forming the alkyl species. It was also shown that in some cases after formation of the alkyl species, subsequent CO-insertion/methyl migration leads to the final acyl species[11].

In the current study, both the intermediate alkyl and the final acyl products could be isolated in the solid state and structurally characterized. It is thus the first time that both these Rh(III) products could be studied this way, yielding the single crystal structures of the Rh(III)-alkyl complex, [Rh(dmavk)(I)(CH_3)(CO)(PPh_3)] and Rh(III)- acyl complex , [Rh(dmavk)(I)($COCH_3$)(PPh_3)].

5.2 EXPERIMENTAL

A summary of the general crystal data and refinement parameters for the complexes of [Rh(dmavk)(CO)(PPh_3)], [Rh(dmavk)(CO)($AsPh_3$)], [Rh(dmavk)(I)(CH_3)(CO)-(PPh_3)].CH_3I and [Rh(dmavk)(I)($COCH_3$)(PPh_3)] are given in Table 5.1. All data collections were done at 293(2)° K on an Enraf Nonius CAD 4 diffractometer (MoK_α = 0.71073 Å), except in the case of [Rh(dmavk)(CO)($AsPh_3$)] which was done on a Siemens Smart system (MoK_α = 0.71073 Å). The densities of all the crystals were determined by flotation in aqueous NaI, and the data were corrected for Lorentz and polarization effects and for absorption when necessary. The [Rh(dmavk)(I)(CH_3)(CO)(PPh_3)] crystals were sealed with Canada Balsam to prevent the evaporation of iodomethane molecules from the crystal lattice, thus resulting in cracking of the crystals.

Details of the preparation of the complexes and the growth of the crystals were given in Chapter 4, while supplementary data containing complete lists of atomic coordinates, anisotropic displacement parameters, bond distances and angles as well as hydrogen coordinates are given in Par. 8.1. Selected bond lengths and angles are given for each structure under each heading as well as a figure showing the atom numbering scheme.

All structures were solved by conventional Patterson and Fourier methods and refined by full-matrix least squares calculations using the SHELXL 97 program[12], with $\Sigma(/Fo/-/Fc/)^2$ being minimized. All non-hydrogen atoms were refined anisotropically unless otherwise stated. Phenyl and methyl hydrogen atom positions were calculated using a riding model,

however, in all cases the hydrogen on the nitrogen atom of the avk ligand was obtained from a difference Fourier map.

Table 5.1 Crystallographic data for complexes studied

	RAVP [a]	RAVAS [b]	RAVALK [c]	RAVACY [d]
Formula	$C_{24}H_{23}NO_2PRh$	$C_{20}H_{16}AsN_2O_2Rh$	$C_{26}H_{30}I_2NO_2PRh$	$C_{50}H_{44}I_2N_2O_4P_2Rh_2$
Formula Weight	491.3	494.2	776.2	1258.4
Crystal System	Orthorhombic	Triclinic	Triclinic	Monoclinic
Space group	$Pca2_1$	$P\bar{1}$	$P\bar{1}$	$P2_1/c$
a(Å)	16.500(4)	10.0317(12)	10.3550(10)	17.124(7)
b(Å)	8.512(3)	11.1000(13)	10.8100(10)	17.941(8)
c(Å)	16.229(4	12.0359(14)	14.0780(10)	18.313(7)
α(°)	90	113.295(2)	82.869(10)	90
β(°)	90	97.156(2)	85.303(10)	117.79(4)
γ(°)	90	107.963(2)	68.876(10)	90
V(Å^3)	2279.3(1)	1123.4(2)	1457.4(2)	4977(4)
Z	4	2	2	4
Flack parameter	0.17(4)	-	-	-
ρ (g cm^{-3})	1.432	1.461	1.769	1.679
Crystal Dimensions (mm^3)	0.50 0.25 0.15	0.48 0.22 0.18	0.44 0.32 0.06	0.30 0.15 0.10
μ (mm^{-1})	0.838	2.235	2.781	16.061
Number of data Collected	1656	12684	2763	3860
Number of Unique data used	1656	5485	2763	3860
R [e]	2.04	3.88	4.77	6.72
wR_2 [f]	5.28	7.31	15.25	16.51
Diffractometer	Enraf-Nonius CAD4F	Siemens Smart	Enraf-Nonius CAD4F	Enraf-Nonius CAD4F

[a] RAVP = $[Rh(dmavk)(CO)(PPh_3)]$ [b] RAVAS = $[Rh(dmavk)(CO)(AsPh_3)]$
[c] RAVALK = $[Rh(dmavk)(I)(CH_3)(CO)(PPh_3)].CH_3I$ [d] RAVACY = $[Rh(dmavk)(I)(COCH_3)(PPh_3)]$

[e] $R = [(\Sigma \Delta F)/(\Sigma F_o)]$, [f] $wR_2 = \Sigma[w(F_o^2 - F_c^2)^2]/\Sigma[w(F_o^2)^2]^{\frac{1}{2}}$

5.3 THE CRYSTAL STRUCTURE OF [Rh(dmavk)(CO)(PPh_3)][13]

5.3.1 Results and discussion

The complex crystallizes as square planar moieties in the asymmetric orthorombic space group $Pca2_1$ with four independent molecules per unit cell, see Fig. 5.1.

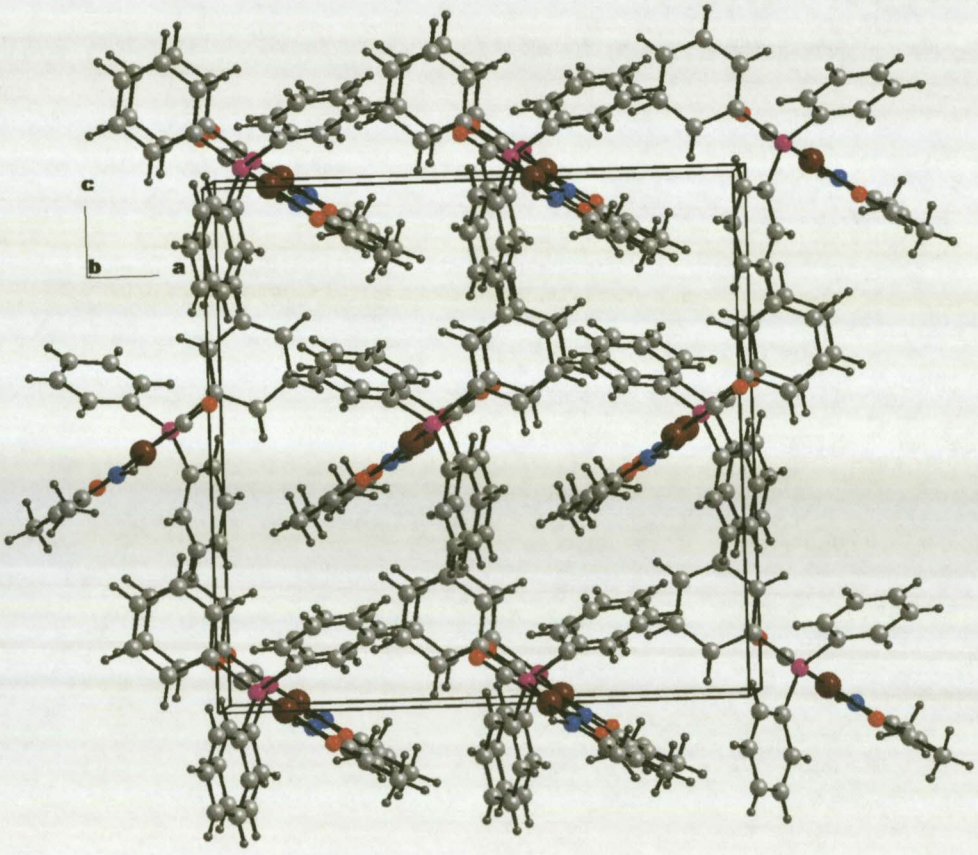

Fig. 5.1 Packing diagram of [Rh(dmavk)(CO)(PPh_3)] (view along the b-axis)

The closest contacts in the unit cell are of the order of 3.3 Å between H32 (phenyl) and O2 (carbonyl), typical of Van der Waal interactions. There are specifically no significant Rh-Rh interactions, with the closest Rh-Rh distance in the order of 8 Å. Of interest is the fact that the dmavk ligands are stacked in channel-like cavities, along the b-axis which are formed by the surrounding phenyl groups of the PPh_3-ligands (see Fig. 5.1) with

contact distances between the avk methyl group and the outer phenyl protons of *ca.* 3.1 Å. The methyl protons of the avk ligand shows interaction (Van der Waals; e.g. H16-H51 = 3.2 Å) with the phenyl protons. Finally, it is noteworthy that this channel-like structure thus results in a crystallographically pure "enantiomers", as confirmed by the Flack parameter of 0.17(4).

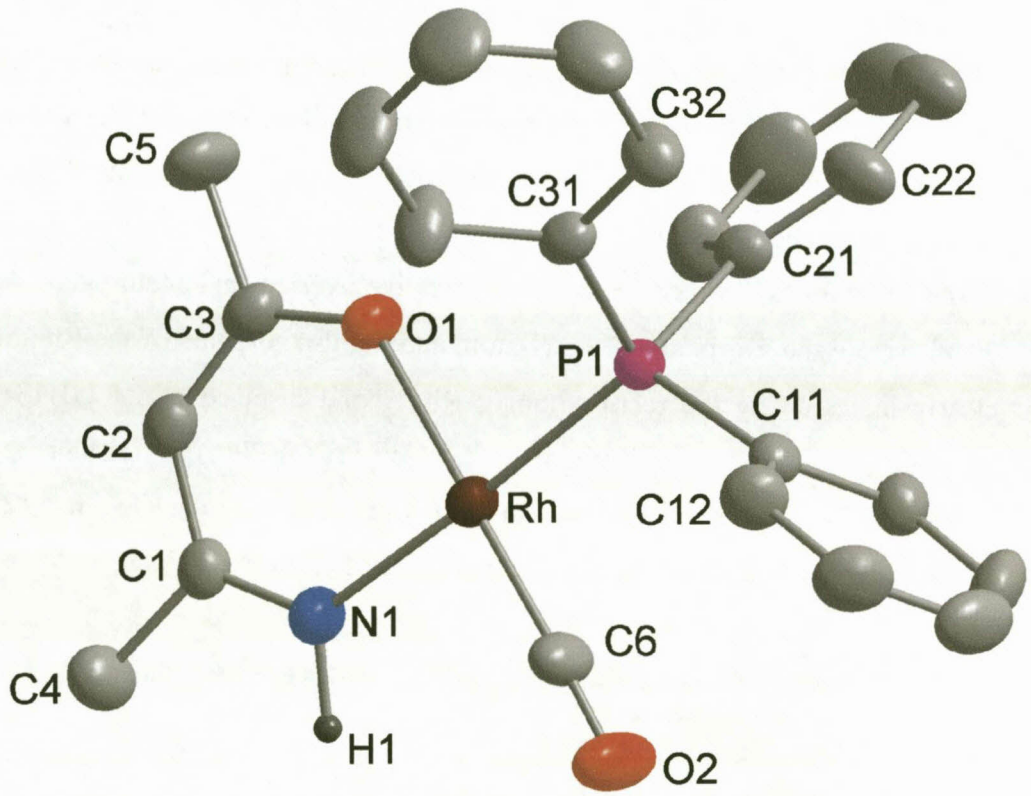

Fig. 5.2 Atom numbering scheme in [Rh(dmavk)(CO)(PPh_3)]. Thermal ellipsoids are at 30 % probability. Hydrogen atoms are omitted for clarity. Only the first two atoms of each phenyl ring are labeled. The first digit on the label indicate the ring number, and the second, the atom number within the ring.

The molecular structure and atom labeling of [Rh(dmavk)(CO)(PPh_3)] are shown in Fig. 5.2. Crystallographically it is difficult to distinguish between an oxygen and a nitrogen atom in a compound (small difference in electron density). However, by interchanging the identities of the N(1) and O(1) atoms, i.e., refining the N(1) atom as an oxygen, and

the O(1) atom as a N-atom, an R=2.45% was obtained, compared to an R=2.17% when the correct atom identities were used. This significant decrease in the R-value suggests that the assignment as in Fig. 5.2 was correct. More convincing evidence however is obtained from the fact that the H-atom of the amino nitrogen could indeed be placed from the Fourier map (See Fig. 5.2), unambiguously confirming the *trans*-N-Rh-P assignment.

Selected structural parameters are given in Table 5.2. The rhodium atom exhibits the typical distorted square planar geometry. The Rh-O and Rh-N bond distances are 2.044(3) and 2.045(4) Å, with the Rh-C and Rh-P bond distances 1.784(5) and 2.2751(13) Å respectively. All the *trans*-ligand-rhodium-ligand angles are nearly linear and correspond well to similar square planar complexes[14,15], while the P-C distances are normal. Since the ß-aminovinylketonato ligand forms a six-membered ring once chelated to the Rh atom, one would expect very effective overlap (bidentate ligand bite angle of 90°) between the π-orbitals of the N-atom and the dsp^2-orbitals of the Rh-atom. This is clearly indicated by the relative longer Rh-P bond distance of 2.2751(13) Å for this structure and 2.281(2) Å found in $[Rh(salnr)(CO)(PPh_3)]$[16] (Hsalnr = N-*o*-tolyl-salicyldiamine) compared to those found in five membered chelate rings (2.261(2) Å)[5] (formed by, i.e., 8-hydroxy quinolinata and 2-carboxylato N,O bidentate ligands).

Table 5.2 Selected interatomic bond distances(Å) and angles (°) for $[Rh(dmavk)(CO)(PPh_3)]$ with esd's in parentheses.

Rh-C(6)	1.784(5)	P(1)-C(11)	1.811(3)
Rh-N(1)	2.045(4)	P(1)-C(31)	1.836(5)
Rh-O(1)	2.044(3)	P(1)-C(21)	1.843(5)
Rh-P(1)	2.2751(13)	C(6)-O(2)	1.142(6)
C(6)-Rh-N(1)	92.6(2)	O(2)-C(6)-Rh	177.9(5)
C(6)-Rh-O(1)	179.3(2)	O(1)-Rh-P(1)	89.69(11)
N(1)-Rh-O(1)	87.43(15)	N(1)-Rh-P(1)	177.12(12)
C(6)-Rh-P(1)	90.3(2)		

This structure determination showed that, as expected, the *trans*-(N-Rh-PPh_3) complex was obtained in the solid state, also being the predominant isomer in solution. Further

correlations with the other structures in this study are discussed in Par. 5.7, while other comparisons with literature examples are given in Par. 5.8.

5.4 THE CRYSTAL STRUCTURE OF [Rh(dmavk)(CO)($AsPh_3$)]

5.4.1 Results and discussion

The complex crystallizes as square planar moieties in the space group $P\bar{1}$ with two molecules per unit cell. It is interesting to note that this $AsPh_3$-complex does not exhibit isomorphism to the PPh_3-complex discussed in Par. 5.3. Of further special interest is the fact that in this $AsPh_3$-complex the Rh-moieties form pairs (see Fig. 5.3) in the unit cell which are inter connected by quite strong Rh-Rh interactions of *ca* 4.0 Å; thus significant d_z^2 interactions. This effect favours the racemic crystallization mode, and further results in the pairs of two Rh-moieties being shielded from other interactions by the phenyl groups of the $AsPh_3$ ligands.

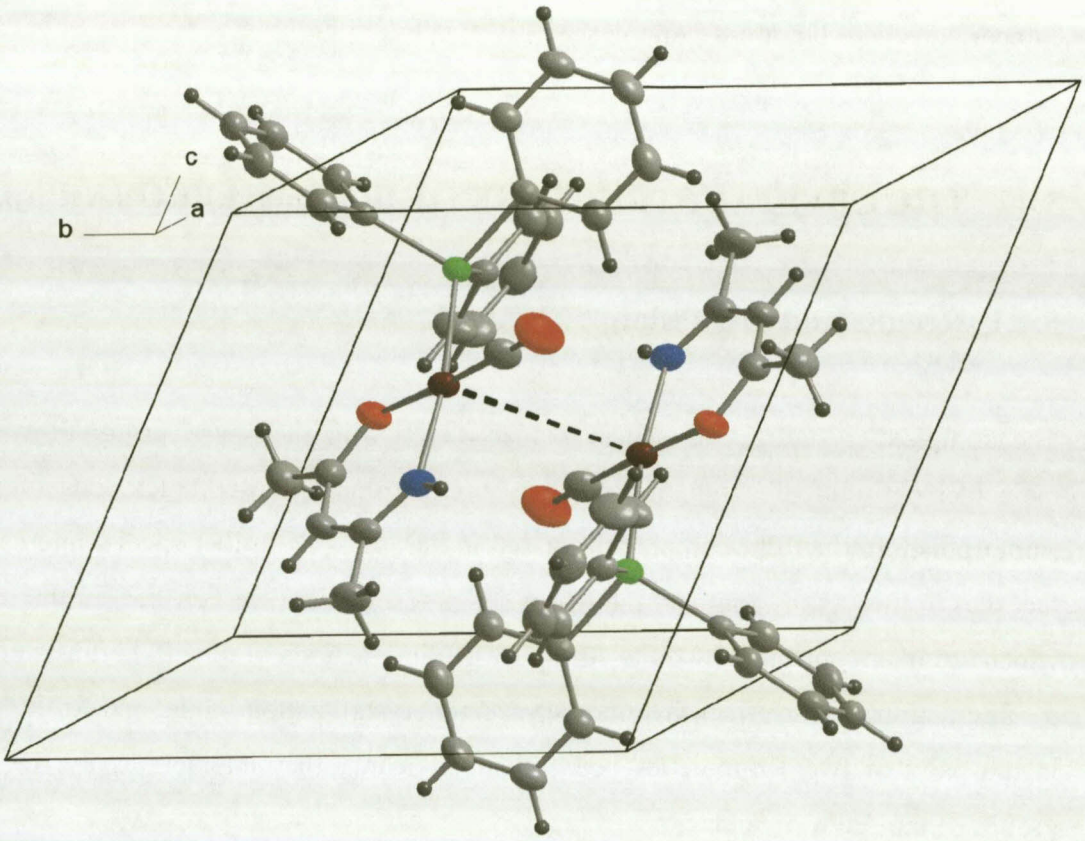

Fig. 5.3 Packing diagram of [Rh(dmavk)(CO)($AsPh_3$)]

The molecular structure and atom labeling of [Rh(dmavk)(CO)($AsPh_3$)] are shown in Fig. 5.4.

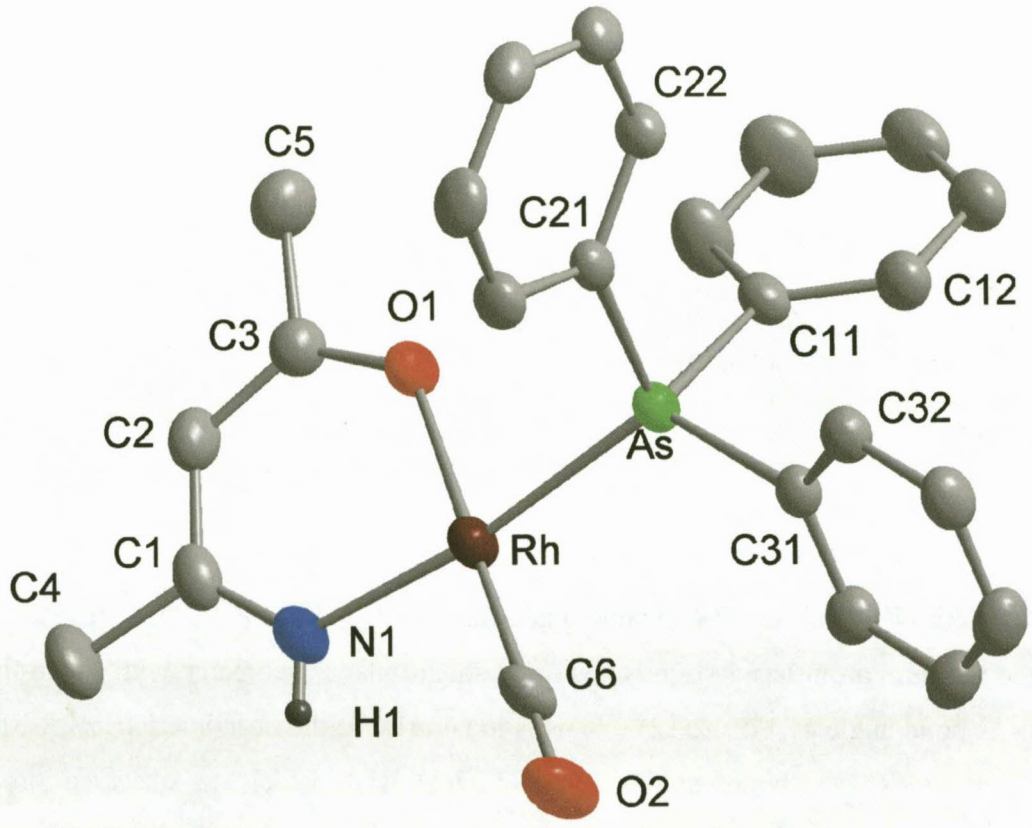

Fig. 5.4 Atom numbering scheme in [Rh(dmavk)(CO)($AsPh_3$)]. Thermal ellipsoids are at 30 % probability. Hydrogen atoms omitted for clarity. Only the first two atoms of each phenyl ring are labeled. The first digit on the label indicate the ring number, and the second the atom number within the ring.

The structure indicates that the most thermodynamic stable isomer obtained in the solid state, is the one in which the carbonyl *trans* to the nitrogen atom is displaced by $AsPh_3$ similar to the PPh_3 complex discussed in par 5.3. This is in agreement with the larger *trans*-influence of the N-atom compared to the oxygen atom of the bidentate moiety. This structure describes the first example of an $AsPh_3$ complex of Rh(I) containing a *trans*-N-Rh-As moiety[17]. Selected bond distances and angles for this complex are given in Table 5.3

Table 5.3 Selected interatomic bond distances(Å) and angles (°) for [Rh(dmavk)(CO)($AsPh_3$)] with esd's in parentheses.

Rh-C(6)	1.793(5)	C(6)-O(2)	1.151(5)
Rh-O(1)	2.026(3)	O(1)-C(3)	1.288(5)
Rh-N(1)	2.032(4)	N(1)-C(1)	1.300(6)
Rh-As	2.3834(6)	As-C(21)	1.944(4)
As-C(31)	1.944(4)	As-C(11)	1.954(4)
C(6)-Rh-O(1)	177.42(17)	O(2)-C(6)-Rh	178.3(4)
C(6)-Rh-N(1)	93.02(19)	C(3)-O(1)-Rh	127.3(3)
O(1)-Rh-N(1)	88.50(15)	C(1)-N(1)-Rh	127.4(4)
C(6)-Rh-As	93.11(14)	N(1)-C(1)-C(2)	123.8(4)
O(1)-Rh-As	85.20(8)	N(1)-C(1)-C(4)	119.3(5)
N(1)-Rh-As	172.12(12)		

The O(1)-Rh-N(1) and As-Rh-CO bond angles are 88.50(15) and 93.11(14)° respectively, and the rhodium atom has a slightly distorted square planar geometry with a non-linear N-Rh-As bond angle of 172.12(12)°. This is in contrast to the near linear *trans* S-Rh-As and *trans* O-Rh-As bond angles of 177.57(3) and 177.5(3)° observed in the [Rh(tfba)(CO)($AsPh_3$)][18] and [Rh(dbbtu)(CO)($AsPh_3$)][19] complexes respectively. The Rh-O and Rh-N bond distances are 2.026(3) and 2.032(4) Å, with the Rh-C and Rh-P bond distances 1.793(5) and 2.3834(6) Å respectively. The Rh-As bond length of 2.3834(6) Å is significantly longer than the corresponding bond length of 2.354(1) Å in [Rh(tfba)(CO)($AsPh_3$)] and significantly shorter than the Rh-As bond distance of 2.4089(7) Å in [Rh(dbbtu)(CO)($AsPh_3$)]. This can be nicely explained in terms of the *trans*-influence order of S > N > O for the donor atoms of the bidentate ligand, which is similar to that found for the corresponding PPh_3 complexes.

This structure determination showed that as expected, the *trans*-(N-Rh-$AsPh_3$) complex was obtained in the solid state. Further correlations with the other structures in this study, are discussed in Par. 5.7, while other comparisons with literature examples are given in Par. 5.8.

5.5 THE CRYSTAL STRUCTURE OF [Rh(dmavk)(I)(CH_3)(CO)-(PPh_3)].CH_3I

5.5.1 Results and discussion

The complex crystallizes with a distorted octahedral geometry in the triclinic space group $P\bar{1}$ as two independent Rh(III)-alkyl complexes per unit cell (see Fig. 5.5) and it is further interesting to note that additionally, an iodomethane molecule also crystallizes in the asymmetric unit. The Rh-Rh contacts are around 10 Å and no direct interactions are possible due to the octahedral geometry. The closest contacts between the iodide of the iodomethane molecule (I2) and the Rh complexes are typically of Van der Waals interactions *via* protons and carbon atoms of the phenyl rings, and range from 3.5-5.0 Å. Interestingly, the iodomethane occupies the 'cavity' between the three phenyl rings as illustrated by the contact distances between C11, C12 and C13 of 4.8, 4.3 and 5.0 Å respectively (see Fig. 5.5). This is further illustrated by the Rh-P-I2 'contact' angle of 164.6 °C.

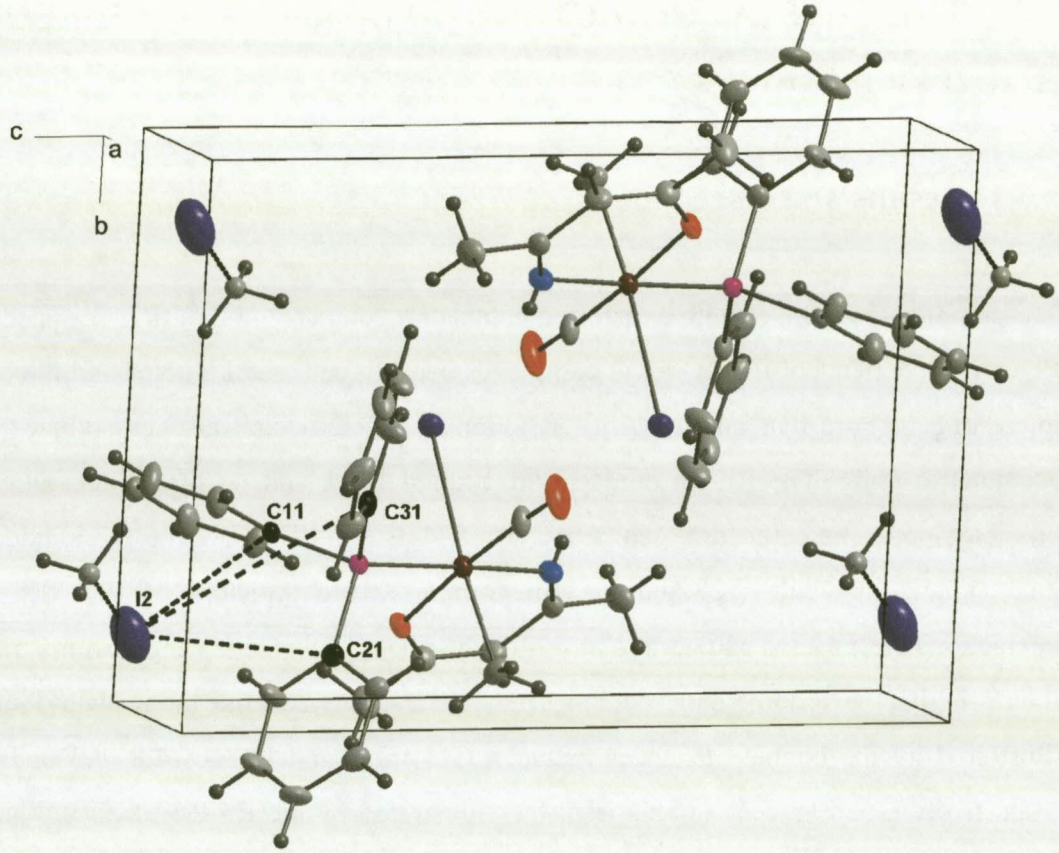

Fig. 5.5 Packing diagram of [Rh(dmavk)(I)(CH_3)(CO)(PPh_3)].CH_3I

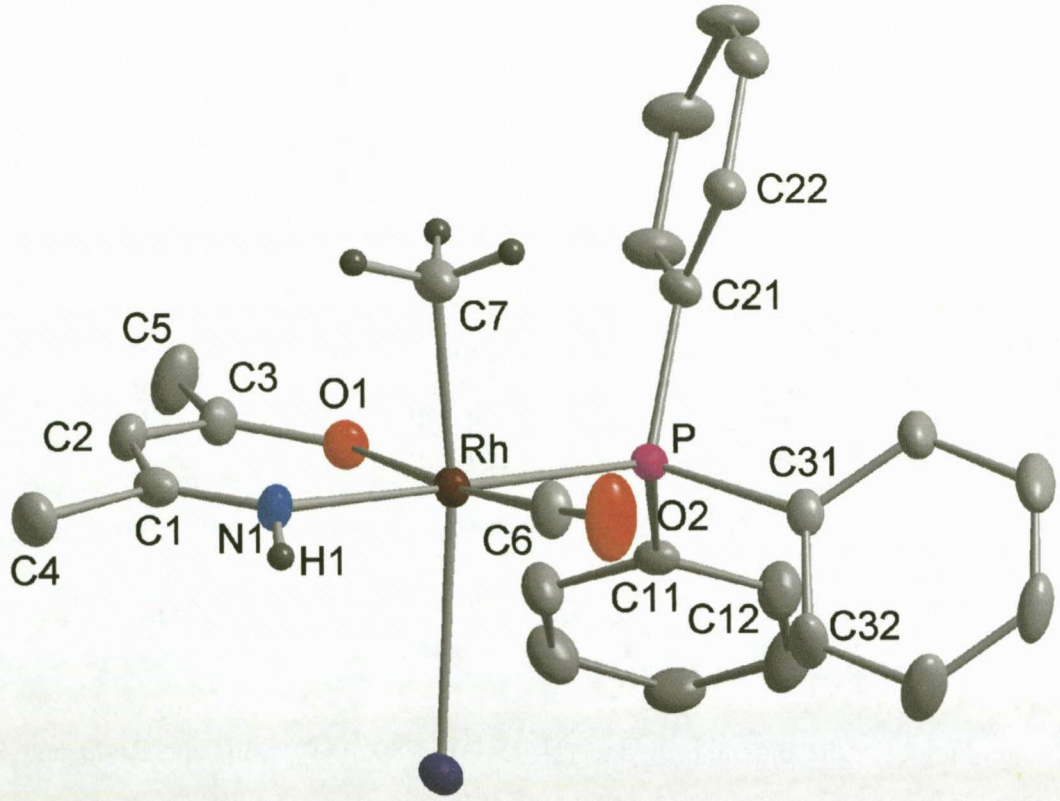

Fig. 5.6 Atom numbering scheme in [Rh(dmavk)(I)(CH_3)(CO)(PPh_3)].CH_3I. Thermal ellipsoids are at 30 % probability. Hydrogen atoms as well as the CH_3I adduct are omitted for clarity. Only the first two atoms of each phenyl ring are labeled. The first digit on the label indicate the ring number, and the second, the atom number within the ring.

The molecular structure and atom labeling of [Rh(dmavk)(I)(CH_3)(CO)(PPh_3)] are shown in Fig. 5.6. The coordination polyhedron corresponds to a distorted octahedron in which the equatorial positions are occupied by the bidentate N-O ligand and the carbonyl and phosphine *trans* to the oxygen and nitrogen respectively; thus the *trans*-N-Rh-P orientation has been retained during the oxidative addition process. The apical positions are occupied by the iodide ligand and methyl group and therefor *trans*-addition of the iodomethane ocurred. Selected bond distances and angles for the complex are given in Table 5.4.

Table 5.4 Interatomic bond distances (Å) and angles (°) for [Rh(dmavk)(I)(CH_3)(CO)(PPh_3)].CH_3I with esd's in parentheses.

Rh-C(6)	1.850(13)	Rh-P	2.356(3)
Rh-O(1)	2.035(7)	Rh-I(1)	2.8489(12)
Rh-N(1)	2.042(11)	C(6)-O(2)	1.116(15)
Rh-C(7)	2.069(12)		
C(6)-Rh-O(1)	175.0(5)	C(3)-O(1)-Rh	126.1(7)
C(6)-Rh-N(1)	91.6(5)	C(1)-N(1)-Rh	127.0(10)
O(1)-Rh-N(1)	89.5(4)	C(6)-Rh-P	91.6(4)
C(6)-Rh-C(7)	90.2(6)	O(1)-Rh-P	87.3(2)
O(1)-Rh-C(7)	85.0(5)	N(1)-Rh-P	176.8(4)
N(1)-Rh-C(7)	86.5(5)	O(2)-C(6)-Rh	177.0(14)
C(7)-Rh-P	93.5(4)	C(7)-Rh-I(1)	172.9(4)
C(6)-Rh-I(1)	90.8(4)	P-Rh-I(1)	93.49(7)
O(1)-Rh-I(1)	94.1(2)	N(1)-Rh-I(1)	86.5(4)

The bite angle of the bidentate ligand (N-Rh-O) is 89.5(4)°, while the Rh-O and Rh-N bond lengths are 2.035(7) and 2.042(11) Å respectively. The Rh-CO bond length of 1.850(13) Å compares well with that found in related complexes and is indicative of a fairly weak Rh-CO bond expected from Rh(III) (also manifested in the high υ_{CO} of 2070 cm^{-1}). The Rh-P bond distance of 2.356(3) Å is significantly longer than the corresponding bond in [Rh(quin)(I)(CH_3)(CO)(P(4-CH_3-C_6H_4)$_3$)][10] and [Rh(cupf)(I)(CH_3)(CO)(PPh_3)][7] (2.334(3) and 2.327(4) Å respectively); the latter two complexes having CH_3I oxidatively added in the *cis* mode. This can be explained in terms of the stronger *trans*-influence of the N atom of the bidentate ligand in [Rh(dmavk)(I)(CH_3)(CO)(PPh_3)] compared to iodide in [Rh)(quin)(I)(CH_3)(CO)(P(4-CH_3-C_6H_4)$_3$)] and [Rh(cupf)(I)(CH_3)(CO)(PPh_3)] respectively. Similarly, the longer Rh-I bond of 2.8489(12) Å compared to similar bonds in the above mentioned two complexes (2.701(2) and 2.708(2) Å respectively) can be explained in terms of the larger *trans*-influence of CH_3 compared to P.

The crystal structure determination clearly indicates a *trans*-addition of CH_3I to [Rh(dmavk)(CO)(PPh_3)], therefore an S_N2 two step mechanism could be suggested. However, although the crystal structure determination of [Rh)(ox)(I)(CH_3)(CO)(PPh_3)][6]

also indicates a *trans*-addition of CH_3I to [Rh(ox)(CO)(PPh_3)], it was proposed that this final product could have resulted *via* isomerization of an initial *cis*-addition. Further correlations between bond distances and NMR data are discussed in par. 5.7 and 5.8.

5.6 THE CRYSTAL STRUCTURE OF [Rh(dmavk)(I)($COCH_3$)-(PPh_3)][20]

5.6.1 Results and discussion

The complex crystallizes in the monoclinic space group $P2_1/c$ with four independent pairs of molecules per unit cell, thus resulting in a total of eight Rh(III)-acyl molecules, see Fig. 5.7. The structure thus consists of two independent, virtually identical, Rh(III) moieties in the asymmetric unit, denoted by molecules 1 and 3 respectively. A complicating factor in solving this structure stemmed from the fact that both these molecules crystallized in a *ca* 3:1 disordered/twinned mode with two components, denoted by molecules 2 and 4 respectively (not indicated in Fig. 5.7).

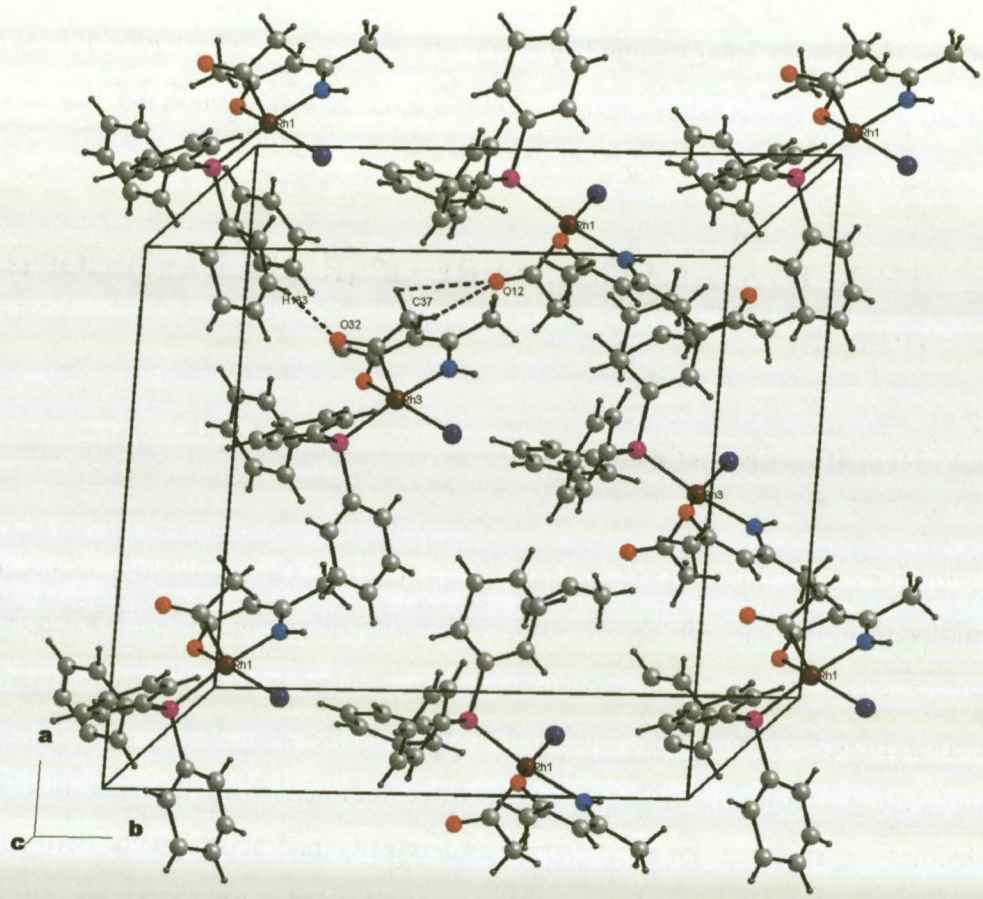

Fig. 5.7 Packing diagram of [Rh(dmavk)(I)($COCH_3$)(PPh_3)]

The disordered mode is illustrated in Fig. 5.8 for molecule 1 (and 2) clearly indicating the positions of the *ca.* 25 % disorder which have all been determined, in general, with an acceptable degree of accuracy (see also supplementary data in Par. 8.1). The reason for this crystallization mode is not clear. However, the structure could, in spite of these internal complicating factors, be solved with a fair degree of accuracy, unambiguously confirming the coordination geometry of the complex. The closest intermolecular interactions between molecules 1 and 3 are between the oxygen of the acyl (O32) and the proton of the phenyl group (H133), as well as the proton of the methyl of the acyl group (H37b) and the oxygen of the acyl (O12), and are around 2.5 and 3.1 Å respectively, while the Rh-Rh contacts are around 8 Å (see Fig. 5.7). The most important individual

structural parameters obtained for the four fragments are given in Table 5.5, showing all four moieties to be structurally equivalent. All the atoms, with the exception of the methine group of the dmavk ligand in molecule 4, and the methyl group of the acetyl in molecule 2, which were placed in calculated positions, were located from difference Fourier maps. The atoms of molecules 1 and 3, as well as the rhodium, iodine and phosphorous atoms in molecules 2 and 4, were refined anisotropically.

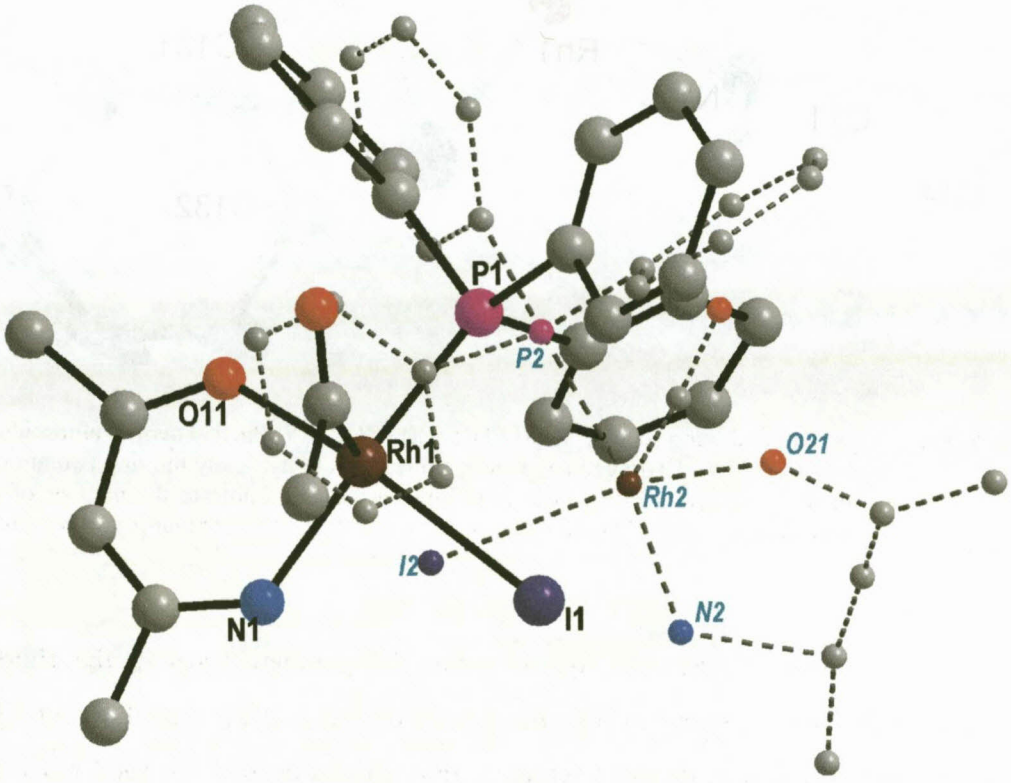

Fig. 5.8 Disordered structure of [Rh(dmavk)(I)($COCH_3$)(PPh_3)]

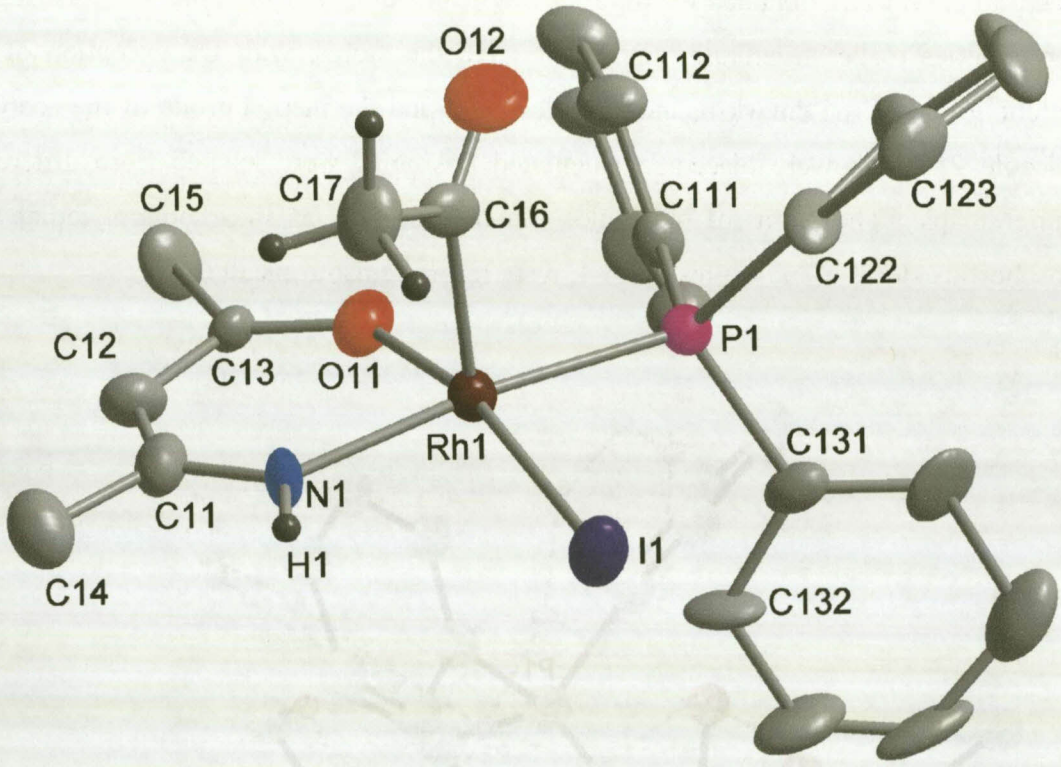

Fig. 5.9 Atom numbering scheme in [Rh(dmavk)(I)($COCH_3$)(PPh_3)]. Thermal ellipsoids are at 30 % probability. Hydrogen atoms are omitted for clarity. Only the first two atoms of each phenyl ring are labelled. The first digit on the label indicate the number of a specific molecule, the second the ring number, and the third, the atom number within the ring.

The structure shows a distorted square pyramidal geometry around the rhodium(III) center with the acetyl moiety in the apical position. It is clear that the *trans*-(N-Rh-P) coordination mode has again been retained, thus indicating that the total reaction (from Rh(I) *via* the Rh(III)-alkyl to the final Rh(III)-acyl complex, see Fig. 6.1) proceeds with retention of configuration with respect to the N,O-BID-ligand and the PPh_3. This is similar to other acyl complexes which were crystallographically characterized, e.g. [Rh(macsm)($COCH_3$)(NSO_2)(PPh_3)][21] and [Rh(mnt)(I)($COCH_3$)(PPh_3)][22]. Selected bond distances and angles are given in Table 5.5.

Table 5.5 Selected interatomic bond distances (Å) and angles (°) for [Rh(dmavk)(I)($COCH_3$)(PPh_3)] with esd's in parentheses.

Bond	Bond Distance(Å)			
	Molecule 1	Molecule 2	Molecule 3	Molecule 4
Rh-I	2.690(2)	2.665(4)	2.670(2)	2.703(4)
Rh-P	2.254(4)	2.250(12)	2.269(5)	2.290(13)
Rh-O(1)	2.054(10)	2.03(4)	2.014(10)	1.87(7)
Rh-N	2.021(9)	1.90(4)	2.014(10)	2.05(3)
Rh-C(6)	1.943(14)	1.91(6)	1.967(13)	1.62(7)
C(6)-O(2)	1.17(2)	1.18(8)	1.19(2)	1.12(7)
C(6)-C(7)	1.50(2)	*	1.41(2)	1.81(7)
Angle	**Bond Angles(°)**			
	Molecule 1	Molecule 2	Molecule 3	Molecule 4
I-Rh-P	91.822(11)	91.0(4)	91.78(11)	88.9(5)
I-Rh-O(1)	166.4(3)	163.2(9)	165.8(3)	163(2)
I-Rh-N	86.7(3)	82.6(12)	86.9(3)	87.5(10)
P-Rh-O(1)	92.5(3)	93.7(10)	94.2(3)	89.9(12)
P-Rh-N	172.7(3)	166.1(13)	172.6(3)	171.2(10)
O(1)-Rh-N	87.4(4)	89(2)	85.5(4)	91.2(14)
C(6)-Rh-P	92.2(4)	93(2)	93.6(5)	93(2)
C(6)-Rh-O(1)	92.0(4)	96(2)	93.2(5)	97(3)
C(6)-Rh-N	95.1(5)	99(2)	93.8(5)	96(3)
Rh-C(6)-O(2)	125.8(13)	112(5)	118.3(12)	134(6)
C(7)-C(6)-O(2)	120(2)	*	123(2)	89(5)
C(7)-C(6)-Rh	114.5(12)	*	118.9(3)	137(4)

* Not located

The respective Rh-I, Rh-P and Rh-$COCH_3$ bond lengths (2.695(2), 2.262(5), 1.955(14) Å; average of molecules 1 and 3, see Table 5.5) in [Rh(dmavk)(I)($COCH_3$)(PPh_3)] are significantly shorter than the corresponding bonds in [Rh(mnt)(I)($COCH_3$)(PPh_3)] (2.709 (1), 2.324(3), 2.006(14) Å) indicating an increase of Lewis acidity of the Rh(III) center for the dmavk ligand. This can be attributed to the difference in the electron-donating ability of the two coordinating atoms (O,N *vs.* S,S) of the bidentate ligands. The more significant distortion of Rh from the square planar plane in dmavk compared to that in the mnt system could be due to internal packing of the molecules (note that the O(1)-Rh-N bond angle differs significantly in the four molecules, see Table 5.6), but more in particular, also from the fact that the mnt ligand forms a 5-membered chelate. Further correlations with other complexes in this study and related systems are done in the following paragraphs.

5.7 CORRELATION OF STRUCTURAL DATA

This section deals with comparisons of structural parameters of the complexes obtained in this thesis. The two monocarbonyl Rh(I) complexes will be firstly discussed, followed by a correlation between the three PPh_3 complexes isolated for the complete oxidative addition/migratory insertion process. Table 5.6 summarizes important bond distances and angles for all four structures.

Table 5.6 Selected interatomic bond distances (Å) and angles(°) for [Rh(dmavk(CO)(PPh_3)], [Rh(dmavk(CO)($AsPh_3$)], [Rh(dmavk(I)(CH_3)(CO)(PPh_3)].CH_3I and [Rh(dmavk)(I)($COCH_3$)(PPh_3)] with esd's in parentheses.

Bond type and angle	Bond distance and angle for the different complexes			
	RAVP [a]	RAVAS [b]	RAVALK [c]	RAVACY [d]
Rh-O1	2.044(3)	2.026(3)	2.035(7)	2.034(10)
Rh-N1	2.045(4)	2.032(4)	2.042(11)	2.018(10)
Rh-P/As	2.2751(13)	2.3834(6)	2.356(3)	2.262(5)
Rh-CO	1.784(5)	1.793(5)	1.850(13)	1.955(14)
Rh-I	-	-	2.8489(12)	2.680(2)
N1-C1	1.302(6)	1.300(6)	1.27(2)	1.29(2)
C1-C2	1.396(7)	1.403(7)	1.43(2)	1.33(3)
C2-C3	1.388(8)	1.363(6)	1.37(2)	1.39(3)
C3-O1	1.282(6)	1.288(5)	1.287(14)	1.26(2)
C1-C4	1.518(8)	1.503(6)	1.52(2)	1.47(2)
C3-C5	1.512(8)	1.503(7)	1.45(2)	1.57(2)
C6-O2	1.142(6)	1.151(5)	1.116(15)	1.46(2)
O1-Rh-N1	87.43(15)	88.50(15)	89.5(4)	86.5(4)
O1-Rh-CO	179.3(2)	177.42(17)	175.0(5)	92.6(5)
O1-Rh-P/As	89.69(11)	85.20(8)	87.3(2)	93.4(3)
N1-Rh-P/As	177.12(12)	172.12(12)	176.8(4)	172.7(3)
N1-Rh-CO	92.6(2)	93.02(19)	91.6(5)	94.5(5)
I1-Rh-CH_3	-	-	172.9(4)	-
I1-Rh-P/As	-	-	93.49(7)	91.80(11)
Rh-C6-O2	177.9(5)	178.3(4)	177.0(14)	122.1(13)
Rh-O1-C3	127.9(3)	127.3(3)	126.1(7)	130.5(10)
O1-C3-C2	126.4(5)	125.8(4)	125.7(11)	122.2(15)
C3-C2-C1	125.0(4)	126.4(4)	126.7(11)	127.0(17)
C2-C1-N1	124.5(5)	123.8(4)	123.9(12)	126.0(11)
C1-N1-Rh	128.5(4)	127.4(4)	127.0(10)	127.0(10)

[a] RAVP = [Rh(dmavk)(CO)(PPh_3)] [b] RAVAS = [Rh(dmavk)(CO)($AsPh_3$)]
[c] RAVALK = [Rh(dmavk)(I)(CH_3)(CO)(PPh_3)].CH_3I [d] RAVACY = [Rh(dmavk)(I)($COCH_3$)(PPh_3)]
υ_{CO} [a] = 1960 cm^{-1}; υ_{CO} [b] = 1956 cm^{-1}; υ_{CO} [c] = 2070 cm^{-1}; υ_{CO} [d] = 1716 cm^{-1} [υ_{CO}-values were determined in KBr]

5.7.1 Comparison of structural data of Rh(I)-complexes: [Rh(dmavk)(CO)(PPh_3)] *vs.* [Rh(dmavk)(CO)($AsPh_3$)]

Both molecules crystallized with the carbonyl substituted by PPh_3 and $AsPh_3$ *trans* to the N-atom of the bidentate ligand, corresponding to the *trans*-influence order of N > O. The Rh-As bond length of 2.3834(6) Å is significantly longer than the Rh-P bond length of 2.2751(13) Å. This can be attributed to the larger covalent radius of arsenic compared to that of phosphorous (1.210 *vs.* 1.100)[23]. The same increase in metal-arsenic bond length compared to metal-phosphorous was observed in [Rh(tfba)(CO)($AsPh_3$)][18] and [Rh(acac)(CO)(PPh_3)][24] of 2.354(1) and 2.244(2) Å; and [Rh(dbbtu)(CO)(PPh_3] and [Rh(dbbtu)(CO)($AsPh_3$][19] of 2.2896(12) and 2.4089(7)Å respectively. Similar results were obtained in [PtCl(CH_3)L_2][25,26] and [Co(Me_3Sn)$(CO)_3$L] (L = PPh_3 and $AsPh_3$).

The bond distances and angles of the bidentate ligand are similar in both structures, with the exception of the O(1)-Rh-N(1) angle which is significantly larger for [Rh(dmavk)(CO)($AsPh_3$)] compared to [Rh(dmavk)(CO)(PPh_3)] (88.50(15) *vs.* 87.43(15)° respectively). This indicates less steric demand by $AsPh_3$ compared to PPh_3 on the ancillary ligands due to the longer Rh-$AsPh_3$ than Rh-PPh_3 bond as discussed previously. The less steric demand of $AsPh_3$ compared to PPh_3 exercised on the ancillary ligands, especially on the O-atom (*cis* relative to the XPh_3 ligand (X = P or As) of the bidentate ligand is further demonstrated by the following bond angles within the coordination polyhedron: O1-Rh-CO [179.3(2); 177.42(17)°], N1-Rh-P/As [177.12(12);172.12(12)°] and O1-Rh-P/As [89.69(11); 85.20(8)°] for the [Rh(dmavk)(CO)(PPh_3)] and [Rh(dmavk)(CO)($AsPh_3$)] complex respectively. Based on these angles, the larger steric demand of PPh_3 compared to $AsPh_3$ thus have an interesting relative effect on the coordination polyhedron for the two complexes. Firstly, the more prominent interaction between the avk O-atom and the PPh_3 (compared to that between the avk O-atom and the $AsPh_3$) results in a decrease in the avk bite angle for the PPh_3 complex (see above). Next, this interaction leads to a larger O-Rh-PPh_3 angle (compared to the O-Rh-$AsPh_3$). The relative differences in the O(1)-Rh-CO and N(1)-Rh-P/As angles cannot be explained but are assumed to be due to packing effects. The Rh-CO

bond distance as well as the bond distance for the CO moieties for both structures are comparable within experimental error. This is further also reflected by the similar υ_{CO} of 1960 and 1956 cm^{-1} observed for the phosphine and arsine complexes respectively (see Chapter 4). These results indicate similar Lewis basicity of PPh_3 and $AsPh_3$ since a stronger Rh-CO bond and hence weaker C-O bond would be expected for an increase in electron density on the rhodium center due to more effective π-back bonding from the metal to the π*-orbitals of the CO moiety. Similar results were for example also found for the *trans*-[RhCl(CO){As(*p*-$C_6H_4CH_3)_3$}$_2$] and *trans*-[RhCl(CO){P(*p*-$C_6H_4CH_3)_3$}$_2$][27] Vaska type complexes.

An important result from this crystallographic study is the fact that it is clearly shown that there is considerable more space available for an entering moiety (such as CH_3I) in the As complex, whereas the electron densities (as obtained from the υ_{CO}-values) are quite similar. This should have an effect on both the stability of the alkyl intermediate, as well as the reactivity of the two complexes towards oxidative addition. These aspects will further be addressed in Chapter 6.

5.7.2 Comparison of structural data of Rh(I)/(III)-complexes: [Rh(dmavk)(CO)(PPh_3)] *vs.* [Rh(dmavk)(I)(CO)(CH_3)-(PPh_3)].CH_3I *vs.* [Rh(dmavk)(I)($COCH_3$)(PPh_3)]

As mentioned above, this study describes the first system wherein the crystallographic characterization of the Rh(I) monocarbonyl, Rh(III) alkyl and Rh(III) acyl for the same starting complex was successfully done. These structures provided further evidence that the oxidative addition by iodomethane to [Rh(L,L'-BID)(CO)(PR_3)] complexes with more nucleophilic donor atoms (e.g. sulfur)[11] proceeds *via* an alkyl intermediate to form an acyliodo complex. This study also clearly indicated the retention of configuration of the phosphine *trans* to nitrogen of the N,O-BID ligand during the complete reaction. The significant lengthening in Rh-P bond distance from the Rh(I)- [2.2751(13) Å] to the

Rh(III)-alkyl [2.356(3) Å] (Table 5.6) complex can be explained in terms of electronic properties, e.g. in spite of an increase of the formal oxidation state on the metal the strong δ-donation by the CH_3^- and I^- will result in a weaker metal-phosphorous interaction, hence a weaker bond. The significant shortening in Rh-P bond again to the Rh(III)-acyl complex [2.262(5) Å] suggests that as soon as the electron rich Rh(III)-center in the alkyl complex rearranges (*via* the migratory CO-insertion process) the PPh_3 ligand again behaves as a stronger electron donor, thus a shorter Rh-P bond.

The bond distances within the bidentate ligand are comparable for all three complexes with the exception of the C(3)-C(5) bond which is significantly longer for the Rh(III)-acyl complex compared to the Rh(I)-monocarbonyl and Rh(III)-alkyl complexes, indicating distortion of the square pyramid around the rhodium center for the acyl complex. The distortion of the square pyramid in Rh(III)-acyl is evident if the distortion from the theoretical value of 90° (expected for bond angles O(1)-Rh-N(1) and O(1)-Rh-P) is considered (Table 5.6), or by observing the deviation of the N-Rh-P and O(1)-Rh-I (also see Table 5.5) bond angles from the theoretical value of 180°.

The C-O bond distance of the carbonyl group in all three structures correspond to the expected υ_{CO}, i.e. in the Rh(I) complex there is more effective back donation from the metal to the sp hybridized C atom of CO, leading to a stronger Rh-CO bond and thus weaker C-O bond. For the Rh(III) alkyl complexes, the less electron density available on the Rh center, limits back donation from the metal to the π*-orbital of the CO, resulting in a weaker Rh-CO bond and thus stronger C-O bond. The weak C-O bond in the acyl complex can be explained in terms of the sp^2 hybridization of C of the carbonyl, thus more double bond character is observed in the C-O moiety.

5.8 CORRELATION OF STRUCTURAL (Rh-P BOND DISTANCES) AND NMR DATA (^{1}J(PRh), ^{1}J(CRh) AND $\delta(^{31}P)$) IN SELECTED Rh(I) AND Rh(III) COMPLEXES

Mather *et al.*[28] have shown that there exists an inverse proportionality between the coupling constant $^1J(^{195}Pt\text{-}^{31}P)$ and the Pt-P bond length in complexes of the type $[PtX_{4-n}(R_3P)_n]^{(n-2)+}$, with X = Br^- or Cl^- and R = Bu or Et. It was observed that the weaker the Pt-P bond, the smaller the coupling constant (^{1}J(PPt)) becomes. This was also done for Rh-complexes by Roodt *et al.*[29]. It was also shown from this and other related work that the principal contribution of the Fermi contact term results from the contribution in s-orbital overlap, i.e. between the 3s P and the 5s Rh orbitals.

The Rh-P bond distances for a range of [Rh(L,L'-BID)(CO)(PPh_3)] complexes, (L,L'-BID = O,O-BID', O,S-BID and N,S-BID) together with the ^{31}P NMR data, are chronologically summarized in Table 5.7, while the graphic correlation is illustrated in Fig. 5.10. The data in Table 5.7 allow more detailed evaluation of the increase in σ-donating ability (larger structural *trans*-effect or *trans*-influence) of the L atom *trans* to the Rh-P bond (causing elongation of the Rh-P bond) and the corresponding decrease in the ^{1}J(PRh) value, as a result of variations in overlap between the 5s(Rh)-3s(P) orbitals. This trend generally holds as further visualized in Fig. 5.10(a) wherein a plot of ^{1}J(PRh) *vs.* Rh-P bond distance is shown[30]. The results obtained in this study are clearly in agreement with the general tendency. It was previously illustrated that the Rh-P bond distance in a [Rh(L,L'-BID)(CO)(PR_3)] complex depends on not only the nature (i.e., O, N or S) of the donor atom in the bidentate ligand, but also on the bite angle of the chelate ring[1]. Separate presentations of six- or five-membered chelates were done and showed better individual linear relationships[30]. However, the general trend is clear, and also holds reasonably well for other complexes, i.e., Rh(III), of which a few examples are included in Table 5.7 and Fig 5.10.

The deviation of the data point plotted for the [Rh(cacsm)(CO)(PPh_3)] (entry 9, Table 5.7) was explained in terms of a large solvent interaction. The ^1J(PRh) value of 144.6 Hz is comparable to the 144.5 Hz for Sacac wherein the Rh-P distance is very long, i.e., 2.300(2) Å. Thus, it seems that the Rh-P bond in the [Rh(cacsm)(CO)(PPh_3)] complex is substantially lengthened in solution by solvent interaction.

Table 5.7 Rh-P bond distances and NMR parameters of [Rh(L,L'-BID)(CO)(PPh_3)] complexes, with L,L'-BID = asymmetric bidentate ligand unless otherwise indicated.

No	L,L'-BID[a]	Ref	L[b]	L'	Ring size	Rh-P distance (Å)	$\delta(^{31}P)$ (ppm)	^1J(PRh) (Hz)
1	tfaa	1,30	O	O	6	2.231(3)	47.73	176.9
2	trop[c]	1,30	O	O	5	2.232(2)	48.66	176.2
3	cupf	1,30	O	O	5	2.232(2)	48.85	171.1
4	acac[c]	1,30	O	O	6	2.244(4)	48.84	175.7
5	tta	1,30	O	O	6	2.245(2)	47.86	177.8
6	dmavk	3,20	N	O	6[d]	2.260(4)	41.25	152.2
7	ox	1,30	N	O	5	2.261(2)	41.40	161.6
8	pic	1,30	N	O	5	2.262(2)	40.24	161.9
9	cacsm	11	S	N	6	2.268(1)	45.20	144.6
10	dmavk	3,13	N	O	6	2.275(1)	41.47	148.0
11	pbtu	19	S	O	6	2.275(2)	36.02	148.1
12	hpt	31	S	O	5	2.278(1)	37.77	157.1
13	hacsm	30,32	S	N	6	2.283(1)	42.70	148.9
14	anmeth	33	S	O	5	2.290(1)	37.04	156.2
15	Sacac	15	S	O	6	2.300(2)	35.36	144.5
16	pbtu	19	P	P	[e]	2.329(2)	33.44	137.2
17	Vaska	27	P	P	[f]	2.331(1)	27.20	118.0
18	dmavk	34	N	O	6[g]	2.356(3)	21.35	107.1
19	acac	35,36	P	P	[h]	2.385(3)	20.01	106.1

[a] L,L'-BID ligands: tfaaH= trifluoroacetylacetone; tropH=tropolone; cupfH=cupferron; acacH=acetylacetone; dmavkH=dimethylaminovinylketone; ttaH=thionyltrifluoroacetylacetone; oxH=8-hydroxyquinoline; picH=picolinic acid; $pbtuH_2$=N-benzoyl-N'-phenylthiourea; hptH=hydoxypyridinethione; anmethH= *p*-hydroxy-N-methylbenzothiohydroxamic acid; SacacH=thioacetylacetone; [b] P atom *trans* to atom L. [c] Symmetric O,O-BID ligand [d] acyl species [e] Vaska type fragment [f] Vaska analogue [g] alkyl species [h] bis PPh_3 Rh(III) complex.

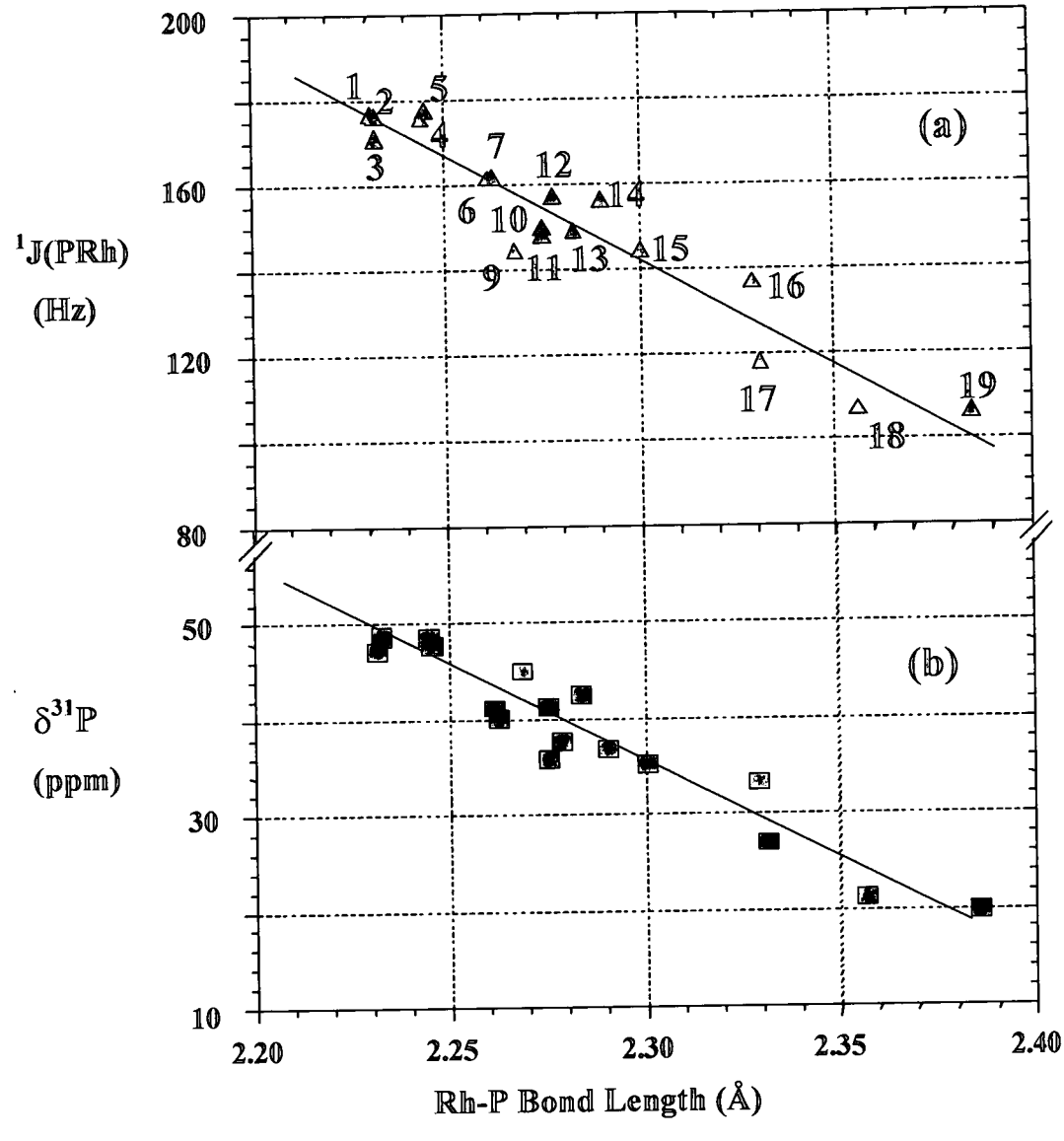

Fig. 5.10: Correlation between Rh-P bond distances and (a) ^{1}J(PRh); (b) $\delta(^{31}P)$; $CDCl_3$, (Data in Table 5.7).

The ^{1}J(CRh) values for the [Rh(L,L'-BID)(CO)(PR_3)] complexes show, as does the ^{1}J(PRh) data, good agreement with the Rh-C bonds. This is illustrated considering an average for Rh-CO bonds of 1.796(8) Å (^{1}J(CRh)= 63.8 Hz) for complexes in which the CO ligand is *trans* to an oxygen atom, compared to the longer Rh-CO bond distance of 1.823(4) Å (hacsm; *trans*-(N-Rh-CO), ^{1}J(CRh) =74.8 Hz). However, since the range of coupling constants is much smaller and less spread out than those of the ^{1}J(PRh), coupled

with the fact that the Rh-CO bond data are less accurate than those of the Rh-P bonds, the correlation is not as convincing as in the case of the ^{31}P.

A similar correlation as discussed above exists between the $\delta(^{31}P)$ *vs.* Rh-P bond distances, see Fig. 5.10(b). Since the chemical shift is dependent on many factors it is thus expected that this parameter will not necessarily, for the range of complexes studied, vary in parallel with the Rh-P bond distance (specifically in PPh_3 complexes). It is therefore remarkable that such a good correlation is obtained, which suggests that the electron density on the P-atom as manifested in the $\delta(^{31}P)$ value does indeed vary reasonably in conjunction with the Rh-P bond strength, and to a large extent thus with the σ-donating ability of the phosphine ligand. Further research to address the effect of different phosphine ligands in these systems in terms of basicity and steric demand, correlated with theoretical calculations and reactivity studies, is obviously required to explain this in more detail.

In summary it can be stated that good correlations in terms of the solid state and solution properties of these complexes were obtained. The complexes were unambiguously characterized and the results obtained are further utilized in Chapter 6 to explain some aspects of the solution behaviour of this system.

REFERENCES

1. Graham, D.E., Lamprecht, G.J., Potgieter, I.M., Roodt, A., and Leipoldt, J.G. 1991, *Transition Met. Chem.*, **16**, 193.
2. Purcell, W., Basson, S.S., Leipoldt, J.G., Roodt, A., and Preston, H. 1995, *Inorg. Chim. Acta*, **234**, 153.
3. Galding, M.R., Cherkasova, T.G., Osetrova, L.V., and Varshavsky, Y.S. 1993, *Rhodium Ex.*, **1**, 14.
4. Poletaeva, I.A., Cherkasova, T.G., Osetrova, L.V., Varshavsky, Y.S., Roodt, A., and Leipoldt, J.G. 1994, *Rhodium Ex.*, **3**, 21.
5. Leipoldt, J.G., Basson, S.S., and Dennis, C.R. 1981, *Inorg. Chim. Acta*, **50**, 121.
6. Van Aswegen, K.G., Leipoldt, J.G., Potgieter, I.M., Lamprecht, J.G., Roodt, A., and Van Zyl, G.J. 1991, *Transition Met. Chem.*, **16**, 369.
7. Basson, S.S., Leipoldt, J.G., Roodt, A., and Venter, J.A. 1987, *Inorg. Chim. Acta,* **128**, 31.
8. Leipoldt, J.G., Basson, S.S., and Botha, L.J. 1990, *Inorg. Chim. Acta*, **168**, 215.
9. Venter, J.A., Leipoldt, J.G., and Van Eldik, R. 1991, *Inorg. Chem.*, **30**, 2207.
10. Cano, M., Herus, J.V., Lobo, M.A., and Pinilla, E. 1992, *Polyhedron*, **11**, 2679.
11. Steyn, G.J.J., Ph.D.-Thesis 1994, Free State University, Bloemfontein, South Africa.
12. Sheldrick, G.M. 1997, SHELXL97, *Program for the refinement of Crystal Structures*, University of Göttingen, Germany.
13. Damoense, L.J., Purcell, W, Roodt, A., and Leipoldt, J.G. 1994, *Rhodium Ex.*, **5**, 10.
14. Leipoldt, J.G., Basson, S.S., and Potgieter, I.M. 1980, *Inorg. Chim. Acta*, **117**, L3.
15. Botha, L.J., Basson, S.S., and Leipoldt, J.G. 1987, *Inorg. Chim. Acta*, **126**, L5.
16. Leipoldt, J.G., Basson, S.S., and Grobler, E.C., Roodt, A. 1985, *Inorg. Chim. Acta*, **99**, 13.
17. Cambridge Crystallographic Data base.
18. Ebenebe, P., Basson, S.S., and Purcell, W. 1996, *Rhodium Ex.*, **16**, 11.
19. Kemp, G., Roodt, A., Purcell, W., and Koch, K.R. 1996, Rhodium Ex., **16**, 17.

20. Damoense, L.J., Purcell, W., and Roodt, A. 1995, *Rhodium Ex.*, **14**, 4.

21. Steyn, G.J.J., Roodt, A., and Leipoldt, J.G. 1993. *Rhodium Ex.*, **0**, 11.

22. Cheng, C.-H, and Eisenberg, R.J. 1977, *J. Am. Chem. Soc.*, **99**, 3003.

23. Diamond Visual Structural information system, Version 2.1.

24. Leipoldt, J.G., Basson, S.S., Bok, L.D.C., and Gerber, T.I.A. 1978, *Inorg. Chim. Acta*, **26**, L35.

25. Bardi, R., and Piazzesi, A.M. 1981, *Inorg. Chim. Acta*, 47, 249.

26. Roodt, A., Otto, S., and Leipoldt, J.G. 1995, *Acta Cryst.*, **C51**, 1105.

27. Mzamane, S.N., Otto, S., and Roodt, A. 1999, *Acta Cryst.*, **C55**, 67.

28. Mather, G.G., Pidcock, A., Rapsey, J.N. 1973, *J. Chem. Soc., Dalton Trans.*, 2095.

29. Roodt, A., Steyn, G.J.J. 2000, Recent Research Developments in Inorganic Chemistry, Transworld Research Network, **2**, 1-23.

30. Steyn, G.J.J., Roodt, A., Poletaeva, I., and Varshavsky, Y.S1997. , *J. Organomet. Chem.*, **536/7**, 797.

31. Basson, S.S., Leipoldt, J.G., Roodt, A., and Preston, H. 1991, *Acta Cryst.*, **C47**, 1961.

32. Steyn, G.J.J., Roodt, and Leipoldt, J.G. 1993, *Rhodium Ex.*, **1**, 25.

33. Preston, H., 1993, Ph.D.-Thesis, Free State University, Bloemfontein, South Africa.

34. Damoense, L.J., Roodt, A., and Purcell, W., (To be published).

35. Shestakova, E.P., Cherkasova, T.G., Osetrova, L.V., Varshavsky. Y.S., Leipoldt, J.G., and Roodt, A. 1994, *Rhodium Express*, **7-8**, 24.

36. Roodt, A., Botha, J.M., Otto, S., Shestakova, A.P., and Varshavsky, Y.S. 1996, Rhodium Express, **17**, 4.

CHAPTER 6

Kinetics of iodomethane oxidative addition to [Rh(aminovinylketonato)(CO)(PR_3)] complexes

6.1 INTRODUCTION

Oxidative addition of iodomethane to various complexes of the type [Rh(L,L'-BID)(CO)(PR_3)] (L,L'-BID = mono anionic bidentate ligand; PR_3 = tertiary phosphine) has been well studied in this laboratory[1,2,3,4,5,6,7,8,9] utilizing techniques such as X-ray crystallography, IR, UV/VIS and ^{1}H- and ^{31}P-NMR. In the course of these studies products were isolated that showed that both *cis*- and *trans*-addition of the iodomethane may occur on the Rh center, forming the corresponding *cis* (as in the case of [Rh(cupf)(I)(CO)(CH_3)(PPh_3)])[3] or *trans* ([Rh(ox)(I)(CO)(CH_3)(PPh_3)])[10] alkyl species (L,L' = O,O and N,O respectively). Acyl complexes (e.g. [Rh(Sacac)(I)($COCH_3$)(PPh_3)][4], [Rh(macsm)(NSO_2)($COCH_3$)(PPh_3)][11] and [Rh(stsc)(I)($COCH_3$)(PCy_3)][12] were isolated in the solid state as products when the bidentate ligand contained a sulfur atom. In general, a reaction scheme as illustrated in Fig. 6.1 was presented for the overall reaction. In some cases, the solvent pathway was found to be absent, e.g. for the reaction between [Rh(Sacac)(CO)(PPh_3)][4] and iodomethane, whereas for the similar reaction for [Rh(cupf)(CO)(PPh_3)][2], substantial solvent interaction was observed. All the reaction steps (excluding solvent pathway) were monitored for the N,S-BID ligand systems, confirming the mechanism to consist of a rapid first oxidative addition equilibrium step followed by the slower acyl formation.

However, uncertainties concerning the reaction scheme for oxidative addition- and CO-insertion reactions for [Rh(acac)(CO)(PR_3)] and its analogues still exist, since no Rh(III)-acyl species have been isolated and specifically crystallographically characterized.

Furthermore, as mentioned earlier, although complexes containing sulfur as donor atom, e.g. in [Rh(Sacac)(I)($COCH_3$)(PPh_3)] and [Rh(macsm)(NSO_2)($COCH_3$)(PPh_3)], have been crystallographically characterized, the mode of addition (*trans* or *cis*) of iodomethane during the oxidative addition step is still not known. This is mainly due to the difficulty to isolate and characterize the Rh(III)-akyl intermediate in these systems.

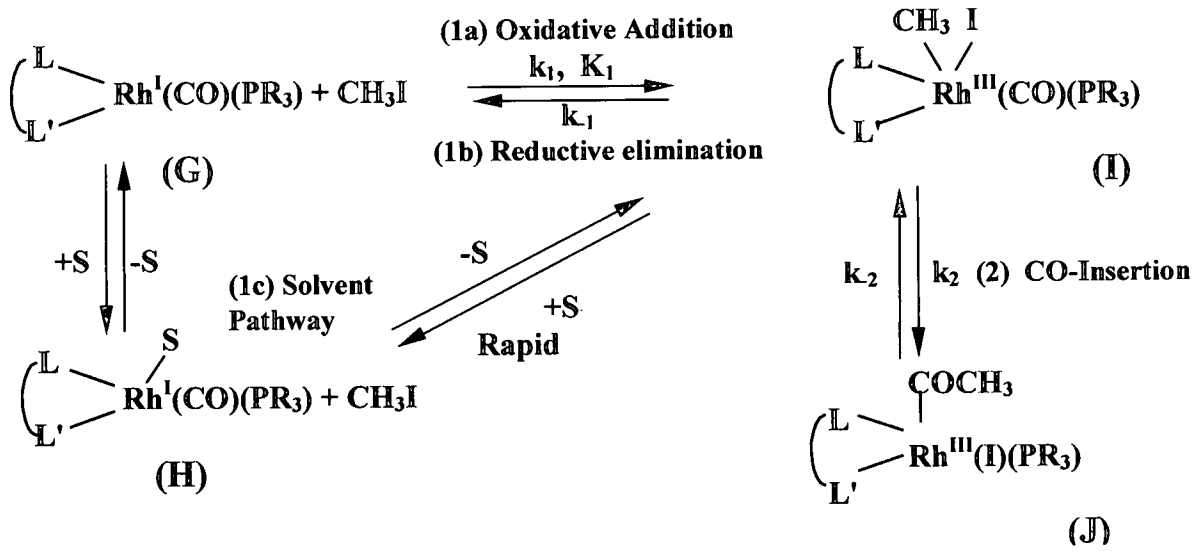

Fig. 6.1 Reaction scheme: Iodomethane Oxidative Addition to [Rh(L,L'-BID)(CO)(PR_3)] complexes (S denotes Solvent).

As a further extension of the research done in our group, the unsymmetrical aminovinylketonato ligand with donor atoms N,O was introduced in this study. The avk ligand is similar to the acac ligand, having the advantage of allowing more effective electronic and steric manipulation close to the metal center by introducing different groups on the N-atom. Also, from our knowledge of the *trans*-influence of donor atoms in these systems, it is expected that the N-atom should donate more electron density to the Rh center compared to the O-atom (*trans*-influence order of S>N>O also indicates electron donating ability in same order), favouring the formation of the acyl species as detected for O,S donor systems. Furthermore, the relative isomeric distribution of the

two isomers in unsymmetrical acac analogues make the study of the oxidative addition difficult since two reactants of comparable concentrations exist in solution. In the case of the avk systems this is virtually eliminated (see Chapters 4 and 5 and below).

Previous investigations on the relative *trans*-influence of nitrogen and oxygen as the donor atoms in the β-aminovinylketonato (avk-) ligand in complexes of the type $[Rh(avk)(CO)(PPh_3)]$[13], utilizing ^{13}C and ^{31}P-NMR, indicated that the reaction of $[Rh(avk)(CO)_2]$ with PPh_3 resulted in the formation of two isomers in a 10:1 ratio, see Fig. 6.2; the ratio indicating towards the larger *trans*-effect, (a kinetic phenomenon) possibly by the larger *trans*-influence of nitrogen in the ground state, see Fig. 6.2. Thus only one reactant is basically ensured.

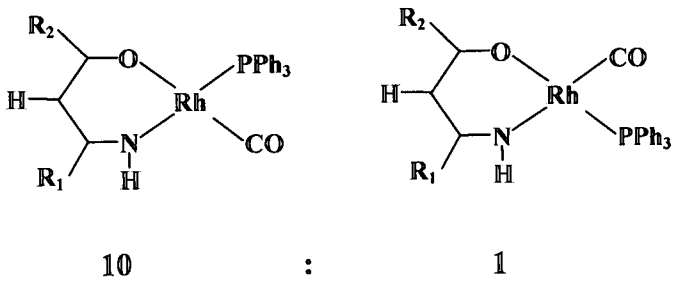

	R_1	R_2
(a)	CH_3	CH_3 (dmavk)
(b)	Ph	Ph
(c)	CF_3	CF_3
(d)	CH_3	CF_3 (tavk)
(e)	CF_3	$C(CH_3)_3$

Fig. 6.2 Isomeric distribution for $[Rh(avk)(CO)(PPh_3)]$ type complexes.

The crystal structure of $[Rh(dmavk)(CO)(PPh_3)]$ ($R_1 = R_2 = CH_3$; Par. 5.3) furthermore confirmed that the principal isomer isolated in the solid state is in agreement with the NMR results, i.e. the *trans*-(N-Rh-PPh_3) orientation was obtained.

We will thus assume that throughout this study, the kinetics of oxidative addition with CH_3I involves mainly the major isomer, i.e. the *trans*-(N-Rh-PPh_3) complex.

The electron density on the metal center was manipulated by the introduction of two different types of avk ligands, where in the first case, $R_1 = R_2 = CH_3$ (dmavk, see Fig.

6.2). Secondly, by substituting R_2 with the electron withdrawing group CF_3, the tavk ligand (see, Fig. 6.2) was obtained. Further electronic manipulations involve different phosphines with different Lewis basicities (PR_3 with R = *p*-Cl-Ph, Ph and *p*-MeO-Ph), while steric effects were addressed by the introduction of $AsPh_3$.

6.2 EXPERIMENTAL

Unless otherwise stated, all reagents and solvents were of analytical grade. The Rh(I) starting complexes were prepared, purified and characterized according to procedures outlined in Section 4.2. For the reaction of [Rh(dmavk)(CO)(PPh_3)] with iodomethane, the rates of formation and disappearance of the different species were selectively monitored on a Hitachi 270-50 infrared spectrophotometer (equipped with a thermostated cell holder, ±0.2 °C) in chloroform as solvent, since chloroform does not exhibit significant absorbency in the 1700-2300 cm^{-1} range. All reactions were monitored under pseudo-first-order conditions, with $[Rh]_{tot} = 7x10^{-3}$ M. Two distinct reaction steps as shown in Fig. 6.3 were observed, i.e. the formation of Rh(III)-alkyl and subsequent formation of the Rh(III)-acyl species.

The two reaction steps as illustrated in Fig.'s 6.1 and 6.3 could also be monitored by UV/visible measurements; the more rapid first reaction was monitored on a Durrum D-110 stopped-flow spectrophotometer while in the case of the slower reactions, the reaction progress was followed on a GBC-916 spectrophotometer. All reactions were monitored under pseudo-first-order conditions, with $[Rh]_{tot} = 2.92x10^{-4}$ M.

Kinetic data were processed according to the following equations by means of software packages including OLIS[14], MINSQ[15] and Scientist[16]:

(a) Determination of the observed rate constant:

$$\textbf{1 process:} \quad A_t = A_\infty - (A_\infty - A_0)e^{-kt} \qquad 6.1$$

Where; A_t = absorbance at time t; A_0 = absorbance at time 0;

A_∞ = absorbance at time ∞; k = rate constant; t = time

$$\textbf{2 process:} \quad A_t = A_{\infty(1)} - (A_{\infty(1)} - A_{0(1)})e^{-k_1 t} + A_{\infty(2)} - (A_{\infty(2)} - A_{0(2)})e^{-k_2 t} \qquad 6.2$$

Where; A_t = absorbance at time t; $A_{0(1)}$ = starting absorbance for the first reaction; $A_{\infty(1)}$ = absorbance at infinity for the first reaction; k_1 = rate constant for the first reaction; $Abs_{0(2)}$ = starting absorbance for the second reaction; $A_{\infty(2)}$ = absorbance at infinity for the second reaction; k_2 = rate constant for the second reaction.

(b) Determination of the thermodynamic activation parameters:

$$\ln(k_1/T) = \ln(k_B/h) + \Delta S/R - \Delta H/RT \qquad 6.3$$

6.3 MECHANISTIC ASPECTS

6.3.1 Reaction Mechanism

The X-ray structural determinations of the [Rh(dmavk)(CO)(PPh_3)] (Par.5.3), its stepwise oxidative addition products with iodomethane, [Rh(dmavk)(I)(CH_3)(CO)(PPh_3)] (Par. 5.5) and [Rh(dmavk)(I)($COCH_3$)(PPh_3)] (Par. 5.6), exactly corresponds with the reaction species proposed in the scheme in Fig. 6.1. Furthermore, ^{31}P-NMR studies confirmed that reactions of the [Rh(avk)(CO)(PPh_3)] compounds with iodomethane proceed *via* the formation of the Rh(III)-alkyl compounds as intermediates which then converts into the Rh(III)-acyl products. Previous studies done by IR spectroscopy on the reaction between iodomethane and [Rh(dmavk)(CO)(PPh_3)] in chloroform showed that upon addition of

iodomethane, the Rh(I)-carbonyl complex (υ_{CO} at 2013 cm^{-1}) disappeared, while simultaneously the Rh(III)-alkyl (υ_{CO} at 2105 cm^{-1}) was formed, followed by the disappearance of the Rh(III)-alkyl signal while the Rh(III)-acyl complex (υ_{CO} at 1710 cm^{-1}) was formed (see also Fig. 6.3).

In general, for the [Rh(avk)(CO)(PR_3)] type complexes, the mechanism as presented in Fig. 6.1, was thus confirmed by IR studies to consist of a rapid first oxidative addition equilibrium step followed by the slower acyl formation. Furthermore, the solvent pathway as shown did not observably contribute to the reaction.

To illustrate the mechanism, consider the formation of the intermediate alkyl complex from the IR data shown in Fig 6.3. The fact that the oxidative addition (reaction 1a, Fig. 6.1) is an equilibrium, is confirmed as follows. For the reaction between [Rh(tavk)(CO)(PPh_3)] and iodomethane at low [CH_3I] (Fig. 6.3(a)), only a relative small amount of the alkyl intermediate I (2080 cm^{-1}) is formed from the Rh(I) reactant G. However, when a large concentration of CH_3I is introduced, a significantly larger amount of the alkyl intermediate is formed -- and much more rapid, see Fig. 6.3(b). In both cases the alkyl intermediate is converted to the acyl species J. This implies that the intermediate Rh(III)-CO-alkyl species is thermodinamically unfavourable (Equilibrium constant K_1 is small), but at high [CH_3I] the equilibrium is indeed shifted towards alkyl formation.

On the other hand, in the case of the reaction between [Rh(dmavk)(CO)(PPh_3)] and iodomethane, even at low [CH_3I], a significantly large amount of the alkyl intermediate is formed (Fig. 6.3 (c); at the same rate as the disappearance of Rh(I) monocarbonyl), followed again by the conversion of alkyl to acyl product. This implies that the formation of the intermediate Rh(III)-CO-alkyl species is thermodinamically favourable (Equilibrium constant K_1 is large) which then converts to the acyl species.

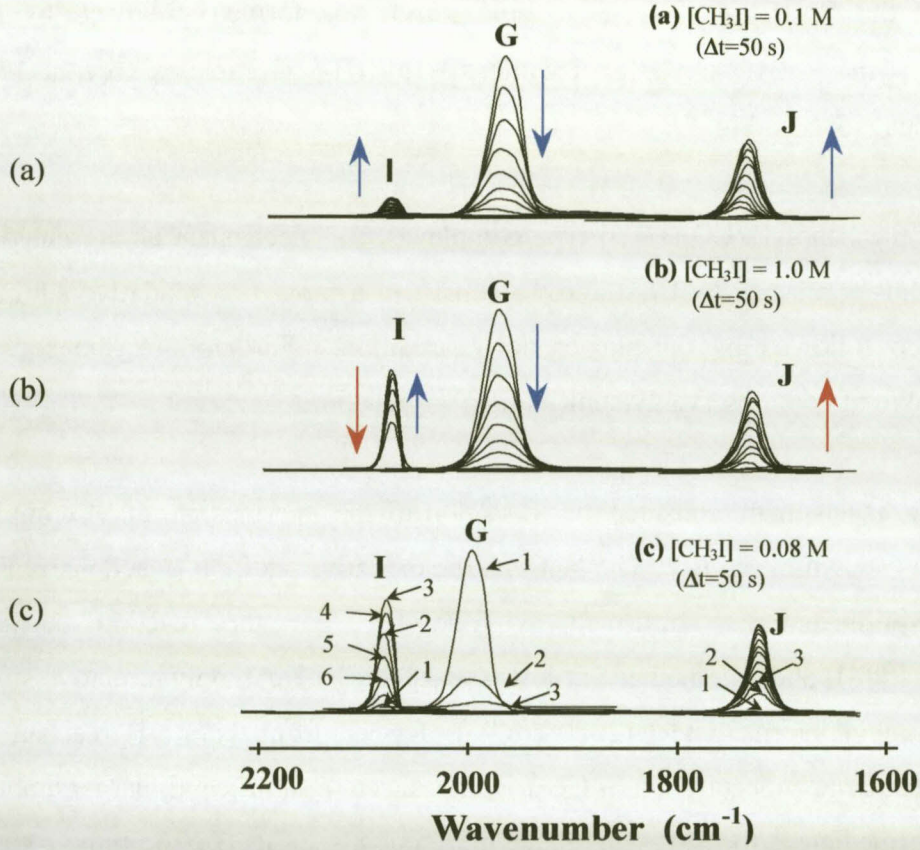

Fig. 6.3: Repetitive IR scans in $CHCl_3$, 25 °C: (a) and (b) is [Rh(tavk)(CO)(PPh_3)]; and (c) is [Rh(dmavk)(CO)(PPh_3)]; G is Rh(I)reactant, I is alkyl and J is acyl.

Both complexes, [Rh(dmavk)(CO)(PPh_3)] and [Rh(tavk)(CO)(PPh_3)], follows the same mechanism as presented in Fig. 6.1. IR studies done on all the complexes utilized in this kinetic study is also in agreement with the mechanism as presented in Fig. 6.1.

6.3.2 Rate Laws for the Iodomethane Oxidative Addition to [Rh(avk)(CO)(PR_3)] complexes

The disappearance of the Rh(I)-carbonyl peak and the formation of the Rh(III)-alkyl-carbonyl peak were monitored by infrared (typically Fig. 6.3) and UV/VIS spectroscopy and gave (within experimental error) identical observed rate constants. Careful study of the Rh(III)-alkyl formation rate dependence on [CH_3I], i.e. a plot of the observed first-

order rate constants *vs.* iodomethane concentration for the oxidative addition to the [Rh(avk)(CO)(PPh_3)] complexes (reaction 1a in Fig. 6.1), yields a linear relationship with a non-zero intercept and in some cases a zero intercept for a range of [Rh(avk)(CO)(PR_3)] complexes (eg., see Fig. 6.4). The results from this study are consistent with the rate expression of an equilibrium reaction as presented for the first step in Fig. 6.1, with k^{OA}_{obsd} the observed pseudo-first-order rate constant for the oxidative addition step, and k_1 and k_{-1} the rate constants for the oxidative addition and reductive elimination steps, respectively.

$$k^{OA}_{obsd} = k_1[CH_3I] + k_{-1} \qquad 6.4$$

On the other hand, plots of the observed first-order rate constants *vs.* [CH_3I] for the formation of the acyl species for most of the [Rh(avk)(CO)(XR_3)] (X = As or P) complexes showed limiting kinetics as depicted for example in Fig. 6.10. The solid curved lines represent the least-squares fits of the k^{CI}_{obsd}-data (k^{CI}_{obsd} = CO insertion step) *vs.* [CH_3I] to Eq. 6.5.

$$k^{CI}_{obsd} = \frac{k_2K_1[CH_3I]}{1 + K_1[CH_3I]} + k_{-2} \qquad 6.5$$

This typically corresponds to a mechanism consisting of a fast pre-equilibrium reaction as it is presented in Fig. 6.1 (K_1 = equilibrium constant), followed by a second slower reaction with a rate constant k_2, defined as an equilibrium with reverse rate constant k_{-2}.

Further confirmation that Eq. 6.5 holds for the avk systems, comes from the data as illustrated in Tables 6.2 and 6.6, depicting the formation of the [Rh(tavk)(I)(CH_3)(CO)(PPh_3)] alkyl and [Rh(tavk)(I)($COCH_3$)(PPh_3)] acyl complexes, respectively. It is clear that an excellent agreement exists between the equilibrium constant (K_1) for the formation of the alkyl complex as determined by monitoring the alkyl formation ($K_1=k_1/k_{-1}$) and CO-insertion steps separately.

Furthermore, in the studies of the complexes containing avk ligands, no evidence to suggest either a solvent pathway, or an equilibrium for the formation of the acyl species (negligible reverse reaction 2, Fig. 6.1) could be obtained. Thus, forward referrals to the mechanism in Fig. 6.1 are always in relation to the mechanism without the solvent pathway and assuming negligible k_{-2} values. In spite of no detectable solvent pathway, significant solvent effects were however indeed observed, see below.

6.4 OXIDATIVE ADDITION AND REDUCTIVE ELIMINATION REACTIONS

In this section, various influences, e.g. the type of β-diketonato ligand, tertiary Group 15 ligands, temperature and solvent effects on the rate of oxidative addition (OA) and reductive elimination (RE) reactions (see Fig. 6.1) are presented.

6.4.1 The influence of the β-diketonato ligand: The reaction between iodomethane and [Rh(dmavk)(CO)(PPh_3)] and [Rh(tavk)-(CO)(PPh_3)]

The oxidative addition of iodomethane to [Rh(dmavk)(CO)(PPh_3)] and [Rh(tavk)(CO)(PPh_3)] is discussed in this section. Manipulation of the electron density on the metal center was accomplished by the introduction of the electron withdrawing CF_3 substituent in place of CH_3 on the bidentate ligand, see Fig. 6.2. Both the β-diketonato ligands have similar steric properties; the only difference thus being the R_2 substituent.

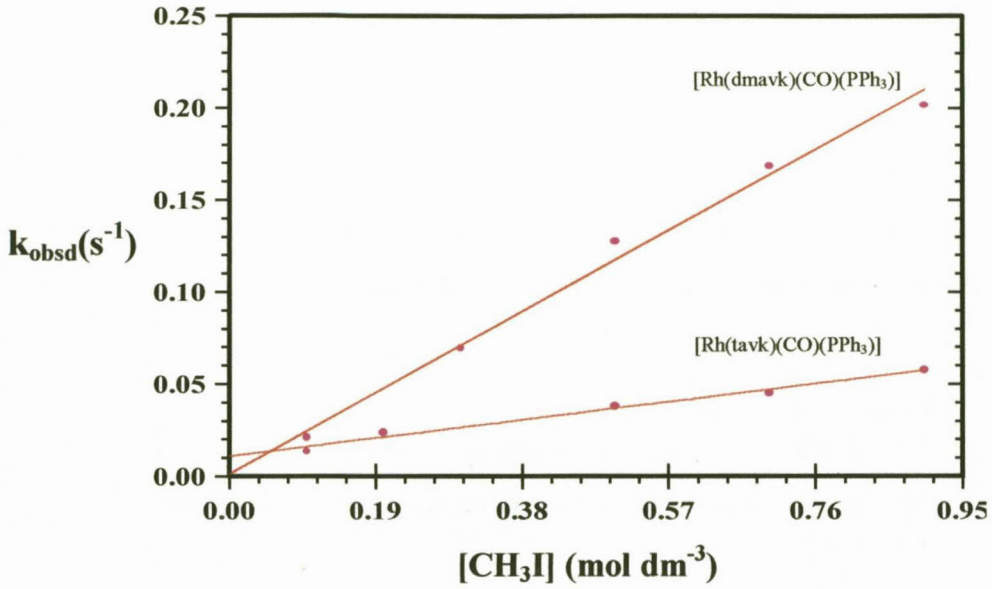

Fig. 6.4 [CH_3I] dependence of the pseudo-first-order rate constant for the formation of [Rh(dmavk)(I)(CH_3)(CO)(PPh_3)] ($[Rh]_{tot} = 2.92x10^{-4}$ M; $\lambda = 385$ nm) and [Rh(tavk)(I)(CH_3)(CO)(PPh_3)] ($[Rh]_{tot} = 2.92x10^{-4}$ M; $\lambda = 374$ nm) in acetone at 25 °C.

The formation of the Rh(III)-alkyl, as illustrated in Fig. 6.4, shows a direct relationship of the pseudo-first-order rate constant on [CH_3I] for both complexes. In the case of the [Rh(dmavk)(CO)(PPh_3)] complex, an approximately zero value was obtained, while for [Rh(tavk)(CO)(PPh_3)] a definite value was observed, see Table 6.1. These results are consistent with the rate expression for the first equilibrium step shown in Eq. 6.4, and also implies that for the formation of [Rh(dmavk)(I)($COCH_3$)(PPh_3)], the equilibrium constant (K_1) is quite large.

Furthermore, the equilibrium constant calculated from $K_1 = k_1/k_{-1}$ for the formation of [Rh(tavk)(I)($COCH_3$)(PPh_3)] is in good agreement with K_1 calculated from the rate expression for the overall reaction (see Eq. 6.5) for the formation of the acyl complex, [Rh(tavk)(I)($COCH_3$)(PPh_3)], see Par. 6.5. This indicates no significant solvent path contribution for this reaction. Due to the small equilibrium constant and subsequent small deviation in absorbance between the [Rh(tavk)(CO)(PPh_3)] and [Rh(tavk)(I)($COCH_3$)(PPh_3)] complexes, it was difficult to monitor the reaction of the

title complex with iodomethane. The rate constants, calculated from the data in Fig. 6.4 are given in Table 6.1.

The introduction of the electron withdrawing CF_3 substituent in place of CH_3, results in a decrease in the rate of oxidative addition (approximately 4 times), a decrease in the equilibrium constant K_1 (about 20 times) and an increase in the rate of the reductive elimination step.

Table 6.1 Kinetic data (constants in Fig. 6.1) for the iodomethane oxidative addition to [Rh(dmavk)(CO)(PPh_3)] and [Rh(tavk)(CO)(PPh_3)] in acetone at 25 °C.

Complex	υ_{CO}(KBr) (cm^{-1})	10^2k_1 ($M^{-1}s^{-1}$)	10^2k_{-1} (s^{-1})	K_1 (M^{-1})
[Rh(dmavk)(CO)(PPh_3)	1960	23(1)	0.3(8)	≥100 [a]
[Rh(tavk)(CO)(PPh_3)]	1974	5.2(4)	1.1(2)	5(1) [b]

[a] Could not be calculated form $K_1 = k_1/k_{-1}$; $k_{-1} \approx 0$, lower limit given [b] Calculated from $K_1 = k_1/k_{-1}$

6.4.2 The influence of group 15 tertiary ligands: The reaction between [Rh(dmavk)(CO)(PX_3)], [Rh(tavk)(CO)(PX_3)], [Rh(tavk)-(CO)($AsPh_3$)] and iodomethane

The oxidative addition of iodomethane to complexes of the type [Rh(avk)(CO)(XR_3)] with X = As or P; R = *para*-chloro-phenyl (*p*-Cl-Ph), phenyl (Ph), *para*-methoxy-phenyl (*p*-OMe-Ph) are discussed in this section. The manipulation of the electron density on the central metal was firstly accomplished by the introduction of functionalized triphenyl phosphines, which have similar Tolman cone angles ($\theta \approx 145$ °), but different Lewis basicities. Their varying effect on the oxidative addition of iodomethane to [Rh(avk)(CO)(PR_3)] complexes will thus mainly be due to electronic rather than steric

differences. This was investigated for both the dmavk and tavk systems. Secondly, the group 15 donor atom was changed from P to As. The carbonyl stretching frequencies for the same bidentate ligand in [Rh(avk)(CO)(XPh_3)] (X = P or As) complexes indicated no significant differences, thereby implying similar donating ability of the P and As phenyl systems, see Chapter 4. The crystal structures of [Rh(dmavk)(CO)(PPh_3)] and [Rh(dmavk)(CO)($AsPh_3$)] showed that the Rh-As bond distance is significantly longer compared to the Rh-P bond distance, indicating much less steric constraints for the arsenic complex which should have an effect on the rate of oxidative addition. All experimental details are summarized under Figures 6.5 to 6.7.

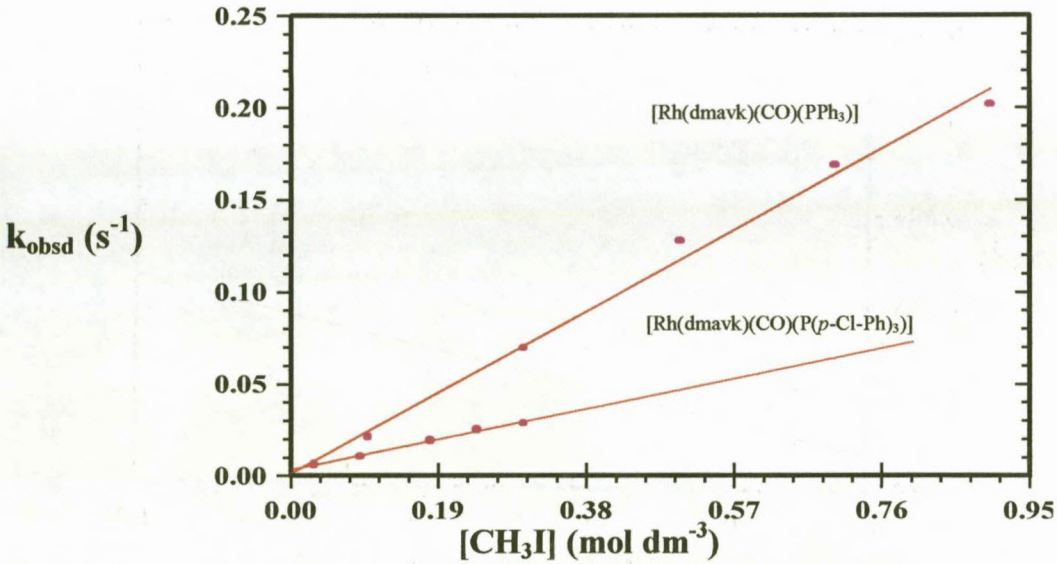

Fig. 6.5 [CH_3I] dependence of the pseudo-first-order rate constant for the formation of [Rh(dmavk)(I)(CH_3)(CO)(PPh_3)] ($[Rh]_{tot}$ = $2.92x10^{-4}$ M; λ = 385 nm) and [Rh(dmavk)(I)(CH_3)(CO)(*p*-Cl-Ph)$_3$P] ($[Rh]_{tot}$ = $2.92x10^{-4}$ M; λ = 390 nm) in acetone at 25 °C.

The formation of the Rh(III)-alkyl complexes from [Rh(dmavk)(CO)(PPh_3)] and [Rh(dmavk)(CO)(P(*p*-Cl-Ph)$_3$)], as illustrated in Fig. 6.5, shows for both reactions a direct relationship of the pseudo-first-order rate constant on [CH_3I], with only the [Rh(dmavk)(CO)(P(*p*-Cl-Ph_3)] complex having a non-zero intercept (see Table 6.2). It is clear that a significant decrease in the OA reaction rate (*ca.* factor of 3) is observed by introducing the P(*p*-Cl-Ph)$_3$ ligand, i.e., a less electron donating moiety. On the other

hand, the RE rate increases – the consequence of this is a smaller effective equilibrium constant K_1 (K_1 is approximately 100 for PPh_3 compared to 23 for P(*p*-Cl-Ph)$_3$. Similar results were obtained for [Rh(tavk)(CO)(PPh_3)], indicating a small equilibrium constant (see Par. 6.4.1). The rate constants that were calculated form the data obtained in Fig. 6.5 are given in Table 6.2.

The electronic effect of tertiary phosphines was further investigated for the reaction between [Rh(tavk)(CO)(PPh_3)] and [Rh(tavk)(CO)(P(*p*-OMe-Ph)$_3$)], i.e. substituting PPh_3 with the more electron donating P(*p*-OMe-Ph)$_3$.

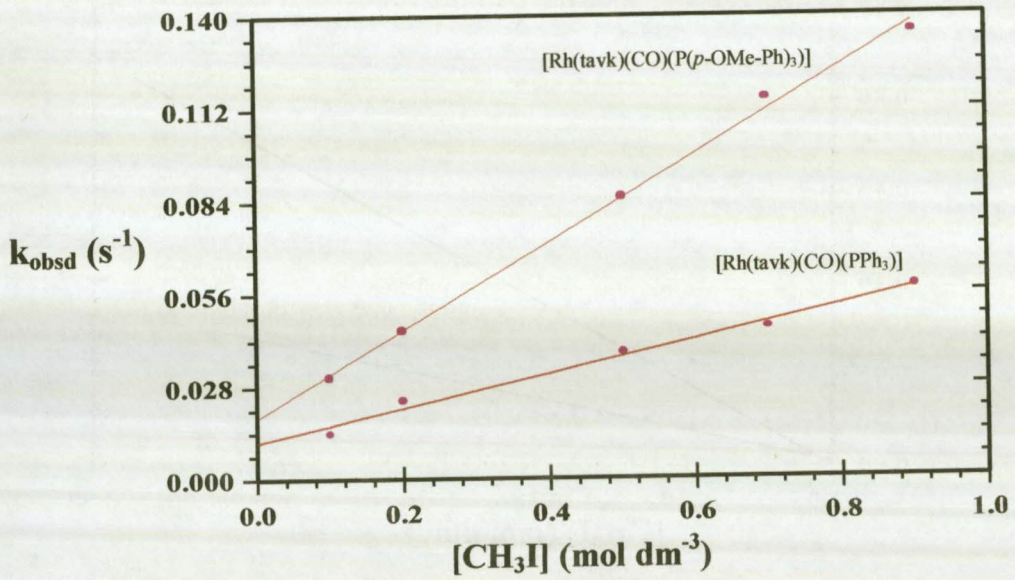

Fig. 6.6 [CH_3I] dependence of the pseudo-first-order rate constant for the formation of [Rh(tavk)(I)(CH_3)(CO)(PPh_3)] ($[Rh]_{tot}$ = $2.92x10^{-4}$ M; λ = 374 nm) and [Rh(tavk)(I)(CH_3)(CO)(P(*p*-OMe-Ph)$_3$] ($[Rh]_{tot}$ = $2.92x10^{-4}$ M; λ = 374 nm) in acetone at 25 °C.

The formation of the Rh(III)-alkyl shows for both reactions, as illustrated in Fig. 6.6, a direct relationship of the pseudo-first-order rate constant on [CH_3I] with a non-zero intercept. It is clear that a significant increase in reaction rate in the tavk system is obtained by introducing the P(*p*-OMe-Ph)$_3$ ligand, i.e. a 2-3 fold increase in OA rate. The equilibrium constants calculated from the data in Fig. 6.6 are in good agreement with

those calculated from the overall reaction (see Table 6.6), again indicating no significant solvent pathway. The rate constants calculated form Fig. 6.6 are given in Table 6.2.

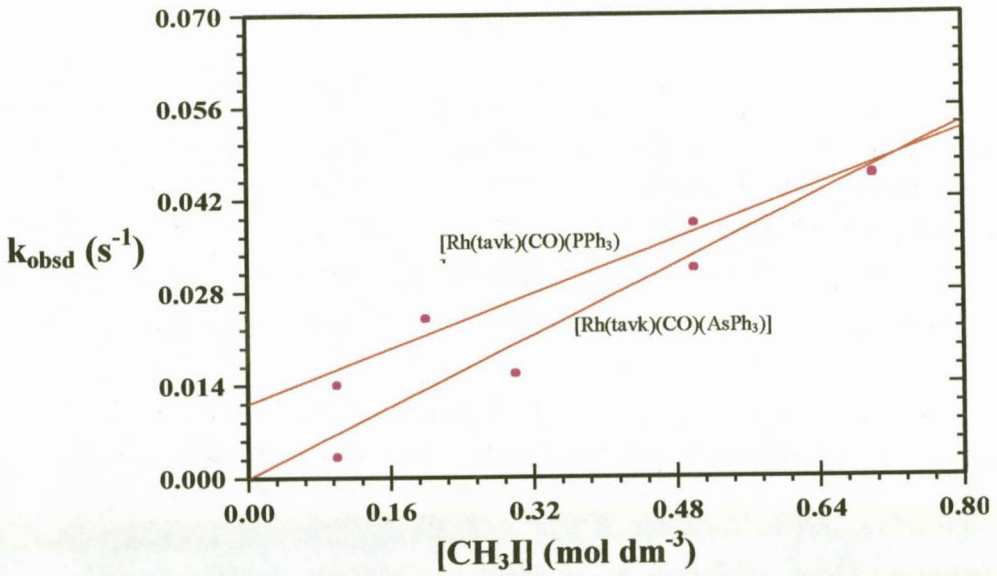

Fig. 6.7 [CH_3I] dependence of the pseudo-first-order rate constant for the formation of [Rh(tavk)(I)(CH_3)(CO)(PPh_3)] ($[Rh]_{tot}$ = $2.92x10^{-4}$ M; λ = 374 nm) and [Rh(tavk)(I)(CH_3)(CO)($AsPh_3$)] ($[Rh]_{tot}$ = $2.92x10^{-4}$ M; λ = 375 nm) in acetone at 25 °C.

Next, the effect of tertiary arsine *vs.* phosphine was investigated for the reaction of iodomethane with [Rh(tavk)(CO)(PPh_3)] and [Rh(tavk)(CO)($AsPh_3$)] and the data are illustrated in Fig. 6.7. The formation of the Rh(III)-alkyl shows for both reactions, as illustrated in Fig. 6.7, a direct relationship of the pseudo-first-order rate constant on [CH_3I]. For the [Rh(tavk)(CO)($AsPh_3$)] complex a zero intercept was observed, indicating a large equilibrium constant and small reductive elimination step. However, the PPh_3 complex was a little less reactive than the $AsPh_3$ species (5.2(4) *vs.* 7.6(3) $M^{-1}s^{-1}$ respectively, see Table 6.2).

Table 6.2 Kinetic data (constants in Fig. 6.1) for the iodomethane oxidative addition to [Rh(dmavk)(CO)(PPh_3)], [Rh(dmavk)(CO)(P(*p*-Cl-Ph)$_3$)], Rh(tavk)(CO)(P(*p*-OMe-Ph)$_3$)] and [Rh(tavk)(CO)(PPh_3)] in acetone at 25 °C.

Complex	PK_a [a]	υ_{CO} (KBr))	10^2k_1	10^2k_{-1}	K_1
		(cm^{-1})	(M^{-1} s^{-1})	(s^{-1})	(M^{-1})
[Rh(dmavk)(CO)(PPh_3)]	2.73	1960	23(1)	0 [b]	≥100 [c]
[Rh(dmavk)(CO)(P(*p*-Cl-Ph)$_3$)]	1.03	1965	8.7(4)	0.35(8)	23(3) [d]
[Rh(tavk)(CO)(P(*p*-OMe-Ph)$_3$)]	4.57	1977	13.2(4)	1.9(2)	5.4(4) [d]
[Rh(tavk)(CO)($AsPh_3$)]	-	1965	7.6(3)	0 [b]	≥100 [c]
[Rh(tavk)(CO)(PPh_3)]	2.73	1974	5.2(4)	1.1(2)	4.7 [d]

[a] Indication of basicity of phosphines [b] Zero within experimental error. Fix as = 0
[c] Could not be calculated form $K_1 = k_1/k_{-1}$; $k_{-1} \approx 0$ [d] Calculated from $K_1 = k_1/k_{-1}$

The relative activation/deactivation induced by the manipulations as performed in this paragraph is further discussed in par. 6.4.5.

6.4.3 Solvent dependence of oxidative addition

In an attempt to investigate the polarity/non-polarity of the transition state for the formation of the Rh(III)-alkyl species (Fig. 6.1), the reaction between iodomethane and [Rh(dmavk)(CO)(PPh_3)] was monitored in a range of solvents, with different polarities and donocities. The effect of solvent was investigated for the [Rh(dmavk)(CO)(PPh_3)] complex to determine the relative activation/deactivation. The data are illustrated in Fig. 6.8 and the rate constants given in Table 6.3.

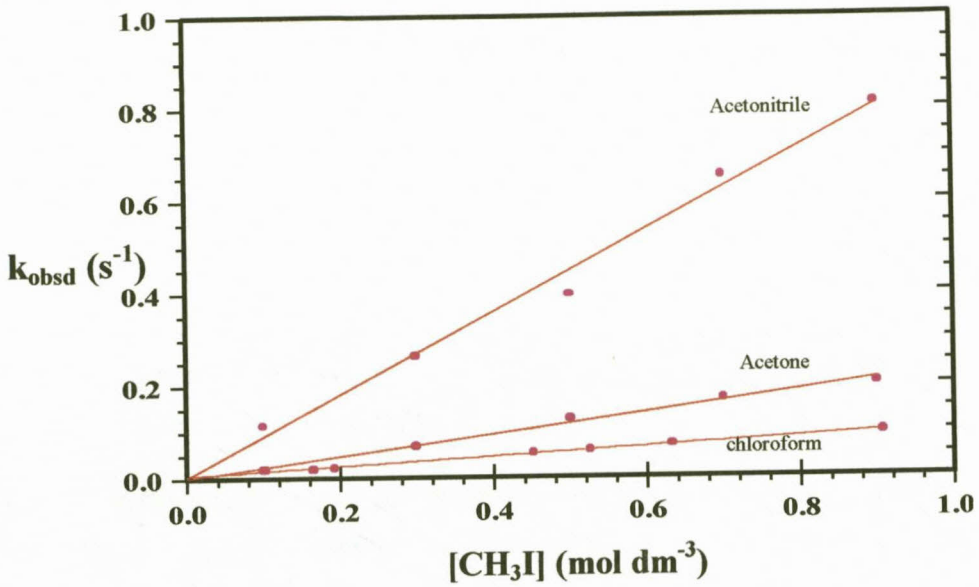

Fig. 6.8 [CH_3I] dependence of the pseudo-first-order rate constant for the formation of [Rh(dmavk)(I)(CH_3)(CO)(PPh_3)] ($[Rh]_{tot}$ = 2.92×10^{-4} M; λ = 385 nm) in acetone, acetonitrile and chloroform at 25 °C.

The rate constants calculated from the data illustrated in Fig. 6.8 using Eq. 6.1 are given in Table 6.3. It is clear that for the [Rh(dmavk)(CO)(PPh_3)] complex an 8-9 fold activation from chloroform to acetonitrile is obtained.

Table 6.3 Kinetic results (data in Fig. 6.1) for the iodomethane oxidative addition to [Rh(dmavk)(CO)(PPh_3)] in different solvents at 25 °C.

Solvent	ε	D_n	10^2k_1 ($M^{-1}s^{-1}$)	10^2k_{-1} (s^{-1})	K_1 (M^{-1})
Chloroform	4.8	4.0	11.4(4)	0 [a]	≥ 100 [b]
Acetone	20.7	17.0	23(1)	0 [a]	≥ 100 [b]
Acetonitrile	38.0	14.1	89(6)	0 [a]	≥ 100 [b]

[a] Zero within experimental error. Fix at = 0 [b] Could not be calculated

6.4.4 Temperature dependence of oxidative addition

The activation parameters were determined for the reaction between [Rh(dmavk)(CO)(PPh_3)] and iodomethane in acetone at different temperatures, see Fig. 6.9.

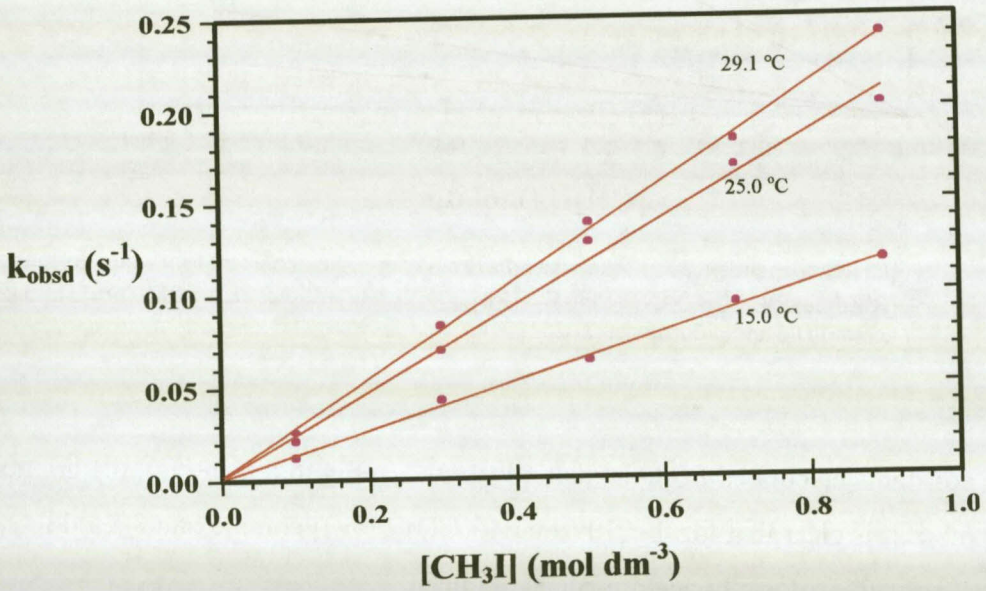

Fig. 6.9 Temperature and [CH_3I] dependence of the pseudo-first-order rate constants for the formation of [Rh(dmavk)(I)(CH_3)(CO)(PPh_3)] ($[Rh]_{tot} = 2.92x10^{-4}$ M; $\lambda = 385$ nm) in acetone.

The rate constants and activation parameters calculated from Eq. 6.3 from the data as illustrated in Fig. 6.9 are given in Table 6.4.

Table 6.4 Kinetic results and activation parameters for the reaction between [Rh(dmavk)(CO)(PPh_3)], and iodomethane in acetone at different temperatures.

Temperature (°C)	k_1 (M^{-1} s^{-1})	k_{-1}(s^{-1}) [a)]
15.0	0.130(4)	≈0
25.0	0.23(1)	≈0
29.1	0.264(6)	≈0
$\Delta H^{\#}$ (kJ mol^{-1})	35(4)	≈0
$\Delta S^{\#}$ (J K^{-1} mol^{-1})	-139(40)	≈0

[a)] assumed ≈ 0 since K_1 very large (see Table 6.3 and Fig. 6.9)

6.4.5 Discussion

In this study, an attempt was made to determine what effect different factors (e.g. electronic, steric, etc.) has on the rate of oxidative addition and reductive elimination reactions for the [Rh(avk)(CO)(XR_3)] type (X = As or P, R = phenyl or functionalized phenyl) of complexes. Electron density manipulation on the metal center was firstly accomplished by the introduction of different substituents (CF_3 in the place of CH_3) on the bidentate ligand, i.e. for the [Rh(tavk)(CO)(PPh_3)] and [Rh(dmavk)(CO)(PPh_3)] complexes respectively. The rate of oxidative addition with iodomethane for the [Rh(dmavk)(CO)(PPh_3)] complex is approximately 4 times higher compared to [Rh(tavk)(CO)(PPh_3)] (see Table 6.1). This can be explained in terms of the higher electron density on the metal center of the dmavk to the tavk complex, as manifested also in the υ_{CO} values.

The second order rate constants (k_1) show a 3 times increase from the [Rh(dmavk)(CO)(P(*p*-Cl-Ph)$_3$)] to the [Rh(dmavk)(CO)(PPh_3)] complex, as is predicted by the pK_a values for P(*p*-Cl-Ph)$_3$ and PPh_3 of 1.03 and 2.73 respectively (Table 6.2). This is in accordance with the higher nucleophilicity of the PPh_3 compared to the P(*p*-Cl-Ph)$_3$ complex, that will in turn enhance the rate of oxidative addition.

An increase in the rate of k_1 was obtained by substituting PPh_3 with $AsPh_3$. The structural determinations of [Rh(dmavk)(CO)(PPh_3)] and [Rh(dmavk)(CO)($AsPh_3$)] in Chapter 5 showed an increase in the bond length form Rh-P to Rh-As, indicating more space available around the metal center which should slightly favour the rate of oxidative addition as was found for the [Rh(tavk)(CO)($AsPh_3$)] compared to the [Rh(tavk)(CO)(PPh_3)] complex ($7.6(3)x10^{-2}$ *vs.* $5.2(4)x10^{-2}$ $M^{-1}s^{-1}$), see Table 6.2.

The magnitude of the equilibrium constant is affected by both the k_1 and k_{-1} reactions, which are both electron and/or sterically controlled, e.g. the large K_1-value for [Rh(tavk)(CO)($AsPh_3$)] compared to [Rh(tavk)(CO)(PPh_3)] is mainly due to the insignificant reductive elimination reaction (k_{-1}) for the former complex. This result is expected since the more steric demand on the metal, as was found for the PPh_3 compared to the $AsPh_3$ complex, will favour the formation of the four coordinate Rh(I) instead of the six coordinate Rh(III)-alkyl complex. However, as mentioned earlier, electron density on the metal center can also influence the magnitude of k_1 and k_{-1}, and thus K_1. The large equilibrium constant for [Rh(dmavk)(CO)(PPh_3)] compared to [Rh(tavk)(CO)(PPh_3)] can therefor be explained in terms of the faster oxidative addition reaction for the former complex. On the other hand, a decrease in electron density on the metal will favour the reductive elimination step (k_{-1}) because of the high formal charge on the metal center in the Rh(III)-alkyl complex, hence further decreasing the equilibrium constant as observed for [Rh(tavk)(CO)(PPh_3)] compared to [Rh(dmavk)(CO)(PPh_3)] (5(1) *vs.* >100, respectively, see Table 6.1). The decrease in the equilibrium constant from [Rh(dmavk)(CO)(PPh_3)] to [Rh(dmavk)(CO)(P(*p*-Cl-Ph)$_3$] can similarly be explained in terms of both the decrease in k_1 and increase in k_{-1}.

Solvent studies were performed on the [Rh(dmavk)(CO)(PPh_3)] complexes. An increase in second-order rate constant (k_1) was observed from chloroform to acetone to acetonitrile, as expected from the ε values. The marked solvent dependence of k_1 for the [Rh(dmavk)(CO)(PPh_3)] complex [k_1(acetonitrile) > k_1(acetone) > k_1(chloroform)] strongly suggests a mechanism in which a polar transition state is established and favoured by more polar solvents. This implies that the function of the solvent is to ease

the charge separation during the rearrangement and formation of a five coordinated intermediate. Conventional activation parameters ($\Delta H^{\#}$, $\Delta S^{\#}$) were determined in acetone to further investigate the character of the transition state. The relative small $\Delta H^{\#}$ values, accompanied by large negative $\Delta S^{\#}$ values, indicate an associative mechanism including bond formation and/or partial charge creation (electrostriction) during the formation of the transition state. The solvent dependence together with the activation parameters thus point to a polar transition state of which the character may vary between a concerted three-center and an ionic S_N2 mechanism. Further evidence for a S_N2 mechanism is the *trans* mode of addition of CH_3I determined for [Rh(dmavk)(I)(CH_3)(CO)(PPh_3)] (Par. 5.3) although isomerization reaction from the *cis*-product to the *trans*-product can also occur.

In general, the results obtained for the oxidative addition step can be summarized as follow: Electron withdrawing substituents decrease the rate of oxidative addition and the magnitude of the equilibrium constant but increase the rate of reductive elimination. Less steric demand on the metal center increase the rate of oxidative addition and also the magnitude of equilibrium constant K_1. Solvents with high polarity increase the rate of oxidative addition and magnitude of the equilibrium constant K_1. An increase in the temperature increase the rate of oxidative addition and K_1 for [Rh(dmavk)(CO)(PPh_3)].

6.5 MIGRATORY CARBONYL INSERTION REACTIONS

In this section, various influences, e.g. the type of β-diketonato ligand, tertiary Group 15 ligands, temperature and solvent effects on the rate of CO-insertion reactions are reported. All these reactions are at least 100 times slower that the oxidative reactions for a specific complex, allowing the k_1 and k_2 steps to be monitored separately.

6.5.1 The influence of the β-diketonato ligand: The reaction between iodomethane and [Rh(dmavk)(CO)(PPh_3)] and Rh(tavk)-(CO)(PPh_3)]

Careful study of the dependence of the rate of Rh(III)-acyl formation on [CH_3I] for the [Rh(dmavk)(CO)(PPh_3)] and [Rh(tavk)(CO)(PPh_3)] complexes, as illustrated in Fig. 6.10 shows limiting kinetics for the relationship of the pseudo-first-order rate constant on [CH_3I]. This result is consistent with the rate expression shown in Eq. 6.5 for which a fast equilibrium reaction exists, then followed by a slower reaction. Even more convincing evidence that the overall reaction for the reaction between [Rh(avk)(PR_3)] type of complexes and iodomethane follows the reaction scheme in Fig. 6.1, is the fact that the equilibrium constant, K_1, obtained from the data in figures 6.10 and 6.4 for the [Rh(tavk)(CO)(PPh_3)] complex, is in good agreement. As mentioned earlier in Section 6.4.1, K_1 for the [Rh(dmavk)(CO)(PPh_3)] complex could not be calculated from the data in Fig. 6.4 due to the zero intercept ($k_{-1} = 0$). From the data in Fig. 6.10, K_1 could however be obtained for [Rh(dmavk)(CO)(PPh_3)], indicating a large equilibrium constant as expected, compared to the smaller K_1 for [Rh(tavk)(CO)(PPh_3)]. The data calculated from figures 6.10 - 6.13 are given in Table 6.6.

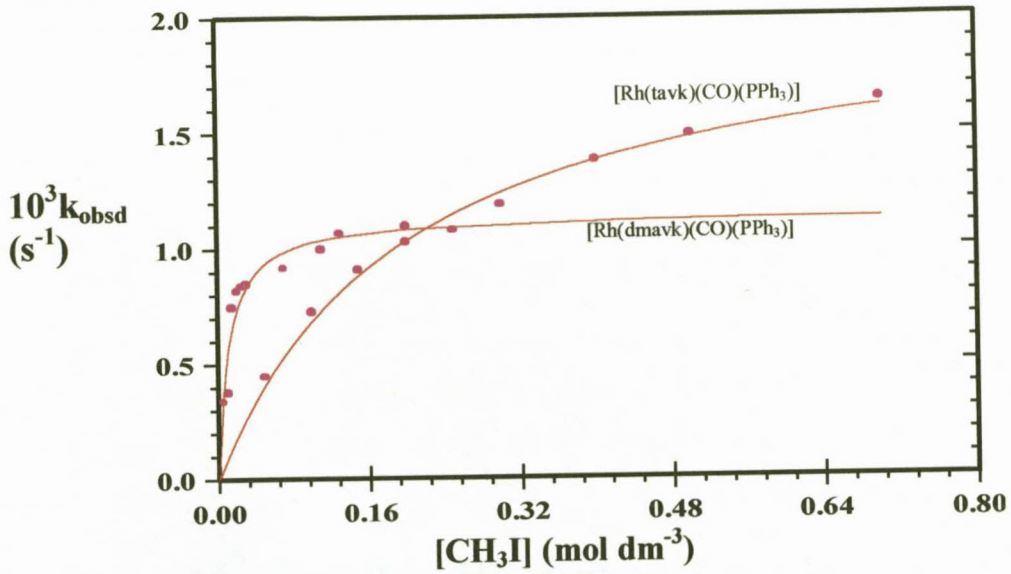

Fig. 6.10 $[CH_3I]$ dependence of the pseudo-first-order rate constant for the formation of $[Rh(dmavk)(I)(COCH_3)(PPh_3)]$ ($[Rh]_{tot}$ = 2.92×10^{-4} M; λ = 350 nm) and $[Rh(tavk)(I)(COCH_3)(PPh_3)]$ ($[Rh]_{tot} = 2.92 \times 10^{-4}$ M; λ = 345 nm) in acetone at 25 °C.

It is important to note that due to the large K_1 for the formation for Rh(III)-alkyl, $[Rh(dmavk)(I)(COCH_3)(PPh_3)]$, the plot in Fig. 6.10 reaches a plateau at fairly low $[CH_3I]$, thus resulting in the relatively large error calculated for K_1 for this complex. The rate constant k_2, is unexpectedly larger for the $[Rh(tavk)(CO)(PPh_3)]$ complex, since it was previously found that increased electron density on the metal center increases the rate of CO-insertion. This was explained in terms of activation energies for the Rh-CH_3 bond breaking process, i.e. high electron density on the metal center would cause lower energy of activation for the bond breaking process[17]. However, similar results found in this study was observed for CO-insertion reactions of $[Rh(N,S\text{-}BID)(CO)(PX_3)]$ complexes[12], where the increase in basicity of the tertiary phosphine led to a decrease in k_2.

Table 6.5 Kinetic results (constants in Fig. 6.1) for the reaction between [Rh(dmavk)(CO)(PPh_3)]; [Rh(tavk)(CO)(PPh_3)] and iodomethane in acetone at 25 °C.

Complex	υ_{CO} (KBr) (cm^{-1})	10^4k_2 /s^{-1}	K_1 /M_{-1}
[Rh(dmavk)(CO)(PPh_3)]	1960	12.0(6)	81(15)
[Rh(tavk)(CO)(PPh_3)]	1974	20.6(7)	5.0(5)

6.5.2 The influence of group 15 tertiary ligands: The reaction between [Rh(dmavk)(CO)(PX_3)], [Rh(tavk)(CO)(PX_3)], [Rh(dmavk)-(CO)($AsPh_3$)] and iodomethane

As a further investigation of the rate of CO-insertion dependence on electronic properties, tertiary phosphine ligands with similar Tolman cone angles, but different Lewis basicities were introduced, i.e. PPh_3, P(*p*-Cl-Ph)$_3$ and P(*p*-OMe-Ph)$_3$. The steric effect on the rate of CO-insertion was addressed by the comparison of PPh_3 and $AsPh_3$ in these reactions. Fig. 6.11 illustrates the formation of [Rh(dmavk)(I)($COCH_3$)(PPh_3)] and [Rh(dmavk)(I)($COCH_3$)(P(*p*-Cl-Ph)$_3$)] and the constants calculated from these results are given in Table 6.6.

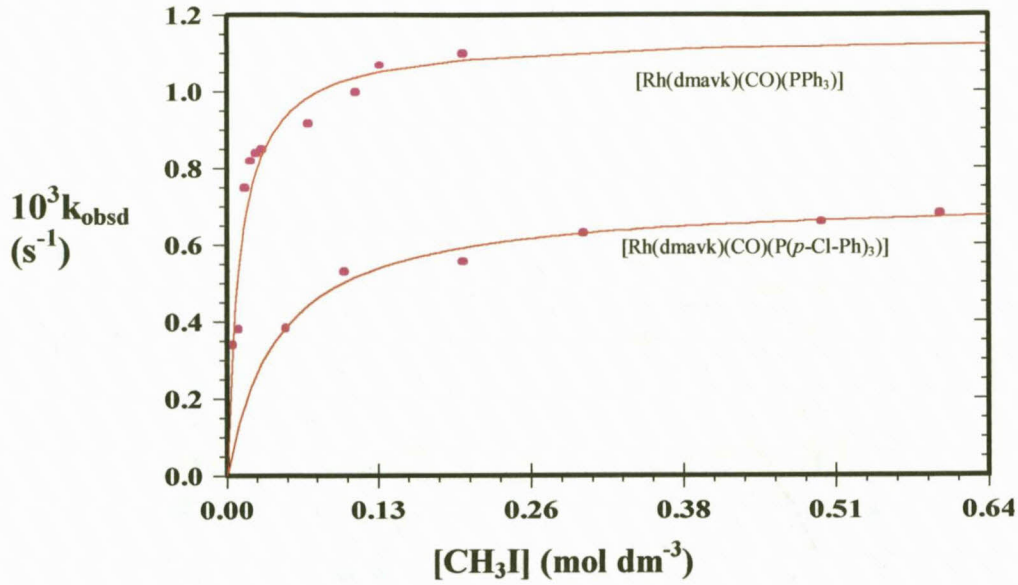

Fig. 6.11 [CH_3I] dependence of the pseudo-first-order rate constant for the formation of [Rh(dmavk)(I)($COCH_3$)(PPh_3)] ($[Rh]_{tot}$ = 2.92×10^{-4} M; λ = 350 nm) and [Rh(dmavk)(I)($COCH_3$)(P(*p*-Cl-Ph)$_3$)] ($[Rh]_{tot}$ = 2.92×10^{-4} M; λ = 360 nm) in acetone at 25 °C.

Fig. 6.12 illustrates the formation of [Rh(tavk)(I)($COCH_3$)(PPh_3)] and [Rh(tavk)(I)($COCH_3$)(P(*p*-OMe-Ph_3)P] and the data calculated from these results are given in Table 6.6.

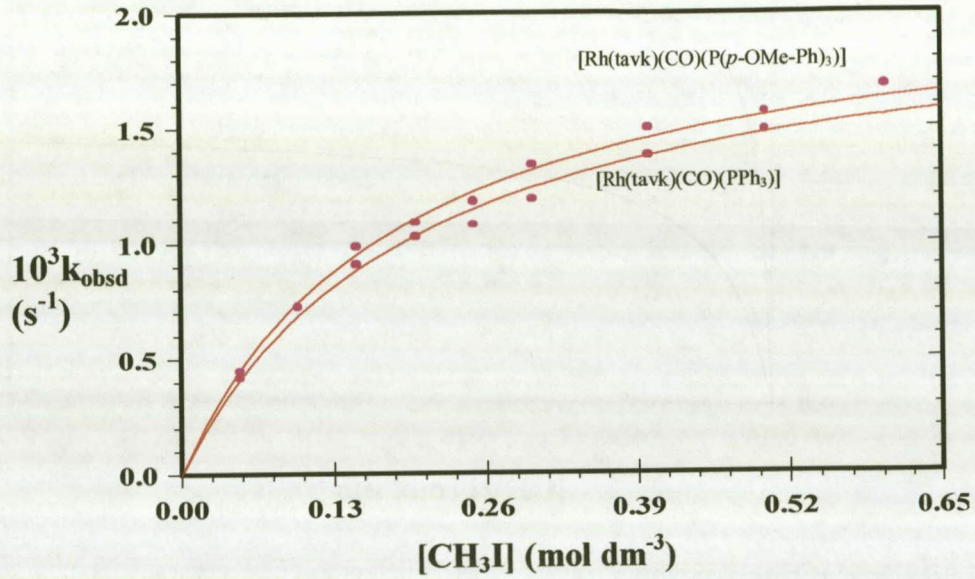

Fig. 6.12 [CH_3I] dependence of the pseudo-first-order rate constant for the formation of [Rh(tavk)(I)($COCH_3$)(PPh_3)] ($[Rh]_{tot}$ = $2.92x10^{-4}$ M; λ = 345 nm) and [Rh(tavk)(I)($COCH_3$)(P(*p*-OMe-$Ph)_3$)] ($[Rh]_{tot}$ = $2.92x10^{-4}$ M; λ = 374 nm) in acetone at 25 °C.

The effect of steric influences on the rate of CO-insertion was determined in the reaction of iodomethane with [Rh(dmavk)(CO)(PPh_3)] and [Rh(dmavk)(CO)($AsPh_3$)]. No limiting kinetics was observed for the formation of Rh(III)- acyl for [Rh(dmavk)(CO)($AsPh_3$)]. This result can be explained as follow. If $k_1[CH_3I] >> k_{-1} >> k_2$ (see Eq. 6.4 and 6.5), the equilibrium is shifted to the right so that K_1 is large and thus $(1+K_1[CH_3I]) \cong K_1[CH_3I]$, which in turn simplifies Eq. 6.5 to $k_{obsd} = k_2$. The latter predicts that the rate at which CO-insertion takes place is independent of [CH_3I] at appreciable high [CH_3I]. A plot of k_{obsd} *vs.* [CH_3I] will thus show a straight line parallel to the [CH_3I] axis and only at very low concentrations of iodomethane will k_{obsd} decrease toward a theoretical value of zero at [CH_3I] = 0 $moldm^{-3}$, as was indeed observed (Fig. 6.13).

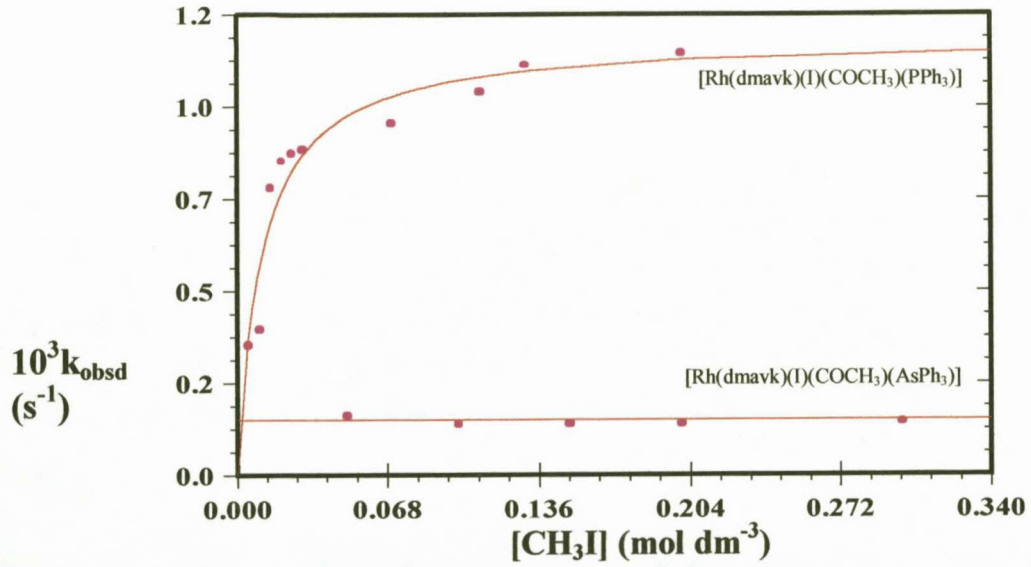

Fig. 6.13 [CH_3I] dependence of the pseudo-first-order rate constant for the formation of [Rh(dmavk)(I)($COCH_3$)(PPh_3)] ($[Rh]_{tot}$ = $2.92x10^{-4}$ M; λ = 350 nm) and [Rh(dmavk)(I)($COCH_3$)($AsPh_3$)] ($[Rh]_{tot}$ = $2.92x10^{-4}$ M; λ = 350 nm) in acetone at 25 °C.

Fig. 6.13 illustrates the formation of [Rh(dmavk)(I)($COCH_3$)(PPh_3)] and [Rh(dmavk)(I)($COCH_3$)($AsPh_3$)] and the results obtained from these data are given in Table 6.6.

Table 6.6 Kinetic results for the reaction (constants in Fig. 6.1) between [Rh(dmavk)(CO)(PPh_3)]; [Rh(tavk)(CO)(PPh_3)], [Rh(dmavk)(CO)(P(*p*-Cl-Ph)$_3$)], [Rh(tavk)(CO)(P(*p*-OMe-Ph)$_3$)] and [Rh(dmavk)(CO)($AsPh_3$)] with iodomethane in acetone at 25 °C.

Complex	υ(CO) (KBr) (cm^{-1})	10^4k_2 $/s^{-1}$	K_1 $/M^{-1}$
[Rh(dmavk)(CO)(PPh_3)]	1960	12.0(6)	81(15)
[Rh(dmavk)(CO)(P(*p*-Cl-Ph)$_3$]	1965	7.2(1)	23(3)
[Rh(tavk)(CO)(PPh_3)]	1974	20.6(7)	5.0(5)
[Rh(tavk)(CO)(P(*p*-OMe-Ph)$_3$]	1977	21.3(4)	5.4(4)
[Rh(dmavk)(CO)($AsPh_3$)]	1956	1.32(2)	>100 [a]

[a] Could not be calculated: Eq. 6.5 simplifies to $k_{obsd} = k_2$.

6.5.3 Solvent and temperature dependence of CO-insertion

Fig. 6.14 illustrates the solvent dependence for CO-insertion for the [Rh(dmavk)(CO)(PPh_3)] complex. Rate constants calculated from the data in Fig. 6.14 as well as plots not illustrated here (see supplementary data in Par. 8.2), are summarized in Table 6.7. Rate constants calculated from the data in figures 6.15, 6.16 and 6.17 (the temperature dependence) are summarized in Tables 6.8.

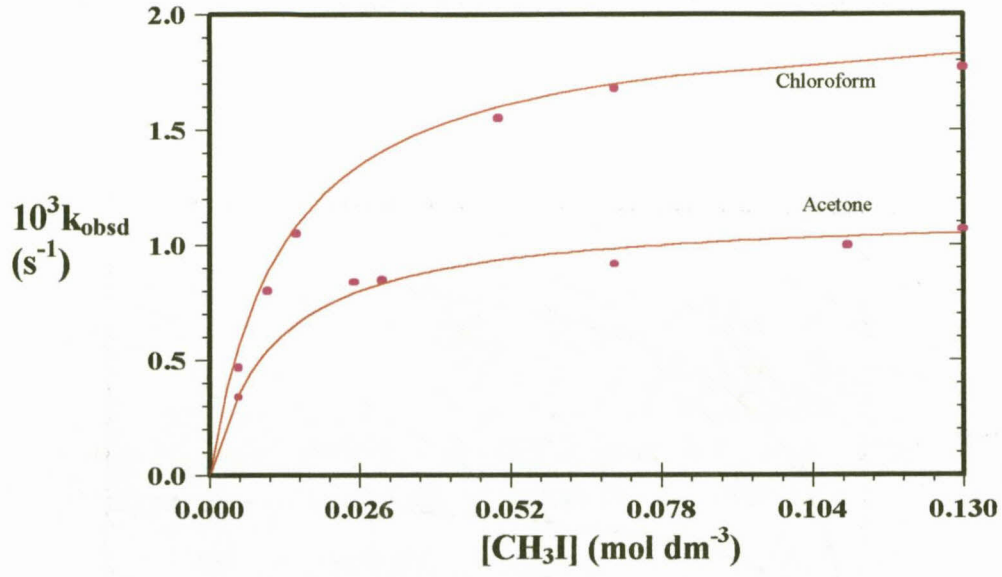

Fig. 6.14 [CH_3I] dependence of the pseudo-first-order rate constant for the formation of [Rh(dmavk)(I)($COCH_3$)(PPh_3)] ([Rh]$_{tot}$ = 2.92x10^{-4} M; λ = 350 nm) in chloroform and acetone at 25 °C.

The rate of CO-insertion is much higher for acetonitrile (see Table 6.7), the most polar solvent. However, there is no significant difference or general trend in terms of rate *vs.* polarity for the other solvents which indicate that the CO-insertion step is not solvent dependent for these systems. Similar results were obtained for the 1-hydroxy-2-piridinethione (hpt) ligand systems[18].

Table 6.7 Kinetic results (data in Fig. 6.1 and Supplementary data, Par. 8.2) for the formation of [Rh(dmavk)(I)($COCH_3$)(PPh_3)] in different solvents at 25 °C.

Solvent	ε	D_n	$10^4 k_2$ /s^{-1}	K_1 /M^{-1}
Benzene	2.3	0.1	25(1)	2.8(4)
Chloroform	4.9	4.0	20(3)	78(12)
Ethyl acetate	6.0	17.1	6.8(2)	52(4)
Dichloromethane	10.4	-	21(3)	32(9)
Acetone	20.7	17.0	12.0(6)	23(3)
Acetonitrile	38.0	14.1	71.9(9)	262(21)

The activation parameters calculated from Eq. 6.3 from the data as illustrated in figures 6.15, 6.16 and 6.17 are given in Table 6.8. The small negative $\Delta S^{\#}$-values in all three

cases indicate that the Rh-CH_3 bond breaking process for CO-insertion is probably more favourable.

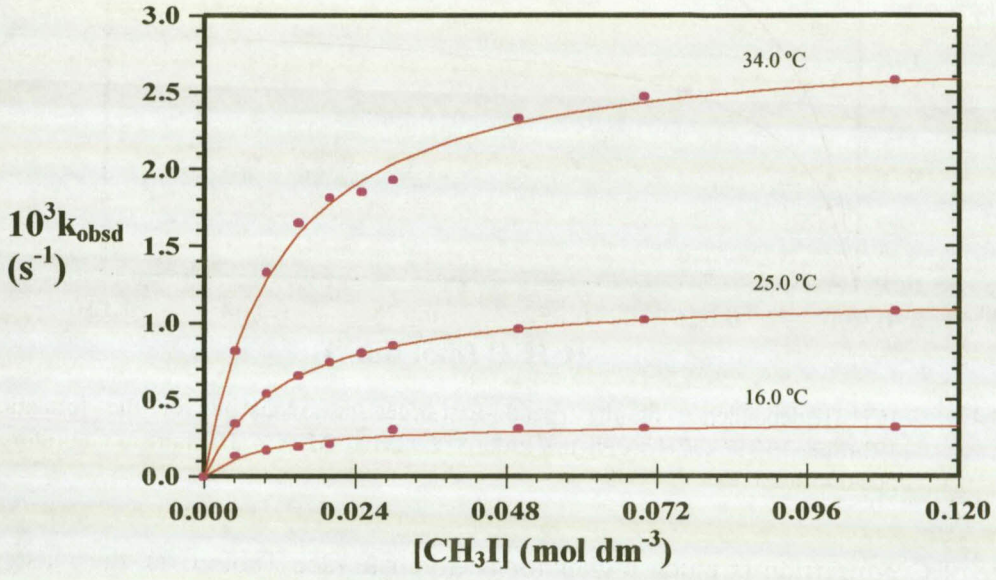

Fig. 6.15 Temperature and [CH_3I] dependence of the pseudo-first-order rate constant for the formation of [Rh(dmavk)(I)($COCH_3$)(PPh_3)] in acetone.

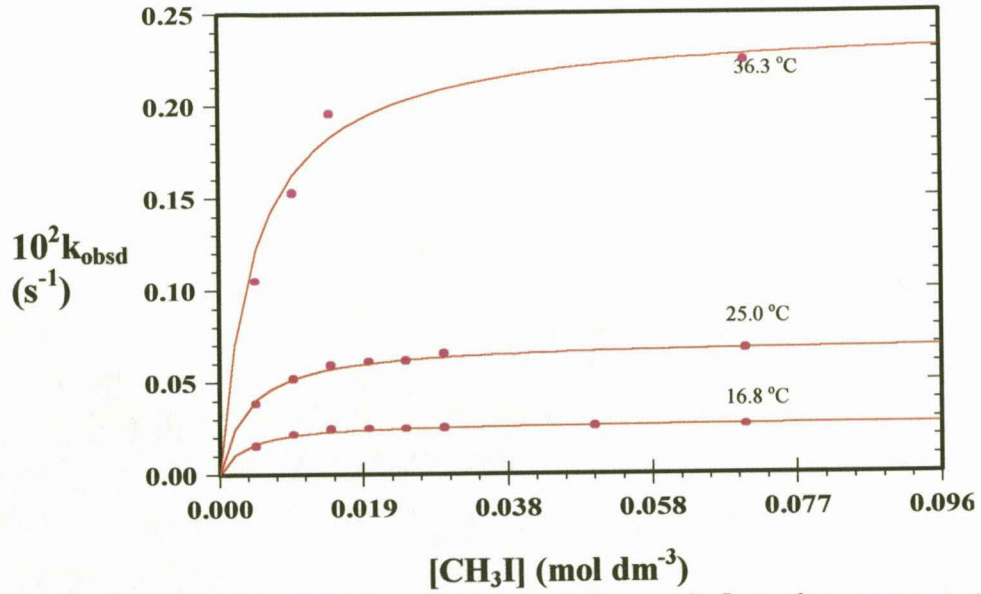

Fig. 6.16 Temperature and [CH_3I] dependence of the pseudo-first-order rate constant for the formation of [Rh(dmavk)(I)($COCH_3$)(PPh_3)] in acetonitrile.

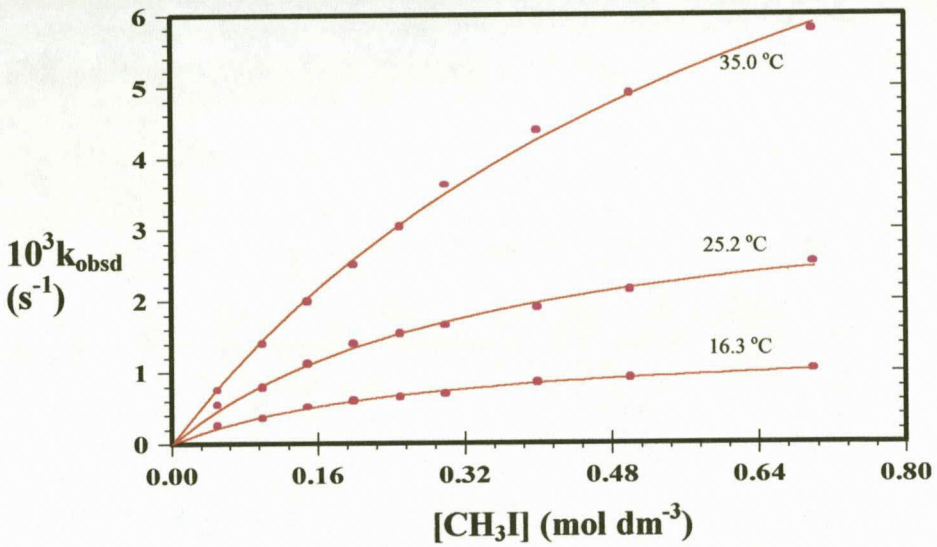

Fig. 6.17 Temperature and [CH_3I] dependence of the pseudo-first-order rate constant for the formation of [Rh(tavk)(I)($COCH_3$)(PPh_3)] in chloroform.

Table 6.8 Kinetic results (constants in Fig. 6.1) and activation parameters for CO-insertion for [Rh(dmavk)(CO)(PPh_3)] (acetone and acetonitrile) and [Rh(tavk)(CO)(PPh_3)]

Complex	Solvent	Temp. (°C)	10^4k_2 (s^{-1})	K_1 (M^{-1})	$\Delta H^{\#}$ (kJ mol^{-})	$\Delta S^{\#}$ (J K^{-1} mol^{-1})
[Rh(dmavk)(CO)(PPh_3)]	Acetone	15.0	3.6(2)	$9(1)x10^{-1}$		
		25.0	12.0(6)	$8(2)x10^{-1}$	77(3)	-42(2)
		34.0	28.5(5)	$8.4(5)x10^{-1}$		
	Acetonitrile	16.8	281(6)	$3.1(5)x10^{-2}$		
		25.0	719(9)	$2.6(2)x10^{-2}$	99(2)	-2.32(7)
		36.3	2430(90)	$2.0(4)x10^{-2}$		
[Rh(tavk)(CO)(PPh_3)]	Chloroform	16.3	14.3(7)	3.6(4)		
		25.2	37(2)	2.8(3)	81(7)	15(2)
		35.0	119(6)	1.4(1)		

6.5.4 Discussion on CO-insertion reactions

An unexpected slight increase for the rate of CO-insertion is observed from the [Rh(dmavk)(CO)(PPh_3)] to the [Rh(tavk)(CO)(PPh_3)] complexes, which follows the reverse order in terms of Lewis basicity, since higher electron density should facilitate the bond braking process (Rh-CH_3) in going from the alkyl to the acyl complex. However, it was also found in the carbonylation of methanol to acetic acid that where Rh is replaced by the more electron rich Ir metal center, the migratory/CO-insertion step is retarded[19] (i.e. the Monsanto *vs.* the "Cativa" process). In the case of tertiary phosphines with similar Tolman angles, the expected order, i.e. an increase in the rate of CO-insertion with an increase in Lewis basicity of the phosphine is found. There is a marked decrease in the rate of CO-insertion when the PPh_3 ligand is replace by $AsPh_3$ in [Rh(tavk)(CO)(PPh_3)], which is expected because more steric demand around the metal center should favour the formation of the five coordinated acyl compared to the six coordinated alkyl complex.

The rate of CO-insertion increase with higher temperatures for all the complexes studied. An interesting observation is that for the [Rh(dmavk)(CO)(PPh_3)] with a large equilibrium constant for the oxidative addition step, higher temperatures has no or little

effect on the magnitude of K_1. On the other hand for the [Rh(tavk)(CO)(PPh_3)] complex with a small K_1 for the equilibrium step, an increase in temperature led to a decrease in K_1. This probably is a result of the fact that high temperatures increase the bond breaking process for Rh-CH_3 and Rh-I due to the faster vibration of the atoms connected in these bonds. This bond breaking process for two adjacent moieties which has the possibility to coordinate is required for the reductive elimination thus, leading to an increase in k_{-1}, and hence a smaller K_1.

6.6 CORRELATION OF THE REACTION BETWEEN IODOMETHANE AND THE [Rh(avk)(CO)(XR_3)] TYPE COMPLEXES AS WELL AS WITH OTHER RELATED COMPLEXES

The electronic and steric manipulation of the [Rh(avk)(CO)(XR_3)] type complexes (X = P or As; R = Ph_3 and its related substituted phenyl analogues) towards oxidative addition and migratory CO-insertion is summarized in Table 6.9.

The electronic manipulation was achieved by firstly the introduction of electron/donating substituents (CH_3/CF_3) on the bidentate ligand and secondly by the interchanging triphenyl phosphine and its derivatives [PPh_3 *vs.* P(*p*-Cl-Ph)$_3$ *vs.* P(*p*-OMe-Ph)$_3$]. Steric manipulation was achieved by interchanging PPh_3 with $AsPh_3$.

From the results in Table 6.9 it is clear that electron withdrawing groups on the phenyl substituent of the P atom results in a decrease in the rate of oxidative addition and an increase in the rate of reductive elimination. A simultaneous decrease in the magnitude of the equilibrium constant was observed. For the CO-insertion step, the introduction of substituents with different electronic properties did not have such a dramatic effect on the reaction rate as observed in the case of oxidative addition.

Table 6.9 Reaction of [Rh(avk)(CO)(XR_3)] and iodomethane in acetone at 25 °C.

Complex	Rate Constants			K_1
	OA	RE	CI	
	$10^2k_1(M^{-1}s^{-1})$	$10^2k_{-1}(s^{-1})$	$10^4k_2(s^{-1})$	M^{-1}
[Rh(dmavk)(CO)(PPh_3)]	23(1)	0 [a]	12.0(6)	81(15) [b]
[Rh(tavk)(CO)(PPh_3)]	5.2(4)	1.1(2)	20.6(7)	5.0(5) [b]
[Rh(dmavk)(CO)(P(*p*-Cl-Ph)$_3$)]	8.7(4)	0.35(8)	7.2(1)	23(3) [b]
[Rh(tavk)(CO)(P(*p*-OMe-Ph)$_3$)]	13.2(4)	1.9(2)	21.3(4)	5.4(4) [b]
[Rh(dmavk)(CO)($AsPh_3$)]	-	-	1.32	>100 [b]
[Rh(tavk)(CO)($AsPh_3$)]	7.6(3)	0 [a]	-	>100

[a] Zero within experimental error. Fix as = 0 [b] Calculated from Eq. 6.2.
[c] Could not be calculated: Eq. 6.2 simplifies to $k_{obsd} = k_2$.

Replacing the PPh_3 ligand by $AsPh_3$ leads to an increase in the rate of oxidative addition and a decrease in the rate of reductive elimination, resulting in an increase in the equilibrium constant for this step. A significant (*ca.* one order of magnitude) decrease in CO-insertion was observed from PPh_3 to $AsPh_3$ ($12.0(6)\times10^{-4}$ compared to 1.32×10^{-4} s^{-1}).

Correlations between the [Rh(dmavk)(CO)(PPh_3)] and other [Rh(BID)(CO)(PPh_3)] complexes are presented in the following paragraphs. In par. 5.8 the correlation between structural (Rh-P bond distances) and NMR data (^1J(PRh) and $\delta(^{31}P)$) for selected Rh(I) complexes was already highlighted. These results indicated that an increase in Rh-P bond distance (and simultaneous decrease in ^1J(PRh) and $\delta(^{31}P)$) was observed for an increase in the *trans*-influence of the ligand *trans* to the P-atom. This lead to the conclusion that the Rh-P bond strength might be an indication of the relative electron density on the rhodium center originating from the electron donating capability of the *trans*-P-Rh-ligand. Thus, the results obtained in this study and other related work done in this laboratory are correlated below.

The structural, NMR and the reactivity towards oxidative addition [Rh(L,L'-BID)(CO)(PPh_3)] complexes are given in Table 6.10 and these results are graphically displayed in Figures 6.18(a) and (b).

Table 6.10 Rate and equilibrium data for the oxidative addition step to [Rh(L,L'-BID)(CO)(PX_3)] complexes in $CHCl_3$ at 25 °C.

No	L,L'-BID	L	L'	Ring size	Rh-P	^1J(PRh)	10^3k_1 M^{-1} s^{-1}	Ref
1	cupf	O	O	5	2.232(2)	171.1	1.2	**[20,21,22]**
2	acac	O	O	6	2.244(3)	175.7	24	**[20,21,1]**
3	ox	N	O	5	2.261(2)	161.6	30	**[20,21,23]**
4	pic	N	O	5	2.262(2)	161.9	10	**[20,21]**
5	cacsm	S	N	6	2.268(1)	144.6	56	**[12]**
6	dmavk	O	N	6	2.275(1)	148.0	114	**This work**
7	hpt	S	O	5	2.278(1)	157.1	51	**[24,18]**
8	hacsm	N	S	6	2.283(1)	148.9	27	**[21,25]**

L'=ligand *trans* to the P-atom.

In both figures the x-axis represent the rate of oxidative addition and the y-axis the Rh-P bond distance and the coupling constant, ^{1}J(PRh) in Fig. (a) and (b) respectively. The red columns represent the O,O-BID, the purple the N,O-BID, the light blue the O,S-BID and the yellow the N,S-BID ligands.

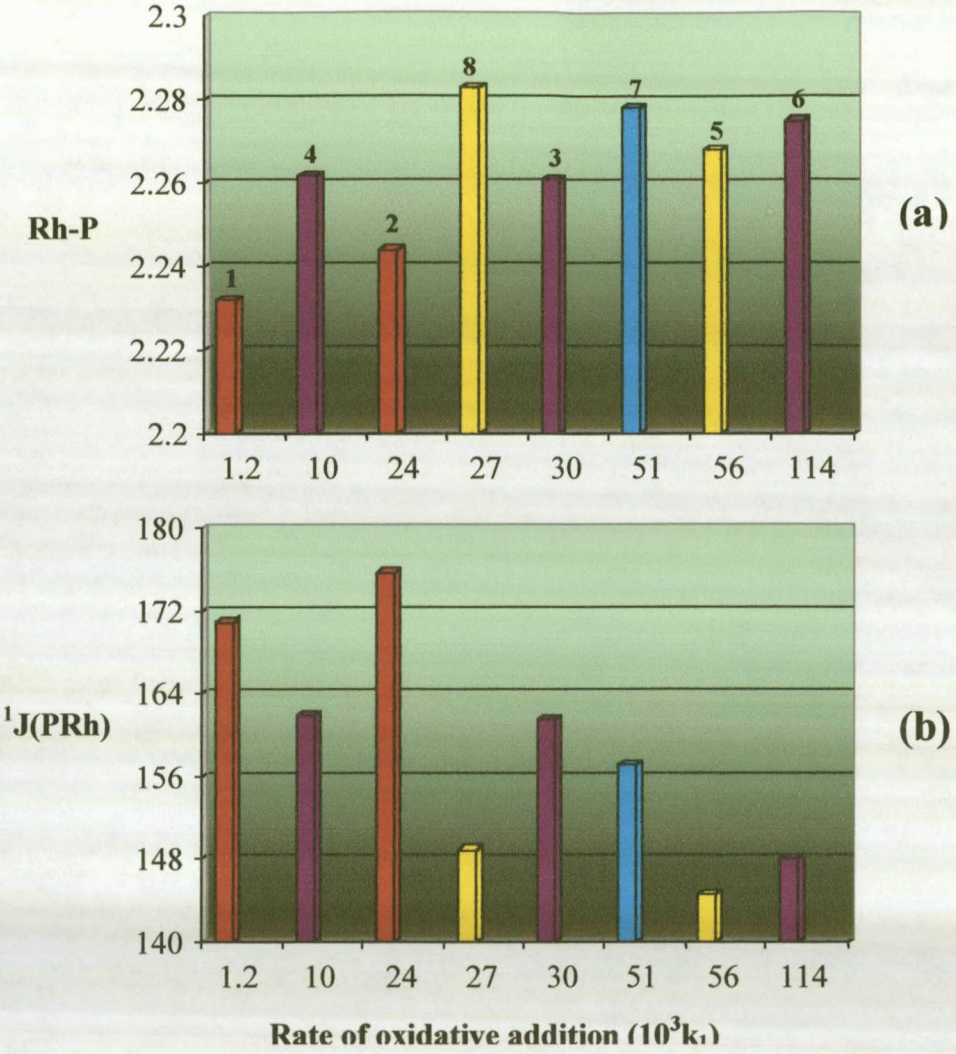

Fig. 6.18 Correlations between oxidative addition rate and Rh-P, ^{1}J(PRh) correlations (Results in Table 6.10).

In general, for the same donor atom BID-ligand system an increase in the rate of iodomethane oxidative addition is observed with an increase in Rh-P bond distance (Fig. 6.18(a)), indicating an increase in electron density on the metal center. Although the trend is by no means convincing, one has to take into account that these BID-ligands constitute different bite angle sizes and steric groups on donor atoms (e.g. the cacsm-ligand). Also, in the case of these cacsm and hacsm complexes, although both complexes contains the N,S-BID ligand, the donor atom *trans* to the P-atom is N and S respectively,

which should have an effect on the Rh-P bond distance due the difference in *trans* influence for N and S.

The relationship between the rate of oxidative addition and NMR parameters, see Fig. 6.18(b) shows a better defined trend, i.e. k_1 increases with a decrease in $^1J(PRh)$. It is important to note that in this case, both parameters (k_1 and $^1J(PRh)$) are measured in solution compared to the solid state Rh-P bond distance obtained from X-ray crystallography.

This kinetic study has (together with the structural results presented in Chapter 5) further confirmed that the basic mechanism for the [Rh(L,L'-BID)(CO)(PR_3)] complexes is consistent with the mechanism proposed in Fig. 6.1. Successful manipulations (both electronic and steric) has been achieved for the Rh(I)-center towards oxidative addition and CO-insertion. Furthermore, this work contributed towards a more fundamental understanding of the intrinsic mechanism of the reactivity of [Rh(L,L'-BID)(CO)(PR_3)] complexes in important industrial applicable reactions.

REFERENCES

1. Basson, S.S., Leipoldt, J.G., and Nel, J.T. 1984, *Inorg. Chim. Acta*, **86**, 167.
2. Basson, S.S., Leipoldt, J.G., Roodt, A., Venter, J.A., and van der Walt, T.J., 1986 *ibid.*, **119**, 35.
3. Basson, S.S., Leipoldt, J.G., Roodt, A., and Venter, J.A. 1987, *ibid.*, **128**, 31.
4. Leipoldt, J.G., Basson, S.S. and Botha, L.J. 1990, *ibid.*, **168**, 215
5. Leipoldt, J.G., Steynberg, E.C., and van Eldik, R. 1987, *Inorg. Chem.*, **26**, 3068.
6. Van Zyl, G.J., Lamprecht, G.J., Leipoldt, J.G., and Swaddle, T.W. 1988, *Inorg. Chim. Acta*, **143**, 223.
7. Leipoldt, J.G., Lamprecht, G.J., and van Zyl, G.J., 1985, *ibid.*, **96**, L31.
8. Van Zyl, G.J., Lamprecht, G.J., and Leipoldt, J.G. 1985, *ibid.*, **102**, L1.
9. Lamprecht, G.J., Leipoldt, J.G., and van Zyl, G.J. 1985, *ibid.*, **97**, 31.
10. Van Aswegen, K.G., Leipoldt, J.G., Potgieter, I.M., Lamprecht, J.G., Roodt, A., and Van Zyl, G.J. 1991, *Transition Met. Chem.*, **16**, 369
11. Steyn, G.J.J., Roodt, A., and Leipoldt, J.G. 1993, Rhodium Express, **0**, 11.
12. Steyn, G.J.J., Ph.D.-Thesis, 1994, Free State University, Bloemfontein, South Africa.
13. Galding, M.R., Cherkasova, T.G., Osetrova, L.V., Varshavsky, Y.S., *Rhodium Ex.*, 1993, **1**, 14.
14. The Olis Kinfit routines, On-line Instrument Systems Inc., Jefferson, U.S.A., 1987.
15. Minsq, Least Squares Parameter Optimisation V 3.12, Micromath, 1990.
16. Micromath Scientist for Windows, Version 2.0, 1986-2995.
17. Erasmus, J.J.C., PhD-Thesis, University of the Free State, 1997.
18. Preston, H., PhD-Thesis, University of the Free State, 1993.
19. Maitlis, P.M., Haynes, A., Sunley, G.J., and Howards, M.J. 1996, *J. Chem. Soc. Dalton Trans.*, 2187.
20. Graham, D.E., Lamprecht, G.J., Potgieter, I.M., Roodt, A., and Leipoldt, J.G. 1991, *Transition Met. Chem.*, **16**, 193.

21. Steyn, G.J.J., Roodt, A., Poletaeva, I., and Varshavsky, Y.S1997. , *J. Organomet. Chem.*, **536/7**, 797.

22. Basson, S.S., Leipoldt, J.G., Roodt, A., and Venter, J.A. 1990, *Inorg. Chim. Acta*, **128**, 31

23. Van Aswegen, K.G., 1990, M.Sc.-Thesis, Free State University, Bloemfontein, South Africa.

24. Basson, S.S., Leipoldt, J.G., Roodt, A., and Preston, H. 1991, *Acta Cryst.*, **C47**, 1961.

25. Steyn, G.J.J., Roodt, and Leipoldt, J.G. 1993, *Rhodium Ex.*, **1**, 25.

CHAPTER 7

Evaluation of this study

The relevance and success of this study are briefly discussed (Section 7.1) in terms of the pre-set aims as outlined in Chapter 1, while some future research aspects are presented in Section 7.2.

7.1 SCIENTIFIC RELEVANCE

Previously, oxidative addition of iodomethane to [Rh(L,L'-BID)(CO)(PR_3)] complexes (L,L' = O,O-BID, O,N-BID (five membered), O,S-BID and N,S-BID ligands) was studied mechanistically in this laboratory and the mechanisms presented, varied largely. Thus, the research program was extended by the inclusion of the avk-type ligands into the square complexes of Rh(I), i.e. [Rh(N,O-BID)(CO)(PR_3)].

The kinetic data (UV/VIS, IR and ^{31}P-NMR) showed a two-step mechanism for the [Rh(avk)(CO)(PR_3)] complexes towards oxidative addition as presented below.

$$[Rh(L,L'\text{-BID})(CO)(PR_3)] + CH_3I \underset{k_{-1}}{\overset{k_1}{\rightleftharpoons}} [Rh(L,L'\text{-BID})(I)(CH_3)(CO)(PPh_3)]$$

alkyl

$$\downarrow k_2$$

$$[Rh(L,L'\text{-BID})(I)(COCH_3)(PR_3)]$$

acyl

Further evidence that the above mechanism holds for [Rh(avk)(CO)(PR_3)] complexes came from the crystal structure determination of [Rh(dmavk)(CO)(PPh_3)], [Rh(dmavk)(I)(CH_3)(CO)(PPh_3)] and [Rh(dmavk)(I)($COCH_3$)(PPh_3)]. The structure of

[Rh(dmavk)(I)(CH_3)(CO)(PPh_3)] showed that the mode of iodomethane addition to [Rh(avk)(CO)(PPh_3)] is *trans*, indicating an S_N2 two step mechanism. However, as was pointed out earlier in Chapter 3, one has to be cautious since isomerization of *cis* addition products can also lead to *trans* products. The ^{31}P-NMR study on [Rh(dmavk)(CO)(PPh_3)] and [Rh(dmavk)(I)(CH_3)(CO)(PPh_3)] indicated a decrease in ^{1}J(PRh) as the Rh-P bond length (determined by X-ray crystallography) increases, thus indicating a decrease in electron density on rhodium. These results correlate well with similar studies performed on different [Rh(L,L'-BID)(CO)(PPh_3)] complexes in this laboratory. Of specific noteworthy mention is the fact that the starting compounds, intermediate alkyl and final acyl species could for the first time be structurally characterized.

The fact that N has a greater *trans* influence than O in these avk ligands was also confirmed by the structure determination of [Rh(dmavk)(CO)(PPh_3)] and [Rh(dmavk)(CO)($AsPh_3$)], wherein both the PPh_3 and $AsPh_3$ ligand were *trans* to nitrogen (thus the expected substitution pattern). Also, retention of configuration (*trans*-Rh-P) was observed for the oxidative addition products of [Rh(dmavk)(CO)(PPh_3)]. Furthermore, it was found that the Rh-As bond is significantly longer than the Rh-P bond, indicating a less steric demand around the Rh(I) metal.

The effect of different factors (e.g. electronic, steric, etc.) on the reactivity of the Rh(I) center was also kinetically studied. Electron density manipulation on the metal center was firstly accomplished by the introduction of different substituents (CF_3 in the place of CH_3) on the bidentate ligand, i.e. for the [Rh(tavk)(CO)(PPh_3)] and [Rh(dmavk)(CO)(PPh_3)] complexes respectively, as well as different functionalised phosphine ligands. The influence of steric ligands on the Rh(I) reactivity was addressed by substituting As by P in PPh_3. In general, the kinetic observations can be summarised as follow:

(1) Electron withdrawing ligands decrease the rate of oxidative addition and increase the rate of reductive elimination, thus decreasing the equilibrium constant (K_1) for alkyl formation. Although no great dependence of the rate of CO-insertion/methyl (k_2)

migration was observed on the basicity of the Rh(I) complex, it appeared that k_2 decreases with increasing basicity of the metal complex.

(2) Less steric demand on the metal center (i.e. replacing P with As in PPh_3) increase the rate of oxidative addition and the magnitude of K_1. However, the rate for the CO-insertion step is deactivated considerably.

The structural and NMR data and the reactivity towards oxidative addition for [Rh(dmavk)(CO)(PPh_3)] were correlated with other [Rh(L,L'-BID)(CO)(PPh_3)] complexes. These results indicated that in general the rate of oxidative addition (k_1) increases with an increase in Rh-P bond distance and a decrease in ^1J(PRh). Thus, it was further illustrated that knowledge of NMR data can give an indication of the reactivity of these [Rh(L,L'-BID)(CO)(PPh_3)] complexes towards oxidative addition.

7.2 FUTURE RESEARCH

Although the mechanism for the reaction between iodomethane and [Rh(N,O-BID)(CO)(PR_3)] complexes was established as proceeding according to the one presented above, and the limited solvent study indicated a polar transition state, for the initial oxidative addition step, a high pressure study of this reaction would provide valuable information about the transition state. Since two reaction steps can be monitored (i.e., oxidative addition and subsequent Rh(III)-acyl formation) the high pressure study can also be expanded to the second reaction.

Further manipulation of electron density on the rhodium(I) center may be accomplished by the introduction of alkyl or aryl groups on the nitrogen atom. This will also allow the introduction of steric groups close to the metal.

Substituting CH_3 with CF_3 on the bidentate ligand, i.e. yielding the [Rh(dmavk)(CO)(PPh_3)] and [Rh(tavk)(CO)(PPh_3)] complexes respectively, showed that during oxidative addition with iodomethane, the reductive elimination step is significantly enhanced. Also, temperature studies showed that the equilibrium constant

increases with temperature for [Rh(dmavk)(CO)(PPh_3)], whereas in the case of [Rh(tavk)(CO)(PPh_3)], the opposite was observed, probably indicating that electron withdrawing ligands increase the rate of reductive elimination. Further studies could include a more detailed temperature and solvent study to investigate these effects.

From the ^{13}C- and ^{31}P-NMR study, it is clear that two isomers of the [Rh(avk)(CO)(PR3)] complexes are present in solution and the relative rates of reaction of these isomers with iodomethane could be explored. The interconversion rates, as well as factors influencing this can also be investigated in future.

CHAPTER 8

Supplementary data

8.1 Supplementary data for structure determinations

Supplementary data for the structures discussed in Chapter 5, are given in this section. For each structure three tables are given under a heading consisting of the formula of the complex for which the structure was studied, containing: (1) a table containing all bond distances and angles, (2) a table containing the anisotropic thermal parameters and (3) a table with the hydrogen coordinates.

8.1.1 [Rh(dmavk)(CO)(PPh_3)], paragraph 5.3

Table 8.1
Interatomic bond distances (Å) and angles (°) for [Rh(dmavk)(CO)(PPh_3)] with Esd's in parentheses.

Rh-C(6)	1.784(5)	C(11)-C(16)	1.4184(14)
Rh-N(1)	2.045(4)	C(3)-C(2)	1.388(8)
Rh-O(1)	2.044(3)	C(3)-C(5)	1.512(8)
Rh-P(1)	2.2751(13)	C(16)-C(15)	1.383(8)
P(1)-C(11)	1.811(3)	C(21)-C(26)	1.377(7)
P(1)-C(31)	1.836(5)	C(15)-C(14)	1.367(11)
P(1)-C(21)	1.843(5)	C(36)-C(35)	1.389(8)
O(1)-C(3)	1.282(6)	C(34)-C(33)	1.357(10)
C(22)-C(21)	1.371(8)	C(34)-C(35)	1.381(11)
C(22)-C(23)	1.383(9)	C(23)-C(24)	1.352(11)
C(31)-C(36)	1.368(7)	C(24)-C(25)	1.360(12)
C(31)-C(32)	1.368(7)	C(25)-C(26)	1.378(9)
C(1)-N(1)	1.302(6)	C(13)-C(14)	1.353(9)
C(1)-C(2)	1.396(7)	C(13)-C(12)	1.379(8)
C(1)-C(4)	1.518(8)	C(6)-O(2)	1.142(6)
C(32)-C(33)	1.398(8)		
C(11)-C(12)	1.373(7)		
C(6)-Rh-N(1)	92.6(2)	C(16)-C(11)-P(1)	119.95(14)
C(6)-Rh-O(1)	179.3(2)	O(1)-C(3)-C(2)	126.4(5)
N(1)-Rh-O(1)	87.43(15)	O(1)-C(3)-C(5)	114.6(5)
C(6)-Rh-P(1)	90.3(2)	C(2)-C(3)-C(5)	119.1(5)
N(1)-Rh-P(1)	177.12(12)	C(15)-C(16)-C(11)	119.0(4)
O(1)-Rh-P(1)	89.69(11)	C(22)-C(21)-C(26)	118.5(5)
C(11)-P(1)-C(31)	102.9(2)	C(22)-C(21)-P(1)	123.3(4)
C(11)-P(1)-C(21)	103.6(2)	C(26)-C(21)-P(1)	118.2(4)
C(31)-P(1)-C(21)	103.8(2)	C(3)-C(2)-C(1)	125.0(4)
C(11)-P(1)-Rh	116.39(15)	C(14)-C(15)-C(16)	121.4(6)
C(31)-P(1)-Rh	114.1(2)	C(1)-N(1)-Rh	128.5(4)
C(21)-P(1)-Rh	114.4(2)	C(31)-C(36)-C(35)	121.1(6)
C(3)-O(1)-Rh	127.9(3)	C(33)-C(34)-C(35)	119.4(6)
C(21)-C(22)-C(23)	120.3(7)	C(24)-C(23)-C(22	121.2(7)
C(36)-C(31)-C(32)	118.7(5)	C(36)-C(35)-C(34)	119.8(6)
C(36)-C(31)-P(1)	118.6(4)	C(25)-C(24)-C(23)	118.8(7)
C(32)-C(31)-P(1)	122.7(4)	C(24)-C(25)-C(26)	121.2(7)
N(1)-C(1)-C(2)	124.5(5)	C(14)-C(13)-C(12)	121.1(6)
N(1)-C(1)-C(4)	117.7(5)	C(34)-C(33)-C(32)	120.4(6)
C(2)-C(1)-C(4)	117.8(4)	C(11)-C(12)-C(13)	121.0(5)
C(31)-C(32)-C(33)	120.6(5)	C(21)-C(26)-C(25)	120.1(6)
C(12)-C(11)-C(16)	118.1(3)	C(13)-C(14)-C(15)	119.4(6)
C(12)-C(11)-P(1)	121.7(3)	O(2)-C(6)-Rh	177.9(5)

Table 8.2
Anisotropic displacement parameters ($Å^2 \times 10^3$) for [Rh(dmavk)(CO)(PPh_3)].

	U11	U22	U33	U23	U13	U12
Rh	43(1)	44(1)	48(1)	2(1)	8(1)	2(1)
P(1)	40(1)	43(1)	40(1)	-1(1)	-1(1)	1(1)
O(1)	53(2)	53(2)	65(2)	2(2)	18(2)	6(2)
C(22)	90(4)	56(3)	69(3)	-12(3)	-22(3)	2(3)
C(31)	45(2)	53(3)	46(2)	-3(2)	-5(2)	8(2)
C(1)	44(2)	57(3)	49(3)	7(2)	-2(2)	-2(2)
C(32)	63(3)	59(3)	70(3)	9(3)	-17(3)	1(3)
C(4)	85(4)	61(4)	90(4)	5(3)	30(4)	-8(3)
C(11)	48(2)	34(2)	48(3)	6(2)	4(2)	-2(2)
C(3)	49(3)	66(3)	53(3)	-2(3)	7(2)	8(2)
C(16)	52(3)	61(3)	65(3)	1(3)	2(2)	-5(3)
C(21)	50(2)	53(3)	46(3)	-8(2)	-10(2)	6(2)
C(2)	45(2)	66(3)	50(3)	3(3)	2(2)	-1(2)
C(15)	44(3)	86(4)	123(6)	9(5)	14(3)	0(3)
N(1)	52(2)	51(2)	71(3)	7(2)	16(2)	-1(2)
C(36)	54(3)	89(4)	87(4)	36(4)	-12(3)	-7(3)
C(34)	82(5)	103(6)	91(5)	19(5)	-28(4)	28(4)
C(23)	91(5)	66(4)	106(6)	-23(4)	-36(4)	5(4)
C(35)	54(3)	123(6)	116(6)	37(5)	-27(4)	5(4)
C(24)	90(5)	124(7)	88(6)	-54(6)	-34(5)	22(5)
C(25)	101(5)	171(9)	45(3)	-26(5)	-4(3)	8(6)
C(13)	100(5)	83(4)	51(3)	-5(3)	19(3)	10(4)
C(33)	104(5)	65(4)	89(5)	17(4)	-30(4)	4(4)
C(12)	74(4)	74(4)	47(3)	-5(3)	4(3)	-1(3)
C(26)	73(3)	98(4)	42(3)	-3(3)	7(2)	-13(3)
C(14)	94(5)	74(4)	93(5)	10(4)	52(4)	8(4)
C(5)	81(5)	80(5)	130(7)	-12(4)	48(5)	15(4)
C(6)	70(3)	41(3)	86(4)	9(3)	27(3)	2(2)
O(2)	105(3)	67(3)	138(4)	6(3)	73(3)	14(3)

Table 8.3
Hydrogen coordinates ($x10^{-3}$) and isotropic displacement parameters ($Å^2x10^3$) for [Rh(dmavk)(CO)(PPh_3)]

	x	y	Z	Ueq
H(22)	-61(4)	-4586(6)	160(4)	97(5)
H(32)	816(3)	-4596(6)	1234(4)	97(5)
H(41)	2923(26)	5085(80)	-1411(24)	97(5)
H(42)	2082(25)	5413(69)	-1039(29)	97(5)
H(43)	2833(28)	5352(70)	-478(26)	97(5)
H(16)	-970(2)	-1635(11)	199(3)	97(5)
H(2)	3332(3)	2379(7)	-1381(3)	97(5)
H(15)	-2055(3)	-1468(9)	1095(5)	97(5)
H(36)	2438(3)	-1269(8)	770(4)	97(5)
H(34)	3103(4)	-5148(10)	1993(5)	97(5)
H(23)	-400(4)	-6098(9)	-965(5)	97(5)
H(35)	3421(4)	-2711(10)	1447(5)	97(5)
H(24)	-142(5)	-5241(12)	-2272(6)	97(5)
H(25)	478(4)	-2861(12)	-2458(4)	97(5)
H(13)	-571(4)	-1319(8)	3006(4)	97(5)
H(33)	1809(4)	-6088(9)	1877(4)	97(5)
H(12)	530(4)	-1508(7)	2149(3)	97(5)
H(26)	860(3)	-1354(9)	-1348(3)	97(5)
H(14)	-1856(4)	-1327(8)	2490(5)	97(5)
H(51)	3510(31)	-1286(62)	-891(26)	97(5)
H(52)	3135(32)	-1371(61)	-1791(27)	97(5)
H(53)	3838(24)	-152(65)	-1594(28)	97(5)
H(1)	1364(24)	4013(20)	-279(32)	93(24)

8.1.2. [Rh(dmavk)(CO)($AsPh_3$)], paragraph 5.4

Table 8.4
Interatomic bond distances (Å) and angles (°) for [Rh(dmavk)(CO)($AsPh_3$)] with Esd's in parentheses.

Rh-C(6)	1.793(5)	C(6)-O(2)	1.151(5)
Rh-O(1)	2.026(3)	O(1)-C(3)	1.288(5)
Rh-N(1)	2.032(4)	N(1)-C(1)	1.300(6)
Rh-As	2.3834(6)	C(4)-C(1)	1.503(6)
As-C(31)	1.944(4)	C(1)-C(2)	1.403(7)
As-C(21)	1.944(4)	C(2)-C(3)	1.363(6)
As-C(11)	1.954(4)	C(3)-C(5)	1.503(7)
C(6)-Rh-O(1)	177.42(17)	O(2)-C(6)-Rh	178.3(4)
C(6)-Rh-N(1)	93.02(19)	C(3)-O(1)-Rh	127.3(3)
O(1)-Rh-N(1)	88.50(15)	C(1)-N(1)-Rh	127.4(4)
C(6)-Rh-As	93.11(14)	N(1)-C(1)-C(2)	123.8(4)
O(1)-Rh-As	85.20(8)	N(1)-C(1)-C(4)	119.3(5)
N(1)-Rh-As	172.12(12)	C(2)-C(1)-C(4)	116.9(4)
O(1)-C(3)-C(5)	113.7(4)	C(3)-C(2)-C(1)	126.4(4)
C(2)-C(3)-C(5)	120.5(4)	O(1)-C(3)-C(2)	125.8(4)

Table 8.5
Anisotropic displacement parameters ($Å^2 \times 10^3$) for [Rh(dmavk)(CO)($AsPh_3$)].

	U11	U22	U33	U23	U13	U12
Rh	38(1)	53(1)	41(1)	19(1)	4(1)	13(1)
As	36(1)	48(1)	39(1)	20(1)	7(1)	14(1)
C(6)	36(2)	73(3)	63(3)	29(3)	3(2)	7(2)
O(2)	61(2)	129(3)	105(3)	78(3)	17(2)	3(2)
O(1)	48(2)	66(2)	51(2)	31(2)	2(1)	11(2)
N(1)	44(2)	59(2)	47(2)	16(2)	3(2)	14(2)
C(4)	65(3)	89(4)	71(3)	20(3)	-14(3)	25(3)
C(1)	53(3)	64(3)	43(2)	13(2)	2(2)	30(2)
C(2)	68(3)	62(3)	43(3)	22(2)	-1(2)	25(3)
C(3)	62(3)	56(3)	46(2)	21(2)	10(2)	21(2)
C(5)	91(4)	86(4)	71(3)	45(3)	18(3)	32(3)
C(11)	38(2)	49(2)	41(2)	15(2)	9(2)	14(2)
C(12)	52(3)	68(3)	69(3)	36(2)	21(2)	27(2)
C(13)	54(3)	73(3)	86(4)	38(3)	23(3)	31(3)
C(14)	52(3)	74(3)	85(4)	25(3)	30(3)	29(3)
C(15)	82(4)	140(5)	65(3)	50(4)	45(3)	46(4)
C(16)	65(3)	122(4)	56(3)	44(3)	26(3)	44(3)
C(21)	37(2)	50(2)	37(2)	22(2)	6(2)	16(2)
C(22)	46(2)	53(2)	56(3)	24(2)	13(2)	23(2)
C(23)	53(3)	59(3)	58(3)	28(2)	1(2)	17(2)
C(24)	70(3)	49(2)	54(3)	20(2)	3(2)	27(2)
C(25)	69(3)	71(3)	68(3)	32(3)	27(3)	47(3)
C(26)	46(3)	66(3)	61(3)	33(2)	18(2)	25(2)
C(31)	38(2)	53(2)	42(2)	24(2)	11(2)	20(2)
C(32)	47(2)	60(3)	50(2)	28(2)	14(2)	22(2)
C(33)	53(3)	81(3)	45(2)	32(2)	13(2)	25(2)
C(34)	73(3)	89(4)	68(3)	53(3)	28(3)	43(3)
C(35)	65(3)	68(3)	85(4)	50(3)	25(3)	31(3)
C(36)	54(3)	59(3)	57(3)	28(2)	18(2)	26(2)

Table 8.6
Hydrogen coordinates ($x10^{-3}$) and isotropic displacement parameters ($Å^2x10^3$) for [Rh(dmavk)(CO)($AsPh_3$)]

	x	y	Z	Ueq
H(1)	1890(5)	5310(5)	4450(5)	69(17)
H(1A)	776	5073	1897	82(3)
H(1B)	545	6474	2656	82(3)
H(1C)	98	5231	3027	82(3)
H(3)	3120(5)	7610(5)	2810(4)	66(13)
H(5A)	6498	9907	4551	82(3)
H(5B)	5373	9290	3240	82(3)
H(5C)	6502	8611	3379	82(3)
H(12)	9475	7772	8409	82(3)
H(13)	11630	7928	7863	82(3)
H(14)	11902	8152	6098	82(3)
H(15)	10078	8319	4901	82(3)
H(16)	7884	8124	5405	82(3)
H(22)	9199	10698	8461	82(3)
H(23)	9650	13066	9703	82(3)
H(24)	7836	13697	10423	82(3)
H(25)	5550	12001	9864	82(3)
H(26)	5034	9625	8582	82(3)
H(32)	7795	9301	10252	82(3)
H(33)	8056	8588	11804	82(3)
H(34)	7219	6180	11248	82(3)
H(35)	6213	4517	9174	82(3)
H(36)	5977	5227	7614	82(3)

8.1.3 [Rh(dmavk)(I)(CH_3)(CO)(PPh_3)].CH_3I, paragraph 5.5

Table 8.7

Selected Interatomic Bond Distances (Å) and Angles(°) for [Rh(dmavk)(I)(CH_3)(CO)(PPh_3)].CH_3I with Esd'd in Parentheses

Rh-C6	1.850(13)	C21-C26	1.39(2)
Rh-O1	2.035(7)	C21-C22	1.41(2)
Rh-N1	2.042(11)	C22-C23	1.39(2)
Rh-C7	2.069(12)	C23-C24	1.34(2)
Rh-P	2.356(3)	C24-C25	1.36(2)
Rh-I1	2.8489(12)	C25-C26	1.38(2)
I2-C8	1.577(15)	C31-C36	1.35(2)
P-C21	1.824(11)	C31-C32	1.39(2)
P-C31	1.831(11)	C32-C33	1.38(2)
P-C11	1.830(10)	C33-C34	1.35(2)
O1-C3	1.287(14)	C34-C35	1.37(2)
N1-C1	1.27(2)	C35-C36	1.43(2)
C11-C12	1.37(2)	C1-C2	1.43(2)
C11-C16	1.37(2)	C1-C4	1.52(2)
C12-C13	1.37(2)	C2-C3	1.37(2)
C13-C14	1.37(2)	C3-C5	1.45(2)
C14-C15	1.35(2)	C6-O2	1.116(15)
C15-C16	1.38(2)		
C6-Rh-O1	175.0(5)	C3-O1-Rh	126.1(7)
C6-Rh-N1	91.6(5)	C1-N1-Rh	127.0(10)
O1-Rh-N1	89.5(4)	C12-C11-C16	118.7(11)
C6-Rh-C7	90.2(6)	C12-C11-P	119.2(9)
O1-Rh-C7	85.0(5)	C16-C11-P	121.9(9)
N1-Rh-C7	86.5(5)	C11-C12-C13	120.8(13)
C6-Rh-P	91.6(4)	C14-C13-C12	120.4(13)
O1-Rh-P	87.3(2)	C15-C14-C13	119.1(12)
N1-Rh-P	176.8(4)	C14-C15-C16	120.9(13)
C7-Rh-P	93.5(4)	C11-C16-C15	120.0(12)
C6-Rh-I1	90.8(4)	C26-C21-C22	118.9(11)
O1-Rh-I1	94.1(2)	C26-C21-P	121.1(9)
N1-Rh-I1	86.5(4)	C22-C21-P	119.9(9)
C7-Rh-I1	172.9(4)	C23-C22-C21	118.6(12)
P-Rh-I1	93.49(7)	C24-C23-C22	122.1(13)
C21-P-C31	104.6(5)	C23-C24-C25	118.6(13)
C21-P-C11	102.2(5)	C26-C25-C24	122.9(14)
C31-P-C11	102.9(5)	C25-C26-C21	118.7(12)
C21-P-Rh	113.9(4)	C36-C31-C32	119.0(12)
C31-P-Rh	114.9(4)	C36-C31-P	123.6(10)
C11-P-Rh	116.7(4)		

Table 8.8
Anisotropic displacement parameters ($Å^2 \times 10^3$) for $[Rh(dmavk)(I)(CH_3)(CO)(PPh_3)].CH_3I$.

	U11	U22	U33	U23	U13	U12
Rh	34(1)	41(1)	32(1)	-7(1)	0(1)	-15(1)
I(1)	39(1)	47(1)	56(1)	-8(1)	-2(1)	-9(1)
I(2)	128(2)	250(3)	140(2)	-69(2)	17(1)	-49(2)
P	32(1)	35(2)	32(1)	-4(1)	-3(1)	-11(1)
O(1)	53(5)	55(5)	37(4)	-18(4)	2(4)	-21(4)
N(1)	43(6)	45(7)	53(7)	-13(6)	10(5)	-25(6)
C(8)	40(7)	22(6)	197(17)	-63(8)	-25(9)	-14(5)
C(11)	45(6)	33(6)	29(6)	-6(5)	0(5)	-5(5)
C(12)	64(8)	84(10)	42(7)	-7(7)	0(6)	-40(8)
C(13)	108(13)	105(13)	39(8)	5(8)	4(8)	-67(11)
C(14)	85(10)	54(8)	38(7)	0(6)	-13(7)	-13(7)
C(15)	54(8)	99(12)	45(8)	-10(8)	-11(6)	-21(8)
C(16)	44(7)	83(10)	45(7)	9(7)	-8(6)	-26(7)
C(21)	37(6)	42(7)	44(7)	-3(5)	1(5)	-6(5)
C(22)	43(7)	46(7)	52(7)	1(6)	0(6)	-12(6)
C(23)	41(7)	54(8)	67(9)	10(7)	-5(6)	-9(6)
C(24)	75(10)	30(7)	88(11)	-10(7)	-12(9)	3(7)
C(25)	105(13)	48(9)	87(11)	-31(8)	-18(10)	-7(9)
C(26)	74(9)	44(8)	58(8)	-20(6)	-21(7)	-3(7)
C(31)	42(7)	57(8)	27(5)	-4(5)	-4(5)	-25(6)
C(32)	52(8)	62(9)	100(11)	-37(8)	27(8)	-30(7)
C(33)	94(12)	79(11)	111(13)	-54(10)	38(10)	-59(10)
C(34)	80(11)	103(13)	49(8)	-22(8)	12(7)	-72(10)
C(35)	48(8)	106(14)	84(11)	37(10)	-25(8)	-42(9)
C(36)	41(7)	66(9)	69(9)	13(7)	-10(6)	-25(7)
C(1)	46(7)	43(7)	42(7)	-1(5)	3(5)	-8(6)
C(2)	49(7)	49(8)	67(9)	-6(6)	3(6)	-28(6)
C(3)	45(7)	54(7)	51(7)	-9(6)	-7(6)	-27(6)
C(4)	57(8)	70(10)	74(9)	-17(8)	21(7)	-25(7)
C(5)	103(12)	99(12)	65(9)	-25(8)	8(8)	-73(11)
C(6)	55(8)	84(10)	32(6)	-8(6)	-1(6)	-37(7)
C(7)	49(7)	56(8)	55(8)	9(6)	3(6)	-13(6)
O(2)	109(9)	175(13)	56(6)	-45(7)	5(6)	-96(9)

Table 8.9
Hydrogen coordinates ($x10^{-3}$) and isotropic displacement parameters ($Å^2x10^3$) for $[Rh(dmavk)(I)(CH_3)(CO)(PPh_3)].CH_3I$.

	x	y	z	U_{eq}
H(1)	9838(172)	6774(149)	5151(116)	64(63)
H(8A)	7952(70)	2592(65)	8806(24)	74(8)
H(8B)	9265(13)	1925(30)	9424(56)	74(8)
H(8C)	7998(73)	3100(38)	9794(36)	74(8)
H(12)	5360(15)	6148(15)	9152(9)	74(8)
H(13)	6048(18)	5401(17)	10692(9)	74(8)
H(14)	8035(16)	5575(13)	11190(9)	74(8)
H(15)	9329(15)	6474(16)	10130(9)	74(8)
H(16)	8709(13)	7131(14)	8559(9)	74(8)
H(22)	4060(12)	9193(12)	6414(9)	74(8)
H(23)	2501(13)	11315(13)	6627(10)	74(8)
H(24)	2519(16)	12323(13)	7942(12)	74(8)
H(25)	4270(18)	11348(14)	8978(12)	74(8)
H(26)	5870(15)	9247(13)	8837(9)	74(8)
H(32)	6981(15)	4655(14)	7075(11)	74(8)
H(33)	5777(19)	3280(17)	6899(12)	74(8)
H(34)	3412(17)	4089(18)	6924(9)	74(8)
H(35)	2220(15)	6236(19)	7291(11)	74(8)
H(36)	3445(13)	7635(14)	7525(10)	74(8)
H(2)	11143(13)	9094(13)	5939(9)	74(8)
H(4A)	11682(58)	8523(16)	4253(43)	74(8)
H(4B)	11491(48)	7221(76)	4017(31)	74(8)
H(4C)	12533(18)	7142(71)	4790(17)	74(8)
H(5A)	10151(87)	8939(28)	8195(20)	74(8)
H(5B)	9118(36)	10261(48)	7693(43)	74(8)
H(5C)	10704(60)	9807(76)	7410(30)	74(8)
H(7A)	6721(75)	9784(20)	6129(16)	74(8)
H(7B)	6141(45)	9164(22)	5390(53)	74(8)
H(7C)	7522(34)	9442(36)	5146(41)	74(8)

8.1.4 Rh(dmavk)(I)($COCH_3$)(PPh_3)]

Table 8.10
Interatomic bond distances (Å) and angles (°) for [Rh(dmavk)(I)($COCH_3$)($PPPh_3$)] with Esd's in parentheses.

Rh(1)-C(211)	1.82(3)	C(121)-C(236)	1.87(5)
Rh(1)-C(16)	1.943(14)	C(121)-C(232)	1.98(4)
Rh(1)-N(1)	2.021(9)	C(122)-C(123)	1.40(3)
Rh(1)-O(11)	2.054(10)	C(123)-C(124)	1.41(3)
Rh(1)-P(1)	2.254(4)	C(124)-C(125)	1.34(2)
Rh(1)-I(2)	2.323(3)	C(125)-C(126)	1.42(2)
Rh(1)-P(2)	2.590(12)	C(131)-C(136)	1.33(3)
Rh(1)-I(1)	2.690(2)	C(131)-C(132)	1.38(2)
I(1)-Rh(2)	2.240(3)	C(131)-C(26)	1.45(7)
I(1)-I(2)	2.718(4)	C(131)-O(22)	1.70(6)
P(1)-P(2)	0.883(14)	C(131)-P(2)	1.84(2)
P(1)-C(221)	1.22(3)	C(131)-Rh(2)	1.889(13)
P(1)-C(111)	1.833(12)	C(132)-C(133)	1.35(2)
P(1)-C(131)	1.842(13)	C(133)-C(134)	1.15(3)
P(1)-C(121)	1.861(12)	C(134)-C(135)	1.42(3)
P(1)-C(211)	1.97(2)	C(135)-C(136)	1.50(3)
P(1)-Rh(2)	2.704(5)	Rh(3)-C(421)	1.92(4)
N(1)-C(11)	1.28(2)	Rh(3)-C(36)	1.967(13)
O(11)-C(13)	1.25(2)	Rh(3)-O(31)	2.014(10)
O(11)-C(43)#1	1.89(5)	Rh(3)-N(3)	2.014(10)
O(12)-C(16)	1.17(2)	Rh(3)-I(4)	2.209(4)
O(12)-C(211)	1.65(3)	Rh(3)-P(3)	2.269(5)
C(11)-C(41)#1	0.83(4)	Rh(3)-C(422)	2.60(5)
C(11)-C(45)#1	1.02(5)	Rh(3)-P(4)	2.62(2)
C(11)-C(12)	1.29(2)	Rh(3)-I(3)	2.670(2)
C(11)-C(14)	1.49(2)	I(3)-Rh(4)	2.293(4)
C(11)-C(42)#1	1.67(6)	I(3)-I(4)	2.649(4)
C(12)-C(13)	1.42(2)	P(3)-P(4)	0.82(2)
C(13)-C(43)#1	0.76(4)	P(3)-C(411)	1.27(3)
C(13)-C(42)#1	1.15(5)	P(3)-C(331)	1.813(8)
C(13)-C(15)	1.57(2)	P(3)-C(311)	1.834(12)
C(13)-C(44)#1	1.70(6)	P(3)-C(321)	1.897(11)
C(16)-C(211)	1.29(2)	P(3)-C(421)	1.95(3)
C(16)-C(17)	1.50(2)	P(3)-Rh(4)	2.597(5)
C(16)-C(215)	1.76(3)	N(3)-C(31)	1.30(2)
C(111)-C(221)	1.05(3)	O(31)-C(33)	1.26(2)
C(111)-C(112)	1.35(2)	O(31)-C(23)#2	1.79(7)
C(111)-C(116)	1.41(2)	O(32)-C(36)	1.19(2)
C(111)-C(223)	1.79(3)	O(32)-C(421)	1.60(4)
C(111)-C(225)	1.94(3)	C(31)-C(21)#2	0.88(5)
C(112)-C(113)	1.36(2)	C(31)-C(22)#2	1.29(9)
C(113)-C(114)	1.37(2)	C(31)-C(32)	1.37(3)
C(114)-C(115)	1.33(2)	C(31)-C(34)	1.45(2)
C(115)-C(116)	1.37(2)	C(31)-C(24)#2	1.48(5)
C(121)-C(231)	0.92(4)	C(32)-C(33)	1.36(3)
C(121)-C(126)	1.31(2)	C(33)-C(35)	1.56(2)
C(121)-P(2)	1.35(2)	C(33)-C(22)#2	1.59(9)
C(121)-C(122)	1.41(2)	C(33)-C(25)#2	1.62(10)

C(33)-C(23)#2	0.63(6)	C(221)-C(226)	1.39
C(36)-C(421)	1.39(4)	C(222)-C(223)	1.39
C(36)-C(37)	1.41(2)	C(223)-C(224)	1.39
C(311)-C(411)	0.96(3)	C(224)-C(225)	1.39
C(311)-C(316)	1.38(2)	C(225)-C(226)	1.39
C(311)-C(312)	1.40(2)	C(231)-C(232)	1.39
C(311)-C(415)	1.75(3)	C(231)-C(236)	1.39
C(311)-C(413)	2.02(3)	C(232)-C(233)	1.39
C(312)-C(313)	1.43(2)	C(233)-C(234)	1.39
C(313)-C(314)	1.37(2)	C(234)-C(235)	1.39
C(314)-C(315)	1.40(2)	C(235)-C(236)	1.39
C(315)-C(316)	1.36(2)	Rh(4)-C(46)	1.62(7)
C(321)-C(431)	0.93(3)	Rh(4)-O(41)	1.87(7)
C(321)-P(4)	1.29(2)	Rh(4)-N(4)	2.05(3)
C(321)-C(326)	1.31(2)	Rh(4)-P(4)	2.290(13)
C(321)-C(322)	1.43(2)	Rh(4)-I(4)	2.703(4)
C(321)-C(436)	1.86(4)	P(4)-C(411)	1.77(3)
C(322)-C(323)	1.40(2)	P(4)-C(421)	1.84(4)
C(323)-C(324)	1.32(2)	P(4)-C(431)	1.89(3)
C(324)-C(325)	1.42(2)	N(4)-C(43)	1.44(6)
C(325)-C(326)	1.44(2)	N(4)-C(15)#1	1.47(4)
C(325)-C(434)	2.02(3)	O(41)-C(41)	1.63(8)
C(331)-C(46)	1.25(6)	C(46)-O(42)	1.12(7)
C(331)-C(332)	1.39	C(46)-C(47)	1.81(7)
C(331)-C(336)	1.39	C(411)-C(412)	1.39
C(331)-O(42)	1.53(5)	C(411)-C(416)	1.39
C(331)-Rh(4)	1.788(10)	C(412)-C(413)	1.39
C(331)-P(4)	1.883(13)	C(413)-C(414)	1.39
C(332)-C(333)	1.39	C(414)-C(415)	1.39
C(333)-C(334)	1.39	C(415)-C(416)	1.39
C(334)-C(335)	1.39	C(421)-C(422)	1.39
C(335)-C(336)	1.39	C(421)-C(426)	1.39
Rh(2)-C(26)	1.91(6)	C(422)-C(423)	1.39
Rh(2)-N(2)	1.90(4)	C(423)-C(424)	1.39
Rh(2)-O(21)	2.03(4)	C(424)-C(425)	1.39
Rh(2)-P(2)	2.250(12)	C(425)-C(426)	1.39
Rh(2)-I(2)	2.665(4)	C(431)-C(432)	1.39
P(2)-C(221)	1.79(3)	C(431)-C(436)	1.39
P(2)-C(231)	1.81(3)	C(432)-C(433)	1.39
P(2)-C(211)	1.93(2)	C(433)-C(434)	1.39
C(26)-O(22)	1.18(8)	C(434)-C(435)	1.39
O(21)-C(21)	1.41(6)	C(435)-C(436)	1.39
O(21)-C(22)	1.86(8)	C(21)-C(31)#2	0.88(5)
O(21)-C(34)#2	1.87(4)	C(21)-C(22)	1.09(10)
N(2)-C(23)	1.83(8)	C(21)-C(34)#2	1.34(6)
N(2)-C(35)#2	1.89(4)	C(21)-C(32)#2	1.39(7)
C(211)-C(212)	1.39	C(21)-C(24)	1.61(8)
C(211)-C(216)	1.39	C(22)-C(32)#2	0.52(5)
C(212)-C(213)	1.39	C(22)-C(31)#2	1.29(9)
C(213)-C(214)	1.39	C(22)-C(23)	1.39(12)
C(214)-C(215)	1.39	C(22)-C(33)#2	1.59(9)
C(215)-C(216)	1.39	C(23)-C(33)#2	0.63(6)
C(221)-C(222)	1.39	C(23)-C(32)#2	1.26(8)
C(23)-C(35)#2	1.41(7)	C(42)-C(12)#1	0.54(4)
C(23)-C(25)	1.67(12)	C(42)-C(13)#1	1.15(5)
C(23)-O(31)#2	1.79(7)	C(42)-C(43)	1.15(7)

C(24)-C(34)#2	1.30(5)	C(42)-C(11)#1	1.67(6)
C(24)-C(31)#2	1.48(5)	C(43)-C(13)#1	0.76(4)
C(24)-N(3)#2	1.61(5)	C(43)-C(15)#1	1.15(4)
C(25)-C(35)#2	0.99(10)	C(43)-C(44)	1.49(7)
C(25)-C(33)#2	1.62(10)	C(43)-C(12)#1	1.58(5)
C(41)-C(11)#1	0.83(4)	C(43)-O(11)#1	1.89(5)
C(41)-C(12)#1	1.06(4)	C(44)-C(15)#1	1.04(6)
C(41)-C(42)	1.37(7)	C(44)-C(13)#1	1.70(6)
C(41)-C(45)	1.38(7)	C(45)-C(11)#1	1.02(5)
C(41)-C(14)#1	1.45(5)	C(45)-C(14)#1	1.07(6)
		C(45)-N(1)#1	1.39(6)

C(211)-Rh(1)-C(16)	40.1(8)	C(221)-P(1)-C(121)	87.6(17)
C(211)-Rh(1)-N(1)	130.3(8)	C(111)-P(1)-C(121)	106.9(6)
C(16)-Rh(1)-N(1)	95.1(5)	C(131)-P(1)-C(121)	102.4(6)
C(211)-Rh(1)-O(11)	109.2(8)	P(2)-P(1)-C(211)	74.8(10)
C(16)-Rh(1)-O(11)	92.0(4)	C(221)-P(1)-C(211)	135.9(19)
N(1)-Rh(1)-O(11)	87.4(4)	C(111)-P(1)-C(211)	115.9(8)
C(211)-Rh(1)-P(1)	56.5(7)	C(131)-P(1)-C(211)	140.3(8)
C(16)-Rh(1)-P(1)	92.2(4)	C(121)-P(1)-C(211)	72.7(9)
N(1)-Rh(1)-P(1)	172.7(3)	P(2)-P(1)-Rh(1)	102.4(8)
O(11)-Rh(1)-P(1)	92.5(3)	C(221)-P(1)-Rh(1)	141.6(16)
C(211)-Rh(1)-I(2)	135.6(7)	C(111)-P(1)-Rh(1)	109.2(4)
C(16)-Rh(1)-I(2)	165.5(4)	C(131)-P(1)-Rh(1)	111.9(5)
N(1)-Rh(1)-I(2)	81.0(3)	C(121)-P(1)-Rh(1)	121.6(4)
O(11)-Rh(1)-I(2)	101.8(3)	C(211)-P(1)-Rh(1)	50.6(8)
P(1)-Rh(1)-I(2)	91.85(13)	P(2)-P(1)-Rh(2)	50.7(8)
C(211)-Rh(1)-P(2)	48.2(7)	C(221)-P(1)-Rh(2)	124.5(16)
C(16)-Rh(1)-P(2)	88.0(5)	C(111)-P(1)-Rh(2)	146.1(5)
N(1)-Rh(1)-P(2)	160.7(4)	C(131)-P(1)-Rh(2)	44.3(4)
O(11)-Rh(1)-P(2)	111.6(4)	C(121)-P(1)-Rh(2)	92.5(4)
P(1)-Rh(1)-P(2)	19.4(3)	C(211)-P(1)-Rh(2)	96.1(7)
I(2)-Rh(1)-P(2)	91.3(3)	Rh(1)-P(1)-Rh(2)	81.93(13)
C(211)-Rh(1)-I(1)	83.9(8)	C(11)-N(1)-Rh(1)	126.4(10)
C(16)-Rh(1)-I(1)	100.8(4)	C(13)-O(11)-C(43)#1	15.3(13)
N(1)-Rh(1)-I(1)	86.7(3)	C(13)-O(11)-Rh(1)	128.8(9)
O(11)-Rh(1)-I(1)	166.4(3)	C(43)#1-O(11)-Rh(1)	136.1(14)
P(1)-Rh(1)-I(1)	91.82(11)	C(16)-O(12)-C(211)	51.2(13)
I(2)-Rh(1)-I(1)	65.18(10)	C(41)#1-C(11)-C(45)#1	96(5)
P(2)-Rh(1)-I(1)	74.0(3)	C(41)#1-C(11)-C(12)	55(3)
Rh(2)-I(1)-Rh(1)	82.50(9)	C(45)#1-C(11)-C(12)	149(4)
Rh(2)-I(1)-I(2)	64.20(11)	C(41)#1-C(11)-N(1)	152(3)
Rh(1)-I(1)-I(2)	50.88(8)	C(45)#1-C(11)-N(1)	73(4)
P(2)-P(1)-C(221)	115.9(18)	C(12)-C(11)-N(1)	127.3(17)
P(2)-P(1)-C(111)	145.7(9)	C(41)#1-C(11)-C(14)	71(3)
C(221)-P(1)-C(111)	33.2(16)	C(45)#1-C(11)-C(14)	46(3)
P(2)-P(1)-C(131)	76.1(9)	C(12)-C(11)-C(14)	119.6(18)
C(221)-P(1)-C(131)	81.6(17)	N(1)-C(11)-C(14)	113.1(16)
C(111)-P(1)-C(131)	103.3(6)	C(41)#1-C(11)-C(42)#1	54(4)
P(2)-P(1)-C(121)	42.6(8)	C(45)#1-C(11)-C(42)#1	140(4)

C(12)-C(11)-C(42)#1	14.8(15)	C(231)-C(121)-C(122)	49(3)
N(1)-C(11)-C(42)#1	120(2)	C(126)-C(121)-C(122)	119.2(13)
C(14)-C(11)-C(42)#1	124(2)	P(2)-C(121)-C(122)	99.2(12)
C(11)-C(12)-C(13)	128.0(17)	C(231)-C(121)-P(1)	129(3)
C(43)#1-C(13)-C(42)#1	71(4)	C(126)-C(121)-P(1)	121.6(11)

C(43)#1-C(13)-O(11)	139(3)	P(2)-C(121)-P(1)	26.3(6)
C(42)#1-C(13)-O(11)	127(3)	C(122)-C(121)-P(1)	119.2(10)
C(43)#1-C(13)-C(12)	87(4)	C(231)-C(121)-C(236)	45(3)
C(42)#1-C(13)-C(12)	21.1(16)	C(126)-C(121)-C(236)	97.7(16)
O(11)-C(13)-C(12)	122.0(13)	P(2)-C(121)-C(236)	120.5(17)
C(43)#1-C(13)-C(15)	44(3)	C(122)-C(121)-C(236)	21.6(13)
C(42)#1-C(13)-C(15)	109(3)	P(1)-C(121)-C(236)	140.5(14)
O(11)-C(13)-C(15)	120.2(12)	C(231)-C(121)-C(232)	39(2)
C(12)-C(13)-C(15)	117.8(13)	C(126)-C(121)-C(232)	60.6(14)
C(43)#1-C(13)-C(44)#1	61(4)	P(2)-C(121)-C(232)	109.5(12)
C(42)#1-C(13)-C(44)#1	131(3)	C(122)-C(121)-C(232)	87.4(11)
O(11)-C(13)-C(44)#1	87(2)	P(1)-C(121)-C(232)	123.6(10)
C(12)-C(13)-C(44)#1	149(2)	C(236)-C(121)-C(232)	77.3(11)
C(15)-C(13)-C(44)#1	36.8(19)	C(123)-C(122)-C(121)	121.8(15)
O(12)-C(16)-C(211)	84.1(16)	C(122)-C(123)-C(124)	116.1(16)
O(12)-C(16)-C(17)	119.6(16)	C(125)-C(124)-C(123)	120.9(15)
C(211)-C(16)-C(17)	127.5(16)	C(124)-C(125)-C(126)	120.8(15)
O(12)-C(16)-C(215)	122.0(19)	C(121)-C(126)-C(125)	120.7(15)
C(211)-C(16)-C(215)	103.0(15)	C(136)-C(131)-C(132)	119.8(16)
C(17)-C(16)-C(215)	24.6(13)	C(136)-C(131)-C(26)	57(3)
O(12)-C(16)-Rh(1)	125.8(13)	C(132)-C(131)-C(26)	68(3)
C(211)-C(16)-Rh(1)	64.9(13)	C(136)-C(131)-O(22)	14(2)
C(17)-C(16)-Rh(1)	114.5(12)	C(132)-C(131)-O(22)	106(2)
C(215)-C(16)-Rh(1)	108.2(16)	C(26)-C(131)-O(22)	43(3)
C(221)-C(111)-C(112)	128(2)	C(136)-C(131)-P(1)	123.3(14)
C(221)-C(111)-C(116)	103(2)	C(132)-C(131)-P(1)	116.8(11)
C(112)-C(111)-C(116)	116.3(12)	C(26)-C(131)-P(1)	160(3)
C(221)-C(111)-C(223)	113(2)	O(22)-C(131)-P(1)	137(2)
C(112)-C(111)-C(223)	109.3(16)	C(136)-C(131)-P(2)	105.3(15)
C(116)-C(111)-C(223)	11.7(17)	C(132)-C(131)-P(2)	131.6(12)
C(221)-C(111)-P(1)	39.3(18)	C(26)-C(131)-P(2)	134(3)
C(112)-C(111)-P(1)	121.4(10)	O(22)-C(131)-P(2)	116(2)
C(116)-C(111)-P(1)	122.4(11)	P(1)-C(131)-P(2)	27.7(5)
C(223)-C(111)-P(1)	128.2(15)	C(136)-C(131)-Rh(2)	98.6(10)
C(221)-C(111)-C(225)	103.0(19)	C(132)-C(131)-Rh(2)	82.1(9)
C(112)-C(111)-C(225)	56.7(14)	C(26)-C(131)-Rh(2)	68(3)
C(116)-C(111)-C(225)	78.4(15)	O(22)-C(131)-Rh(2)	93(2)
C(223)-C(111)-C(225)	80.4(12)	P(1)-C(131)-Rh(2)	92.9(6)
P(1)-C(111)-C(225)	136.3(13)	P(2)-C(131)-Rh(2)	74.2(6)
C(111)-C(112)-C(113)	121.7(13)	C(133)-C(132)-C(131)	119.6(17)
C(112)-C(113)-C(114)	121.5(15)	C(134)-C(133)-C(132)	123(2)
C(115)-C(114)-C(113)	118.1(13)	C(133)-C(134)-C(135)	126.6(17)
C(114)-C(115)-C(116)	121.7(15)	C(134)-C(135)-C(136)	111.7(16)
C(115)-C(116)-C(111)	120.4(15)	C(131)-C(136)-C(135)	119(2)
C(231)-C(121)-C(126)	91(3)	C(421)-Rh(3)-C(36)	42.0(11)
C(231)-C(121)-P(2)	104(3)	C(421)-Rh(3)-O(31)	109.1(14)
C(126)-C(121)-P(2)	138.3(13)	C(36)-Rh(3)-O(31)	93.2(5)
C(421)-Rh(3)-N(3)	132.2(10)	C(411)-P(3)-Rh(3)	138.0(15)
C(36)-Rh(3)-N(3)	93.8(5)	C(331)-P(3)-Rh(3)	113.6(4)
O(31)-Rh(3)-N(3)	85.5(4)	C(311)-P(3)-Rh(3)	109.3(4)
C(421)-Rh(3)-I(4)	133.4(12)	C(321)-P(3)-Rh(3)	120.6(4)
C(36)-Rh(3)-I(4)	164.0(4)	C(421)-P(3)-Rh(3)	53.6(12)
O(31)-Rh(3)-I(4)	102.1(3)	P(4)-P(3)-Rh(4)	59.4(10)
N(3)-Rh(3)-I(4)	83.0(3)	C(411)-P(3)-Rh(4)	126.5(16)
C(421)-Rh(3)-P(3)	54.8(10)	C(331)-P(3)-Rh(4)	43.5(3)

C(36)-Rh(3)-P(3)	93.6(5)	C(311)-P(3)-Rh(4)	145.6(5)
O(31)-Rh(3)-P(3)	94.2(3)	C(321)-P(3)-Rh(4)	91.5(4)
N(3)-Rh(3)-P(3)	172.6(3)	C(421)-P(3)-Rh(4)	97.2(14)
I(4)-Rh(3)-P(3)	89.8(2)	Rh(3)-P(3)-Rh(4)	84.0(2)
C(421)-Rh(3)-C(422)	31.4(9)	C(31)-N(3)-Rh(3)	127.5(9)
C(36)-Rh(3)-C(422)	31.0(11)	C(33)-O(31)-C(23)#2	13(2)
O(31)-Rh(3)-C(422)	79.8(10)	C(33)-O(31)-Rh(3)	132.2(11)
N(3)-Rh(3)-C(422)	120.1(13)	C(23)#2-O(31)-Rh(3)	132(2)
I(4)-Rh(3)-C(422)	156.9(12)	C(36)-O(32)-C(421)	57.7(16)
P(3)-Rh(3)-C(422)	67.0(12)	C(21)#2-C(31)-C(22)#2	57(5)
C(421)-Rh(3)-P(4)	44.4(11)	C(21)#2-C(31)-N(3)	142(4)
C(36)-Rh(3)-P(4)	86.1(5)	C(22)#2-C(31)-N(3)	126(3)
O(31)-Rh(3)-P(4)	110.4(5)	C(21)#2-C(31)-C(32)	73(5)
N(3)-Rh(3)-P(4)	164.0(5)	C(22)#2-C(31)-C(32)	22(2)
I(4)-Rh(3)-P(4)	92.7(3)	N(3)-C(31)-C(32)	124.7(14)
P(3)-Rh(3)-P(4)	17.5(3)	C(21)#2-C(31)-C(34)	65(4)
C(422)-Rh(3)-P(4)	65.5(13)	C(22)#2-C(31)-C(34)	118(3)
C(421)-Rh(3)-I(3)	84.9(14)	N(3)-C(31)-C(34)	112.4(16)
C(36)-Rh(3)-I(3)	99.3(4)	C(32)-C(31)-C(34)	122.7(18)
O(31)-Rh(3)-I(3)	165.8(3)	C(21)#2-C(31)-C(24)#2	82(5)
N(3)-Rh(3)-I(3)	86.9(3)	C(22)#2-C(31)-C(24)#2	129(3)
I(4)-Rh(3)-I(3)	64.98(11)	N(3)-C(31)-C(24)#2	70(2)
P(3)-Rh(3)-I(3)	91.78(11)	C(32)-C(31)-C(24)#2	151(3)
C(422)-Rh(3)-I(3)	114.4(10)	C(34)-C(31)-C(24)#2	53(2)
P(4)-Rh(3)-I(3)	77.4(4)	C(33)-C(32)-C(31)	125.9(17)
Rh(4)-I(3)-I(4)	65.85(12)	C(23)#2-C(33)-O(31)	140(7)
Rh(4)-I(3)-Rh(3)	81.92(9)	C(23)#2-C(33)-C(32)	67(7)
I(4)-I(3)-Rh(3)	49.06(8)	O(31)-C(33)-C(32)	122.4(17)
P(4)-P(3)-C(411)	113.9(19)	C(23)#2-C(33)-C(35)	64(7)
P(4)-P(3)-C(331)	81.9(10)	O(31)-C(33)-C(35)	121.4(16)
C(411)-P(3)-C(331)	84.0(16)	C(32)-C(33)-C(35)	116.2(16)
P(4)-P(3)-C(311)	137.7(11)	C(23)#2-C(33)-C(22)#2	60(8)
C(411)-P(3)-C(311)	29.2(15)	O(31)-C(33)-C(22)#2	115(2)
C(331)-P(3)-C(311)	103.3(6)	C(32)-C(33)-C(22)#2	18.4(19)
P(4)-P(3)-C(321)	32.9(10)	C(35)-C(33)-C(22)#2	120(2)
C(411)-P(3)-C(321)	89.9(16)	C(23)#2-C(33)-C(25)#2	83(8)
C(331)-P(3)-C(321)	101.5(5)	O(31)-C(33)-C(25)#2	87(4)
C(311)-P(3)-C(321)	106.9(5)	C(32)-C(33)-C(25)#2	149(4)
P(4)-P(3)-C(421)	69.5(16)	C(35)-C(33)-C(25)#2	36(3)
C(411)-P(3)-C(421)	132(2)	C(22)#2-C(33)-C(25)#2	142(4)
C(331)-P(3)-C(421)	140.3(14)	O(32)-C(36)-C(421)	76(2)
C(311)-P(3)-C(421)	116.4(14)	O(32)-C(36)-C(37)	122.8(16)
C(321)-P(3)-C(421)	68.6(13)	C(421)-C(36)-C(37)	126(2)
P(4)-P(3)-Rh(3)	106.5(10)	O(32)-C(36)-Rh(3)	118.3(12)
C(421)-C(36)-Rh(3)	67.3(18)	C(336)-C(331)-Rh(4)	102.7(5)
C(37)-C(36)-Rh(3)	118.9(13)	O(42)-C(331)-Rh(4)	99(3)
C(411)-C(311)-C(316)	129(2)	C(46)-C(331)-P(3)	153(3)
C(411)-C(311)-C(312)	101(2)	C(332)-C(331)-P(3)	117.3(6)
C(316)-C(311)-C(312)	119.6(12)	C(336)-C(331)-P(3)	122.4(6)
C(411)-C(311)-C(415)	123(3)	O(42)-C(331)-P(3)	145(2)
C(316)-C(311)-C(415)	101.5(16)	Rh(4)-C(331)-P(3)	92.3(4)
C(312)-C(311)-C(415)	22.0(14)	C(46)-C(331)-P(4)	132(3)
C(411)-C(311)-P(3)	40(2)	C(332)-C(331)-P(4)	132.5(8)
C(316)-C(311)-P(3)	120.7(10)	C(336)-C(331)-P(4)	105.3(8)
C(312)-C(311)-P(3)	119.4(10)	O(42)-C(331)-P(4)	127(2)

C(415)-C(311)-P(3)	133.8(15)	Rh(4)-C(331)-P(4)	77.1(5)
C(411)-C(311)-C(413)	102(2)	P(3)-C(331)-P(4)	25.6(6)
C(316)-C(311)-C(413)	60.0(14)	C(331)-C(332)-C(333)	120.0
C(312)-C(311)-C(413)	80.1(14)	C(334)-C(333)-C(332)	120.0
C(415)-C(311)-C(413)	78.9(11)	C(333)-C(334)-C(335)	120.0
P(3)-C(311)-C(413)	136.9(13)	C(336)-C(335)-C(334)	120.0
C(311)-C(312)-C(313)	117.6(13)	C(335)-C(336)-C(331)	120.0
C(314)-C(313)-C(312)	121.1(14)	C(26)-Rh(2)-C(131)	45(2)
C(313)-C(314)-C(315)	119.6(12)	C(26)-Rh(2)-N(2)	99(2)
C(316)-C(315)-C(314)	119.4(15)	C(131)-Rh(2)-N(2)	138.1(13)
C(315)-C(316)-C(311)	122.6(14)	C(26)-Rh(2)-O(21)	96(2)
C(431)-C(321)-P(4)	116(3)	C(131)-Rh(2)-O(21)	111.8(10)
C(431)-C(321)-C(326)	84(2)	N(2)-Rh(2)-O(21)	89.3(15)
P(4)-C(321)-C(326)	133.3(12)	C(26)-Rh(2)-I(1)	166(2)
C(431)-C(321)-C(322)	55(2)	C(131)-Rh(2)-I(1)	131.9(4)
P(4)-C(321)-C(322)	102.0(12)	N(2)-Rh(2)-I(1)	76.5(12)
C(326)-C(321)-C(322)	122.9(12)	O(21)-Rh(2)-I(1)	97.1(10)
C(431)-C(321)-C(436)	46(2)	C(26)-Rh(2)-P(2)	93(2)
P(4)-C(321)-C(436)	131.0(17)	C(131)-Rh(2)-P(2)	52.0(5)
C(326)-C(321)-C(436)	93.9(15)	N(2)-Rh(2)-P(2)	166.6(13)
C(322)-C(321)-C(436)	29.1(13)	O(21)-Rh(2)-P(2)	93.7(10)
C(431)-C(321)-P(3)	134(2)	I(1)-Rh(2)-P(2)	90.2(3)
P(4)-C(321)-P(3)	20.3(8)	C(26)-Rh(2)-I(2)	100(2)
C(326)-C(321)-P(3)	118.5(10)	C(131)-Rh(2)-I(2)	83.7(5)
C(322)-C(321)-P(3)	118.6(9)	N(2)-Rh(2)-I(2)	82.6(12)
C(436)-C(321)-P(3)	147.4(13)	O(21)-Rh(2)-I(2)	163.2(9)
C(323)-C(322)-C(321)	117.0(14)	I(1)-Rh(2)-I(2)	66.65(12)
C(324)-C(323)-C(322)	123.6(18)	P(2)-Rh(2)-I(2)	91.0(4)
C(323)-C(324)-C(325)	116.9(15)	C(26)-Rh(2)-P(1)	88(2)
C(324)-C(325)-C(326)	122.0(13)	C(131)-Rh(2)-P(1)	42.9(4)
C(324)-C(325)-C(434)	32.7(13)	N(2)-Rh(2)-P(1)	157.9(12)
C(326)-C(325)-C(434)	136.5(14)	O(21)-Rh(2)-P(1)	110.9(9)
C(321)-C(326)-C(325)	117.0(13)	I(1)-Rh(2)-P(1)	91.77(13)
C(46)-C(331)-C(332)	66(3)	P(2)-Rh(2)-P(1)	17.7(4)
C(46)-C(331)-C(336)	64(3)	I(2)-Rh(2)-P(1)	75.53(14)
C(332)-C(331)-C(336)	120.0	Rh(1)-I(2)-Rh(2)	81.54(12)
C(46)-C(331)-O(42)	46(3)	Rh(1)-I(2)-I(1)	63.94(9)
C(332)-C(331)-O(42)	97(2)	Rh(2)-I(2)-I(1)	49.16(10)
C(336)-C(331)-O(42)	23(2)	P(1)-P(2)-C(121)	111.2(12)
C(46)-C(331)-Rh(4)	62(3)	P(1)-P(2)-C(221)	37.8(13)
C(332)-C(331)-Rh(4)	79.7(5)	C(121)-P(2)-C(221)	86.8(14)
P(1)-P(2)-C(231)	140.0(17)	Rh(1)-C(211)-P(2)	87.2(11)
C(121)-P(2)-C(231)	29.7(14)	C(16)-C(211)-P(1)	135.7(19)
C(221)-P(2)-C(231)	108.8(19)	C(212)-C(211)-P(1)	105.3(16)
P(1)-P(2)-C(131)	76.1(10)	C(216)-C(211)-P(1)	132.2(16)
C(121)-P(2)-C(131)	128.7(10)	O(12)-C(211)-P(1)	120.3(16)
C(221)-P(2)-C(131)	68.9(13)	Rh(1)-C(211)-P(1)	72.9(9)
C(231)-P(2)-C(131)	118.0(16)	P(2)-C(211)-P(1)	26.1(5)
P(1)-P(2)-C(211)	79.0(11)	C(213)-C(212)-C(211)	120.0
C(121)-P(2)-C(211)	85.5(11)	C(214)-C(213)-C(212)	120.0
C(221)-P(2)-C(211)	105.5(15)	C(213)-C(214)-C(215)	120.0
C(231)-P(2)-C(211)	98.4(17)	C(214)-C(215)-C(216)	120.0
C(131)-P(2)-C(211)	143.3(12)	C(214)-C(215)-C(16)	63.4(9)
P(1)-P(2)-Rh(2)	111.7(10)	C(216)-C(215)-C(16)	59.1(8)
C(121)-P(2)-Rh(2)	135.5(11)	C(215)-C(216)-C(211)	120.0

Table 8.11
Anisotropic displacement parameters ($Å^2 \times 10^3$) for [Rh(dmavk)(I)($COCH_3$)(PPh_3)].

	U11	U22	U33	U23	U13	U12
Rh(1)	42(1)	40(1)	31(1)	0(1)	17(1)	2(1)
I(1)	64(1)	60(1)	46(1)	-17(1)	14(1)	7(1)
P(1)	42(2)	41(2)	30(2)	-1(2)	21(2)	-1(1)
N(1)	41(6)	35(5)	27(5)	1(4)	9(5)	16(4)
O(11)	49(6)	82(7)	55(6)	5(5)	22(5)	-2(5)
O(12)	73(9)	101(11)	112(11)	5(7)	71(9)	-7(7)
C(11)	42(9)	75(11)	55(10)	14(9)	17(8)	4(8)
C(12)	65(11)	53(11)	55(10)	-9(8)	24(9)	-15(8)
C(13)	31(7)	42(7)	32(7)	-2(6)	6(6)	-6(6)
C(14)	90(13)	84(12)	81(12)	19(10)	46(11)	19(10)
C(15)	98(12)	69(10)	25(7)	2(6)	28(7)	9(8)
C(16)	60(9)	58(9)	24(6)	-6(6)	16(6)	-14(7)
C(17)	70(11)	100(14)	59(12)	-5(10)	35(10)	23(11)
C(111)	53(8)	43(7)	32(6)	-1(5)	20(6)	4(6)
C(112)	57(8)	55(8)	70(8)	-11(7)	44(7)	-9(7)
C(113)	103(9)	58(8)	75(8)	-11(8)	70(9)	-5(8)
C(114)	82(9)	51(8)	60(8)	-18(7)	41(8)	-24(8)
C(115)	87(9)	68(9)	58(8)	-23(8)	59(8)	3(8)
C(116)	61(10)	66(11)	56(9)	-6(9)	33(8)	-8(7)
C(121)	23(6)	55(8)	29(6)	10(5)	2(5)	-10(5)
C(122)	53(8)	90(9)	49(7)	30(8)	37(7)	2(8)
C(123)	63(11)	104(10)	34(8)	-11(10)	16(7)	-12(9)
C(124)	87(13)	96(9)	76(9)	56(9)	39(11)	17(10)
C(125)	136(17)	47(9)	82(10)	26(8)	54(12)	17(10)
C(126)	69(10)	54(9)	82(8)	10(8)	41(9)	15(7)
C(131)	41(8)	52(8)	60(8)	-19(7)	25(7)	-10(6)
C(132)	64(7)	61(9)	91(11)	-14(8)	58(8)	-33(7)
C(133)	64(8)	134(15)	83(13)	-21(12)	45(10)	-49(11)
C(134)	50(7)	144(14)	68(11)	-47(11)	41(8)	-60(10)
C(135)	52(9)	133(14)	95(14)	-28(13)	23(10)	16(12)
C(136)	56(10)	91(13)	31(9)	-37(8)	-1(9)	-12(10)
Rh(3)	45(1)	37(1)	32(1)	0(1)	19(1)	0(1)
I(3)	68(1)	55(1)	44(1)	13(1)	19(1)	-3(1)
P(3)	47(2)	43(2)	36(2)	4(2)	27(2)	5(1)
N(3)	41(6)	39(5)	29(5)	1(4)	4(5)	1(4)
O(31)	53(6)	82(7)	51(6)	-6(5)	22(5)	6(5)
O(32)	65(8)	57(7)	85(9)	-16(6)	47(6)	13(6)
C(31)	57(9)	51(9)	69(11)	-24(7)	36(9)	-13(7)
C(32)	39(9)	101(15)	75(13)	-11(12)	11(9)	-7(10)
C(33)	49(10)	68(10)	33(9)	-17(7)	5(8)	8(8)
C(34)	130(17)	79(13)	109(15)	-36(11)	67(14)	-54(12)
C(35)	79(11)	86(11)	20(6)	8(7)	16(7)	29(9)
C(36)	53(8)	70(10)	49(8)	-11(7)	37(7)	9(7)
C(37)	65(11)	91(15)	102(18)	14(11)	39(13)	1(10)
C(311)	56(8)	44(7)	29(6)	7(5)	25(6)	-2(6)
C(312)	26(7)	88(12)	49(9)	1(8)	12(7)	6(7)
C(313)	93(9)	68(9)	66(9)	24(9)	59(8)	8(9)
C(314)	95(10)	63(9)	46(7)	28(7)	27(8)	11(9)
C(315)	90(9)	54(8)	68(8)	14(7)	47(9)	14(8)
C(316)	111(13)	47(8)	62(8)	16(7)	55(9)	28(9)
C(321)	47(7)	36(7)	40(7)	-4(5)	27(6)	13(5)

C(433)-C(434)-C(325)	60.8(12)
C(436)-C(435)-C(434)	120.0
C(435)-C(436)-C(431)	120.00(6)
C(435)-C(436)-C(321)	140.6(14)
C(431)-C(436)-C(321)	28.9(14)
C(31)#2-C(21)-C(22)	81(5)
C(31)#2-C(21)-C(34)#2	79(5)
C(22)-C(21)-C(34)#2	151(4)
C(31)#2-C(21)-C(32)#2	70(4)
C(22)-C(21)-C(32)#2	20(2)
C(34)#2-C(21)-C(32)#2	131(4)
C(31)#2-C(21)-O(21)	139(5)
C(22)-C(21)-O(21)	96(4)
C(34)#2-C(21)-O(21)	86(4)
C(32)#2-C(21)-O(21)	93(4)
C(31)#2-C(21)-C(24)	65(4)
C(22)-C(21)-C(24)	135(5)
C(34)#2-C(21)-C(24)	51(3)
C(32)#2-C(21)-C(24)	134(5)
O(21)-C(21)-C(24)	129(5)
C(32)#2-C(22)-C(21)	115(10)
C(21)-C(22)-C(31)#2	43(4)
C(32)#2-C(22)-C(23)	65(10)
C(21)-C(22)-C(23)	179(2)
C(31)#2-C(22)-C(23)	139(4)
C(32)#2-C(22)-C(33)#2	55(10)
C(21)-C(22)-C(33)#2	158(3)
C(31)#2-C(22)-C(33)#2	116(3)
C(23)-C(22)-C(33)#2	23(3)
C(32)#2-C(22)-O(21)	101(9)
C(21)-C(22)-O(21)	49(4)
C(13)#1-C(42)-C(41)	147(4)
C(43)-C(42)-C(41)	173(5)
C(12)#1-C(42)-C(11)#1	7(6)
C(13)#1-C(42)-C(11)#1	118(3)
C(43)-C(42)-C(11)#1	156(4)
C(41)-C(42)-C(11)#1	30(2)
C(13)#1-C(43)-C(42)	71(4)
C(13)#1-C(43)-C(15)#1	108(4)
C(42)-C(43)-C(15)#1	151(3)
C(13)#1-C(43)-N(4)	152(4)
C(42)-C(43)-N(4)	99(4)
C(15)#1-C(43)-N(4)	68(3)
C(13)#1-C(43)-C(44)	92(4)
C(42)-C(43)-C(44)	160(5)
C(15)#1-C(43)-C(44)	44(3)
N(4)-C(43)-C(44)	101(4)
C(13)#1-C(43)-C(12)#1	64(3)
C(42)-C(43)-C(12)#1	14.0(13)
C(35)#2-C(23)-N(2)	70(3)
C(25)-C(23)-N(2)	97(5)
O(31)#2-C(23)-N(2)	167(5)
C(34)#2-C(24)-C(31)#2	63(2)
C(34)#2-C(24)-N(3)#2	103(4)
C(31)#2-C(24)-N(3)#2	49.5(18)
C(34)#2-C(24)-C(21)	53(3)
C(31)#2-C(24)-C(21)	33(2)
N(3)#2-C(24)-C(21)	80(3)
C(35)#2-C(25)-C(33)#2	68(6)
C(35)#2-C(25)-C(23)	57(6)
C(33)#2-C(25)-C(23)	22(3)
C(11)#1-C(41)-C(12)#1	85(4)
C(11)#1-C(41)-C(42)	96(4)
C(12)#1-C(41)-C(42)	21.4(18)
C(11)#1-C(41)-C(45)	48(4)
C(12)#1-C(41)-C(45)	131(5)
C(42)-C(41)-C(45)	136(5)
C(11)#1-C(41)-C(14)#1	76(4)
C(12)#1-C(41)-C(14)#1	145(4)
C(42)-C(41)-C(14)#1	166(3)
C(45)-C(41)-C(14)#1	44(3)
C(11)#1-C(41)-O(41)	155(5)
C(12)#1-C(41)-O(41)	102(4)
C(42)-C(41)-O(41)	98(4)
C(45)-C(41)-O(41)	125(4)
C(14)#1-C(41)-O(41)	86(3)
C(12)#1-C(42)-C(13)#1	109(6)
C(12)#1-C(42)-C(43)	135(7)
C(13)#1-C(42)-C(43)	39(3)
C(12)#1-C(42)-C(41)	46(6)
C(15)#1-C(43)-C(12)#1	139(3)
N(4)-C(43)-C(12)#1	100(3)
C(44)-C(43)-C(12)#1	156(4)
C(13)#1-C(43)-O(11)#1	26(2)
C(42)-C(43)-O(11)#1	87(3)
C(15)#1-C(43)-O(11)#1	104(3)
N(4)-C(43)-O(11)#1	172(3)
C(44)-C(43)-O(11)#1	74(3)
C(12)#1-C(43)-O(11)#1	84(2)
C(15)#1-C(44)-C(43)	50(3)
C(15)#1-C(44)-C(13)#1	65(3)
C(43)-C(44)-C(13)#1	26.6(19)
C(11)#1-C(45)-C(14)#1	91(5)
C(11)#1-C(45)-N(1)#1	62(4)
C(14)#1-C(45)-N(1)#1	140(5)
C(11)#1-C(45)-C(41)	37(3)
C(14)#1-C(45)-C(41)	72(4)
N(1)#1-C(45)-C(41)	96(5)

C(46)-Rh(4)-I(4)	100(2)	P(3)-C(411)-C(412)	135(3)
C(331)-Rh(4)-I(4)	83.3(3)	C(311)-C(411)-C(416)	54.3(19)
O(41)-Rh(4)-I(4)	162.9(17)	P(3)-C(411)-C(416)	98(3)
N(4)-Rh(4)-I(4)	87.5(10)	C(412)-C(411)-C(416)	120.0
P(4)-Rh(4)-I(4)	88.9(5)	C(311)-C(411)-P(4)	131(3)
I(3)-Rh(4)-I(4)	63.43(13)	C(412)-C(411)-P(4)	118(2)
P(3)-Rh(4)-I(4)	73.23(15)	C(416)-C(411)-P(4)	121(2)
Rh(3)-I(4)-I(3)	65.96(11)	C(413)-C(412)-C(411)	120.0
Rh(3)-I(4)-Rh(4)	82.70(13)	C(414)-C(413)-C(412)	120.0
I(3)-I(4)-Rh(4)	50.73(10)	C(414)-C(413)-C(311)	74.0(9)
P(3)-P(4)-C(321)	126.8(16)	C(412)-C(413)-C(311)	48.7(9)
P(3)-P(4)-C(411)	41.0(14)	C(413)-C(414)-C(415)	120.0
C(321)-P(4)-C(411)	95.2(14)	C(416)-C(415)-C(414)	120.0
P(3)-P(4)-C(421)	85.6(18)	C(416)-C(415)-C(311)	40.4(10)
C(321)-P(4)-C(421)	86.2(15)	C(414)-C(415)-C(311)	83.7(10)
C(411)-P(4)-C(421)	110(2)	C(415)-C(416)-C(411)	120.0
P(3)-P(4)-C(331)	72.4(10)	C(422)-C(421)-C(426)	120.0
C(321)-P(4)-C(331)	129.1(11)	C(422)-C(421)-C(36)	58.8(17)
C(411)-P(4)-C(331)	70.1(13)	C(426)-C(421)-C(36)	67.8(16)
C(421)-P(4)-C(331)	144.6(17)	C(422)-C(421)-O(32)	15.3(18)
P(3)-P(4)-C(431)	149.7(17)	C(426)-C(421)-O(32)	104.7(18)
C(321)-P(4)-C(431)	26.3(13)	C(36)-C(421)-O(32)	46.0(14)
C(411)-P(4)-C(431)	110.8(17)	C(422)-C(421)-P(4)	122(3)
C(421)-P(4)-C(431)	100.0(18)	C(426)-C(421)-P(4)	118(3)
C(331)-P(4)-C(431)	113.1(14)	C(36)-C(421)-P(4)	158(3)
P(3)-P(4)-Rh(4)	102.6(11)	O(32)-C(421)-P(4)	137(3)
C(321)-P(4)-Rh(4)	128.9(14)	C(422)-C(421)-Rh(3)	102(2)
C(411)-P(4)-Rh(4)	118.7(13)	C(426)-C(421)-Rh(3)	83(2)
C(421)-P(4)-Rh(4)	112.4(15)	C(36)-C(421)-Rh(3)	70.7(18)
C(331)-P(4)-Rh(4)	49.6(4)	O(32)-C(421)-Rh(3)	102(2)
C(431)-P(4)-Rh(4)	102.6(14)	P(4)-C(421)-Rh(3)	88.5(17)
P(3)-P(4)-Rh(3)	56.0(10)	C(422)-C(421)-P(3)	107(3)
C(321)-P(4)-Rh(3)	133.0(9)	C(426)-C(421)-P(3)	131(3)
C(411)-P(4)-Rh(3)	96.3(14)		
C(36)-C(421)-P(3)	135(3)	C(31)#2-C(22)-O(21)	84(5)
O(32)-C(421)-P(3)	121(3)	C(23)-C(22)-O(21)	130(4)
P(4)-C(421)-P(3)	24.8(7)	C(33)#2-C(22)-O(21)	146(4)
Rh(3)-C(421)-P(3)	71.7(13)	C(33)#2-C(23)-C(32)#2	85(8)
C(423)-C(422)-C(421)	120.0	C(33)#2-C(23)-C(22)	97(8)
C(423)-C(422)-Rh(3)	109.5(16)	C(32)#2-C(23)-C(22)	22(2)
C(421)-C(422)-Rh(3)	46.2(14)	C(33)#2-C(23)-C(35)#2	92(8)
C(422)-C(423)-C(424)	120.0	C(32)#2-C(23)-C(35)#2	137(6)
C(425)-C(424)-C(423)	120.00(7)	C(22)-C(23)-C(35)#2	155(5)
C(424)-C(425)-C(426)	120.00(7)	C(33)#2-C(23)-C(25)	75(8)
C(425)-C(426)-C(421)	120.0	C(32)#2-C(23)-C(25)	158(6)
C(321)-C(431)-C(432)	123(3)	C(22)-C(23)-C(25)	168(6)
C(321)-C(431)-C(436)	105(3)	C(35)#2-C(23)-C(25)	36(4)
C(432)-C(431)-C(436)	120.0	C(33)#2-C(23)-O(31)#2	27(5)
C(321)-C(431)-P(4)	37.6(15)	C(32)#2-C(23)-O(31)#2	96(4)
C(432)-C(431)-P(4)	118(2)	C(22)-C(23)-O(31)#2	98(4)
C(436)-C(431)-P(4)	122(2)	C(35)#2-C(23)-O(31)#2	100(4)
C(431)-C(432)-C(433)	120.0	C(25)-C(23)-O(31)#2	71(5)
C(432)-C(433)-C(434)	120.0	C(33)#2-C(23)-N(2)	156(9)
C(435)-C(434)-C(433)	120.0	C(32)#2-C(23)-N(2)	97(5)
C(435)-C(434)-C(325)	78.0(12)	C(22)-C(23)-N(2)	94(4)

C(221)-P(2)-Rh(2)	121.9(13)	C(111)-C(221)-P(1)	107(3)
C(231)-P(2)-Rh(2)	105.9(15)	C(111)-C(221)-C(222)	60.7(17)
C(131)-P(2)-Rh(2)	53.9(5)	P(1)-C(221)-C(222)	99(3)
C(211)-P(2)-Rh(2)	113.8(9)	C(111)-C(221)-C(226)	73.1(17)
P(1)-P(2)-Rh(1)	58.2(7)	P(1)-C(221)-C(226)	131(3)
C(121)-P(2)-Rh(1)	129.0(8)	C(222)-C(221)-C(226)	120.0
C(221)-P(2)-Rh(1)	95.9(13)	C(111)-C(221)-P(2)	132(3)
C(231)-P(2)-Rh(1)	140.9(16)	P(1)-C(221)-P(2)	26.4(7)
C(131)-P(2)-Rh(1)	98.8(7)	C(222)-C(221)-P(2)	118(2)
C(211)-P(2)-Rh(1)	44.6(8)	C(226)-C(221)-P(2)	121(2)
Rh(2)-P(2)-Rh(1)	84.6(4)	C(221)-C(222)-C(223)	120.00(6)
O(22)-C(26)-C(131)	80(5)	C(222)-C(223)-C(224)	120.0
O(22)-C(26)-Rh(2)	112(5)	C(222)-C(223)-C(111)	45.0(10)
C(131)-C(26)-Rh(2)	67(3)	C(224)-C(223)-C(111)	80.1(10)
C(21)-O(21)-C(22)	35(3)	C(225)-C(224)-C(223)	120.0
C(21)-O(21)-C(34)#2	46(3)	C(224)-C(225)-C(226)	120.0
C(22)-O(21)-C(34)#2	78(3)	C(224)-C(225)-C(111)	74.6(9)
C(21)-O(21)-Rh(2)	134(4)	C(226)-C(225)-C(111)	49.4(9)
C(22)-O(21)-Rh(2)	99(3)	C(225)-C(226)-C(221)	120.0
C(34)#2-O(21)-Rh(2)	156(2)	C(121)-C(231)-C(232)	116(4)
C(23)-N(2)-Rh(2)	119(3)	C(121)-C(231)-C(236)	106(4)
C(23)-N(2)-C(35)#2	44(2)	C(232)-C(231)-C(236)	120.0
Rh(2)-N(2)-C(35)#2	137(2)	C(121)-C(231)-P(2)	46.5(17)
C(26)-O(22)-C(131)	57(4)	C(232)-C(231)-P(2)	118(3)
C(16)-C(211)-C(212)	52.6(13)	C(236)-C(231)-P(2)	122(3)
C(16)-C(211)-C(216)	72.3(13)	C(231)-C(232)-C(233)	120.0
C(212)-C(211)-C(216)	120.0	C(231)-C(232)-C(121)	24.7(17)
C(16)-C(211)-O(12)	44.6(9)	C(233)-C(232)-C(121)	133.6(17)
C(212)-C(211)-O(12)	15.3(11)	C(234)-C(233)-C(232)	120.0
C(216)-C(211)-O(12)	106.1(11)	C(233)-C(234)-C(235)	120.0
C(16)-C(211)-Rh(1)	75.0(14)	C(236)-C(235)-C(234)	120.0
C(212)-C(211)-Rh(1)	100.9(15)	C(235)-C(236)-C(231)	120.0
C(216)-C(211)-Rh(1)	84.0(15)	C(235)-C(236)-C(121)	136.7(15)
O(12)-C(211)-Rh(1)	106.8(15)	C(231)-C(236)-C(121)	28.2(16)
C(16)-C(211)-P(2)	160(2)	C(46)-Rh(4)-C(331)	43(2)
C(212)-C(211)-P(2)	125.0(17)	C(46)-Rh(4)-O(41)	97(3)
C(216)-C(211)-P(2)	114.9(17)	C(331)-Rh(4)-O(41)	109.4(13)
O(12)-C(211)-P(2)	137.9(17)	C(46)-Rh(4)-N(4)	96(3)
C(331)-Rh(4)-N(4)	134.0(10)	C(421)-P(4)-Rh(3)	47.1(14)
O(41)-Rh(4)-N(4)	91.2(14)	C(331)-P(4)-Rh(3)	97.6(7)
C(46)-Rh(4)-P(4)	93(2)	C(431)-P(4)-Rh(3)	144.2(13)
C(331)-Rh(4)-P(4)	53.3(4)	Rh(4)-P(4)-Rh(3)	83.0(4)
O(41)-Rh(4)-P(4)	89.9(12)	C(43)-N(4)-C(15)#1	47(2)
N(4)-Rh(4)-P(4)	171.2(10)	C(43)-N(4)-Rh(4)	129(3)
C(46)-Rh(4)-I(3)	163(2)	C(15)#1-N(4)-Rh(4)	150(2)
C(331)-Rh(4)-I(3)	133.5(3)	C(41)-O(41)-Rh(4)	126(3)
O(41)-Rh(4)-I(3)	99.6(17)	O(42)-C(46)-C(331)	80(5)
N(4)-Rh(4)-I(3)	78.7(10)	O(42)-C(46)-Rh(4)	134(6)
P(4)-Rh(4)-I(3)	92.5(3)	C(331)-C(46)-Rh(4)	76(3)
C(46)-Rh(4)-P(3)	87(2)	O(42)-C(46)-C(47)	89(5)
C(331)-Rh(4)-P(3)	44.2(3)	C(331)-C(46)-C(47)	113(4)
O(41)-Rh(4)-P(3)	107.5(10)	Rh(4)-C(46)-C(47)	137(4)
N(4)-Rh(4)-P(3)	160.7(10)	C(46)-O(42)-C(331)	54(4)
P(4)-Rh(4)-P(3)	18.0(5)	C(311)-C(411)-P(3)	110(3)
I(3)-Rh(4)-P(3)	93.1(2)	C(311)-C(411)-C(412)	78.4(18)

C(322)	53(8)	72(8)	38(7)	-10(7)	32(6)	-8(7)
C(323)	87(13)	64(8)	51(9)	-14(8)	28(9)	2(8)
C(324)	107(14)	67(7)	62(8)	-28(8)	50(10)	-6(9)
C(325)	70(10)	58(8)	68(7)	-37(7)	36(8)	-15(7)
C(326)	99(12)	33(7)	74(8)	7(6)	60(9)	14(7)
C(331)	39(7)	48(7)	49(7)	6(6)	27(6)	0(6)
C(332)	67(7)	80(10)	72(10)	30(8)	47(8)	40(8)
C(333)	65(10)	88(14)	138(19)	20(14)	64(12)	6(12)
C(334)	59(8)	150(15)	64(12)	41(12)	37(9)	46(11)
C(335)	71(10)	113(13)	102(14)	34(12)	30(11)	-31(11)
C(336)	72(9)	62(11)	55(10)	5(8)	23(9)	9(9)
Rh(2)	73(2)	61(2)	79(2)	2(1)	34(2)	-4(1)
I(2)	98(2)	86(2)	94(2)	20(2)	28(2)	-12(2)
P(2)	50(6)	55(6)	97(10)	-2(7)	29(7)	2(5)
O(21)	81(21)	81(21)	106(23)	-22(17)	-14(18)	17(16)
Rh(4)	83(2)	60(2)	77(2)	-5(1)	37(2)	6(2)
I(4)	104(3)	88(2)	92(2)	-24(2)	21(2)	18(2)
P(4)	60(7)	50(7)	158(15)	18(10)	73(11)	4(5)
O(41)	315(67)	131(34)	349(71)	175(43)	284(64)	152(41)

Table 8.12
Hydrogen coordinates ($x10^{-3}$) and isotropic displacement parameters ($Å^2x10^3$) for [Rh(dmavk)(I)($COCH_3$)(PPh_3)]

	x	y	z	Ueq
H(1)	1664(6)	2970(5)	8312(6)	132(13)
H(12)	2910(12)	3378(9)	10565(11)	132(13)
H(14A)	2973(78)	2406(34)	9119(56)	132(13)
H(14B)	2360(26)	2034(10)	9438(81)	132(13)
H(14C)	3251(53)	2406(33)	10065(31)	132(13)
H(15A)	2309(87)	4346(43)	11302(32)	132(13)
H(15B)	2198(78)	5135(37)	10899(11)	132(13)
H(15C)	3098(16)	4709(77)	11223(40)	132(13)
H(17A)	2115(15)	4020(65)	7363(55)	132(13)
H(17B)	2825(75)	3951(55)	8292(39)	132(13)
H(17C)	2890(71)	4598(12)	7746(89)	132(13)
H(112)	1376(9)	6357(8)	8741(9)	132(13)
H(113)	1727(12)	7022(8)	9907(10)	132(13)
H(114)	885(11)	6942(8)	10585(9)	132(13)
H(115)	-325(11)	6203(9)	10053(9)	132(13)
H(116)	-750(12)	5582(9)	8837(15)	132(13)
H(122)	438(9)	5057(9)	6399(9)	132(13)
H(123)	304(11)	5776(13)	5276(12)	132(13)
H(124)	-282(12)	6991(10)	5152(12)	132(13)
H(125)	-452(13)	7491(9)	6202(11)	132(13)
H(126)	-217(11)	6772(8)	7351(10)	132(13)
H(132)	-729(10)	4071(8)	8181(10)	132(13)
H(133)	-2128(13)	3792(12)	7918(13)	132(13)
H(134)	-3190(12)	4226(13)	6937(11)	132(13)
H(135)	-3153(12)	5346(13)	6275(12)	132(13)
H(136)	-1631(15)	5749(12)	6597(11)	132(13)
H(3)	3504(6)	5380(5)	6563(6)	132(13)
H(32)	2058(11)	5978(17)	4338(14)	132(13)
H(34A)	1917(72)	4983(28)	5727(69)	132(13)
H(34B)	2674(15)	4561(15)	5644(75)	132(13)
H(34C)	1856(66)	4862(38)	4853(16)	132(13)
H(35A)	2883(68)	7018(56)	3756(41)	132(13)
H(35B)	2700(88)	7736(15)	4140(9)	132(13)
H(35C)	1954(19)	7141(67)	3707(36)	132(13)
H(37A)	2968(44)	6621(61)	7797(20)	132(13)
H(37B)	2536(78)	6206(28)	6945(63)	132(13)
H(37C)	2072(41)	6907(38)	7082(77)	132(13)
H(312)	5831(9)	8108(9)	6281(10)	132(13)
H(313)	5403(12)	8797(9)	5048(10)	132(13)
H(314)	4123(12)	9482(8)	4491(9)	132(13)
H(315)	3216(12)	9477(8)	5128(10)	132(13)
H(316)	3609(12)	8797(8)	6294(9)	132(13)
H(322)	4624(9)	7411(8)	8662(8)	132(13)
H(323)	4826(12)	8094(9)	9819(13)	132(13)
H(324)	5129(13)	9321(9)	9938(10)	132(13)
H(325)	5386(10)	9893(8)	8914(9)	132(13)
H(326)	5108(11)	9239(7)	7683(9)	132(13)
H(332)	5865(9)	6578(7)	6912(8)	708(2)
H(333)	7333(12)	6315(9)	7299(12)	708(2)
H(334)	8440(6)	7066(12)	8256(12)	708(2)

H(335)	8079(9)	8079(11)	8827(10)	708(2)
H(336)	6611(11)	8342(7)	8441(10)	708(2)
H(212)	1721(28)	5797(18)	8516(23)	708(2)
H(213)	3165(20)	5511(29)	8830(27)	708(2)
H(214)	3450(20)	4552(34)	8137(39)	708(2)
H(215)	2291(36)	3878(26)	7132(36)	708(2)
H(216)	847(28)	4164(23)	6818(24)	708(2)
H(222)	-445(36)	4919(17)	8595(33)	708(2)
H(223)	-257(38)	5571(31)	9760(26)	708(2)
H(224)	165(39)	6814(30)	9917(24)	708(2)
H(225)	399(38)	7404(16)	8908(34)	708(2)
H(226)	211(37)	6752(26)	7744(27)	708(2)
H(232)	-1458(33)	6193(31)	6272(31)	708(2)
H(233)	-1801(23)	6923(25)	5116(30)	708(2)
H(234)	-845(38)	6971(28)	4545(25)	708(2)
H(235)	456(34)	6288(37)	5130(40)	708(2)
H(236)	799(28)	5558(33)	6286(41)	708(2)
H(412)	4908(38)	9262(26)	7380(26)	708(2)
H(413)	4687(39)	9977(15)	6244(35)	708(2)
H(414)	4780(37)	9431(29)	5138(25)	708(2)
H(415)	5094(41)	8170(31)	5169(27)	708(2)
H(416)	5315(40)	7455(17)	6305(34)	708(2)
H(422)	3315(53)	8296(30)	6584(44)	708(2)
H(423)	1884(39)	7985(41)	6293(39)	708(2)
H(424)	1632(26)	6972(48)	6942(49)	708(2)
H(425)	2810(49)	6270(35)	7882(45)	708(2)
H(426)	4241(35)	6581(31)	8173(31)	708(2)
H(432)	6446(28)	8743(28)	8775(27)	708(2)
H(433)	6781(24)	9458(25)	9939(28)	708(2)
H(434)	5845(32)	9452(25)	10534(21)	708(2)
H(435)	4574(28)	8731(34)	9963(31)	708(2)
H(436)	4239(27)	8016(32)	8799(33)	708(2)

8.2 Kinetic Supplementary data

The tables in this section give the observed first-order rate constants for the reactions described in Chapter 6. The kinetic results for each complex studied are given in tables under a heading for each (consisting of the formula of the complex). If the data in a table were graphically presented in Chapter 6 the number of the figure is given after the table number. The iodomethane concentrations are referred to as $[CH_3I]$ and are given in mol dm^{-3} (M); the observed first-order rate constants (k_{obsd}) are given in the unit (s^{-1}), and temperatures as °C.

Table 8.13 Fig. 6.4 (Par. 6.4.1)

$[CH_3I]$ dependence of the pseudo-first-order rate constant for the formation of $[Rh(dmavk)(I)(CH_3)(CO)(PPh_3)]$ ($[Rh]_{tot} = 2.92x10^{-4}$ M; λ = 385 nm) and $[Rh(tavk)(I)(CH_3)(CO)(PPh_3)]$ ($[Rh]_{tot} = 2.92x10^{-4}$ M; λ = 374 nm) in acetone at 25 °C.

Complex	$[CH_3I]$	k_{obsd}
$[Rh(tavk)(CO)(PPh_3)]$	0.1	$1.4(3)x10^{-2}$
	0.2	$2.4(2)x10^{-2}$
	0.5	$3.8(6)x10^{-2}$
	0.7	$4.57(8)x10^{-2}$
	0.9	$5.79(7)x10^{-2}$
$[Rh(dmavk)(CO)(PPh_3)]$	0.1	$2.118(8)x10^{-2}$
	0.3	$6.99(4)x10^{-2}$
	0.5	$1.278(7)x10^{-1}$
	0.7	$1.689(6)x10^{-1}$
	0.9	$2.02(1)x10^{-1}$

Table 8.14 Fig. 6.5 (Par.6.4.2)

$[CH_3I]$ dependence of the pseudo-first-order rate constant for the formation of $[Rh(dmavk)(I)(CH_3)(CO)(PPh_3)]$ ($[Rh]_{tot} = 2.92x10^{-4}$ M; λ = 385 nm) and $[Rh(dmavk)(I)(CH_3)(CO)(p\text{-Cl-Ph})_3P]$ ($[Rh]_{tot} = 2.92x10^{-4}$ M; λ = 390 nm) in acetone at 25 °C.

Complex	$[CH_3I]$	k_{obsd}
$[Rh(tavk)(CO)(P(p\text{-Cl-Ph})_3)]$	0.03	$6.27(1)x10^{-3}$
	0.09	$1.068(2)x10^{-2}$
	0.18	$1.92(6)x10^{-2}$
	0.24	$2.54(4)x10^{-2}$
	0.3	$2.88(3)x10^{-2}$
$[Rh(dmavk)(CO)(PPh_3)]$	0.1	$2.118(8)x10^{-2}$
	0.3	$6.99(4)x10^{-2}$
	0.5	$1.278(7)x10^{-1}$
	0.7	$1.689(6)x10^{-1}$
	0.9	$2.02(1)x10^{-1}$

Table 8.15 Fig. 6.6 (Par.6.4.2)

$[CH_3I]$ dependence of the pseudo-first-order rate constant for the formation of $[Rh(tavk)(I)(CH_3)(CO)(PPh_3)]$ ($[Rh]_{tot} = 2.92x10^{-4}$ M; λ = 374 nm) and $[Rh(tavk)(I)(CH_3)(CO)(P(p\text{-OMe-Ph})_3]$ ($[Rh]_{tot} = 2.92x10^{-4}$ M; λ = 374 nm) in acetone at 25 °C.

Complex	$[CH_3I]$	k_{obsd}
$[Rh(tavk)(CO)(P(p\text{-OMe-Ph})_3]$	0.1	$3.09(6)x10^{-2}$
	0.2	$4.52(5)x10^{-2}$
	0.5	$8.53(7)x10^{-2}$
	0.7	$1.15(2)x10^{-2}$
	0.9	$1.35(3)x10^{-1}$
$[Rh(tavk)(CO)(PPh_3)]$	0.1	$1.4(3)x10^{-2}$
	0.2	$2.4(2)x10^{-2}$
	0.5	$3.8(6)x10^{-2}$
	0.7	$4.57(8)x10^{-2}$
	0.9	$5.79(7)x10^{-2}$

Table 8.16 Fig. 6.7 (Par.6.4.2)

$[CH_3I]$ dependence of the pseudo-first-order rate constant for the formation of $[Rh(tavk)(I)(CH_3)(CO)(PPh_3)]$ ($[Rh]_{tot} = 2.92x10^{-4}$ M; λ = 374 nm) and $[Rh(tavk)(I)(CH_3)(CO)(AsPh_3)]$ ($[Rh]_{tot} = 2.92x10^{-4}$ M; λ = 375 nm) in acetone at 25 °C.

Complex	$[CH_3I]$	k_{obsd}
$[Rh(tavk)(CO)(AsPh_3)]$	0.1	$3.02(2)x10^{-3}$
	0.2	$1.57(5)x10^{-2}$
	0.5	$3.15(2)x10^{-2}$
	0.7	$4.56(4)x10^{-2}$
	0.9	$6.44(3)x10^{-1}$
$[Rh(tavk)(CO)(PPh_3)]$	0.1	$1.4(3)x10^{-2}$
	0.2	$2.4(2)x10^{-2}$
	0.5	$3.8(6)x10^{-2}$
	0.7	$4.57(8)x10^{-2}$
	0.9	$5.79(7)x10^{-2}$

Table 8.17 Fig. 6.8 (Par.6.4.3)

$[CH_3I]$ dependence of the pseudo-first-order rate constant for the formation of $[Rh(dmavk)(I)(CH_3)(CO)(PPh_3)]$ ($[Rh]_{tot} = 2.92x10^{-4}$ M; λ = 385 nm) in acetone, acetonitrile and chloroform at 25 °C.

Solvent	$[CH_3I]$	k_{obsd}
Acetonitrile	0.1	$1.1(1)x10^{-1}$
	0.3	$2.65(3)x10^{-1}$
	0.5	$3.97(7)x10^{-1}$
	0.7	$6.5(2)x10^{-1}$
	0.9	$8.1(3)x10^{-1}$
Chloroform	0.1	$2.028(7)x10^{-2}$
	0.17	$2.125(4)x10^{-2}$
	0.19	$2.41(2)x10^{-2}$
	0.45	$5.39(2)x10^{-2}$
	0.53	$6.01(4)x10^{-2}$
	0.63	$7.11(5)x10^{-2}$
	0.81	$9.64(7)x10^{-2}$
Acetone	0.1	$2.118(8)x10^{-2}$
	0.3	$6.99(4)x10^{-2}$
	0.5	$1.278(7)x10^{-1}$
	0.7	$1.689(6)x10^{-1}$
	0.9	$2.02(1)x10^{-1}$

Table 8.18 Fig. 6.9 (Par.6.4.4)

Temperature and $[CH_3I]$ dependence of the pseudo-first-order rate constants for the formation of $[Rh(dmavk)(I)(CH_3)(CO)(PPh_3)]$ ($[Rh]_{tot} = 2.92x10^{-4}$ M; λ = 385 nm) in acetone.

Temperature (°C)	$[CH_3I]$	k_{obsd}
15.0	0.1	$1.253(4)x10^{-2}$
	0.3	$4.20(2)x10^{-2}$
	0.5	$6.35(4)x10^{-2}$
	0.7	$9.41(6)x10^{-2}$
	0.9	$1.17(1)x10^{-1}$
	0.1	$2.118(8)x10^{-2}$
	0.3	$6.99(4)x10^{-2}$
	0.5	$1.278(7)x10^{-1}$
	0.7	$1.689(6)x10^{-1}$
	0.9	$2.02(1)x10^{-1}$
	0.1	$2.62(2)x10^{-2}$
	0.3	$8.32(3)x10^{-2}$
	0.5	$1.384(5)x10^{-1}$
	0.7	$1.830(6)x10^{-1}$
	0.9	$2.403(5)x10^{-1}$

Table 8.19 Fig. 6.10 (Par.6.5.1)

$[CH_3I]$ dependence of the pseudo-first-order rate constant for the formation of $[Rh(dmavk)(I)(COCH_3)(PPh_3)]$ ($[Rh]_{tot} = 2.92x10^{-4}$ M; λ = 350 nm) and $[Rh(tavk)(I)(COCH_3)(PPh_3)]$ ($[Rh]_{tot} = 2.92x10^{-4}$ M; λ = 345 nm)in acetone at 25 °C.

Complex	$[CH_3I]$	k_{obsd}
$[Rh(dmavk)(CO)(PPh_3)]$	0.005	$3.5(2)x10^{-4}$
	0.01	$3.8(1)x10^{-4}$
	0.015	$7.5(2)x10^{-4}$
	0.02	$8.2(1)x10^{-4}$
	0.025	$8.4(1)x10^{-4}$
	0.03	$8.5(2)x10^{-4}$
	0.05	$9.18(7)x10^{-4}$
	0.07	$1.00(1)x10^{-3}$
	0.11	$1.07(7)x10^{-3}$
	0.13	$1.10(10)x10^{-3}$
$[Rh(tavk)(CO)(PPh_3)]$	0.05	$4.5(2)x10^{-4}$
	0.1	$7.3(3)x10^{-4}$
	0.15	$9.1(3)x10^{-4}$
	0.2	$1.03(3)x10^{-3}$
	0.25	$1.08(4)x10^{-3}$
	0.3	$1.19(4)x10^{-3}$
	0.4	$1.38(3)x10^{-3}$
	0.5	$1.49(3)x10^{-3}$
	0.7	$1.64(3)x10^{-3}$

Table 8.20 Fig. 6.11 (Par.6.5.1)

$[CH_3I]$ dependence of the pseudo-first-order rate constant for the formation of $[Rh(dmavk)(I)(COCH_3)(PPh_3)]$ ($[Rh]_{tot} = 2.92x10^{-4}$ M; λ = 350 nm) and $[Rh(dmavk)(I)(COCH_3)(P(p\text{-}Cl\text{-}Ph)_3)]$ ($[Rh]_{tot} = 2.92x10^{-4}$ M; λ = 360 nm) in acetone at 25 °C.

Complex	$[CH_3I]$	k_{obsd}
$[Rh(dmavk)(CO)(PPh_3)]$	0.005	$3.5(2)x10^{-4}$
	0.01	$3.8(1)x10^{-4}$
	0.015	$7.5(2)x10^{-4}$
	0.02	$8.2(1)x10^{-4}$
	0.025	$8.4(1)x10^{-4}$
	0.03	$8.5(2)x10^{-4}$
	0.05	$9.18(7)x10^{-4}$
	0.07	$1.00(1)x10^{-3}$
	0.11	$1.07(7)x10^{-3}$
	0.13	$1.10(10)x10^{-3}$
$[Rh(dmavk)(CO)(P(p\text{-}Cl\text{-}Ph)_3)]$	0.05	$4.5(2)x10^{-4}$
	0.1	$7.3(3)x10^{-4}$
	0.15	$9.1(3)x10^{-4}$
	0.2	$1.03(3)x10^{-3}$
	0.25	$1.08(4)x10^{-3}$
	0.3	$1.19(4)x10^{-3}$
	0.4	$1.38(3)x10^{-3}$
	0.5	$1.49(3)x10^{-3}$
	0.7	$1.64(3)x10^{-3}$

Table 8.21 Fig. 6.12 (Par.6.5.2)

[CH_3I] dependence of the pseudo-first-order rate constant for the formation of [Rh(tavk)(I)($COCH_3$)(PPh_3)] ($[Rh]_{tot}$ = 2.92x10^{-4} M; λ = 345 nm) and [Rh(tavk)(I)($COCH_3$)(P(*p*-OMe-Ph)$_3$)] ($[Rh]_{tot}$ = 2.92x10^{-4} M; λ = 374 nm) in acetone at 25 °C.

Complex	[CH_3I]	k_{obsd}
[Rh(tavk)(CO)(PPh_3)]	0.05	4.5(2)x10^{-4}
	0.1	7.3(3)x10^{-4}
	0.15	9.1(3)x10^{-4}
	0.2	1.03(3)x10^{-3}
	0.25	1.08(4)x10^{-3}
	0.3	1.19(4)x10^{-3}
	0.4	1.38(3)x10^{-3}
	0.5	1.49(3)x10^{-3}
	0.7	1.64(3)x10^{-3}
[Rh(tavk)(CO)(P(*p*-OMe-Ph)$_3$)]	0.05	4.2(1)x10^{-4}
	0.1	7.3(2)x10^{-4}
	0.15	9.9(2)x10^{-4}
	0.2	1.18(2)x10^{-3}
	0.25	1.34(3)x10^{-3}
	0.3	1.50(3)x10^{-3}
	0.4	1.57(3)x10^{-3}
	0.5	1.57(3)x10^{-3}
	0.6	1.68(3)x10^{-3}
	0.7	1.70(3)x10^{-3}
	0.9	1.69(4)x10^{-3}

Table 8.22 Fig. 6.13 (Par.6.5.2)

$[CH_3I]$ dependence of the pseudo-first-order rate constant for the formation of $[Rh(dmavk)(I)(COCH_3)(PPh_3)]$ ($[Rh]_{tot} = 2.92x10^{-4}$ M; λ = 350 nm) and $[Rh(dmavk)(I)(COCH_3)(AsPh_3)]$ ($[Rh]_{tot} = 2.92x10^{-4}$ M; λ = 350 nm) in acetone at 25 °C.

Complex	$[CH_3I]$	k_{obsd}
$[Rh(dmavk)(CO)(PPh_3)]$	0.005	$3.5(2)x10^{-4}$
	0.01	$3.8(1)x10^{-4}$
	0.015	$7.5(2)x10^{-4}$
	0.02	$8.2(1)x10^{-4}$
	0.025	$8.4(1)x10^{-4}$
	0.03	$8.5(2)x10^{-4}$
	0.05	$9.18(7)x10^{-4}$
	0.07	$1.00(1)x10^{-3}$
	0.11	$1.07(7)x10^{-3}$
	0.13	$1.10(10)x10^{-3}$
$[Rh(dmavk)(CO)(AsPh_3)]$	0.05	$1.55(2)x10^{-4}$
	0.1	$1.34(2)x10^{-4}$
	0.15	$1.35(2)x10^{-4}$
	0.2	$1.34(2)x10^{-4}$
	0.25	$2.09(2)x10^{-4}$
	0.3	$1.39(2)x10^{-4}$
	0.4	$1.11(4)x10^{-4}$
	0.5	$1.55(2)x10^{-4}$
	0.6	$1.32(1)x10^{-4}$
	0.7	$1.64(3)x10^{-4}$

Table 8.23 Fig. 6.14 (Par.6.5.3)

$[CH_3I]$ dependence of the pseudo-first-order rate constant for the formation of $[Rh(dmavk)(I)(COCH_3)(PPh_3)]$ ($[Rh]_{tot} = 2.92x10^{-4}$ M; λ = 350 nm) in chloroform and acetone at 25 °C.

Solvent	$[CH_3I]$	k_{obsd}
Chloroform	0.005	$4.68(10)x10^{-4}$
	0.01	$8.02(10)x10^{-4}$
	0.015	$1.05(1)x10^{-3}$
	0.02	$1.31(2)x10^{-3}$
	0.025	$1.43(2)x10^{-3}$
	0.03	$1.53(2)x10^{-3}$
	0.05	$1.55(2)x10^{-3}$
	0.07	$1.68(2)x10^{-3}$
	0.13	$1.77(2)x10^{-3}$
Acetone	0.005	$3.5(2)x10^{-4}$
	0.01	$3.8(1)x10^{-4}$
	0.015	$7.5(2)x10^{-4}$
	0.02	$8.2(1)x10^{-4}$
	0.025	$8.4(1)x10^{-4}$
	0.03	$8.5(2)x10^{-4}$
	0.05	$9.18(7)x10^{-4}$
	0.07	$1.00(1)x10^{-3}$
	0.11	$1.07(7)x10^{-3}$
	0.13	$1.10(10)x10^{-3}$

Table 8.24 Data in Table 6.7 (Par.6.5.3)

$[CH_3I]$ dependence of the pseudo-first-order rate constant for the formation of $[Rh(dmavk)(I)(COCH_3)(PPh_3)]$ ($[Rh]_{tot} = 2.92x10^{-4}$ M; λ = 350 nm) in benzene, ethyl acetate, acetonitrile and dichloromethane at 25 °C.

Solvent	$[CH_3I]$	k_{obsd}
Dichloromethane	0.005	$4.21(2)x10^{-4}$
	0.01	$5.86(4)x10^{-4}$
	0.015	$6.48(6)x10^{-4}$
	0.02	$7.05(8)x10^{-4}$
	0.025	$8.9(1)x10^{-4}$
	0.03	$1.107(10)x10^{-3}$
	0.04	$1.16(10)x10^{-3}$
	0.05	$1.23(1)x10^{-3}$
	0.07	$1.31(1)x10^{-3}$
Benzene	0.005	$5.48(5)x10^{-4}$
	0.01	$5.96(4)x10^{-4}$
	0.015	$9.04(5)x10^{-4}$
	0.02	$1.173(7)x10^{-4}$
	0.025	$1.416(9)x10^{-4}$
	0.03	$1.66(1)x10^{-4}$
	0.04	$1.84(1)x10^{-4}$
	0.05	$2.46(2)x10^{-4}$
	0.08	$3.47(3)x10^{-4}$
	0.094	$5.08(2)x10^{-4}$
	0.22	$1.013(3)x10^{-3}$
	0.32	$1.264(9)x10^{-3}$
	0.36	$1.256(6)x10^{-3}$
	0.48	$1.466(5)x10^{-3}$
	0.79	$1.755(3)x10^{-3}$
Ethyl acetate	0.005	$1.15(3)x10^{-4}$
	0.01	$2.20(3)x10^{-4}$
	0.015	$2.98(4)x10^{-4}$
	0.02	$3.56(2)x10^{-4}$
	0.025	$4.05(6)x10^{-4}$
	0.03	$4.29(3)x10^{-4}$
	0.035	$4.26(5)x10^{-4}$
	0.04	$4.49(4)x10^{-4}$
	0.05	$4.90(6)x10^{-4}$
	0.06	$5.03(1)x10^{-4}$
	0.07	$4.24(3)x10^{-4}$
Acetonitrile	0.005	$3.87(3)x10^{-2}$
	0.01	$5.19(3)x10^{-2}$
	0.015	$5.19(2)x10^{-2}$
	0.02	$6.14(1)x10^{-2}$
	0.025	$6.180(9)x10^{-2}$
	0.03	$6.58(2)x10^{-2}$
	0.05	$6.801(8)x10^{-2}$
	0.07	$6.759(7)x10^{-2}$
	0.13	$6.849(8)x10^{-2}$

Table 8.25 Fig. 6.15 (Par.6.5.3)

Temperature and [CH_3I] dependence of the pseudo-first-order rate constant for the formation of [Rh(dmavk)(I)($COCH_3$)(PPh_3)] in acetone.

Temperature (°C)	[CH_3I]	k_{obsd}
16.0	0.005	$1.37(6)\times10^{-4}$
	0.01	$1.69(6)\times10^{-4}$
	0.015	$1.95(6)\times10^{-4}$
	0.02	$2.06(6)\times10^{-4}$
	0.025	$2.09(6)\times10^{-4}$
	0.03	$3.02(2)\times10^{-4}$
	0.05	$3.12(2)\times10^{-4}$
	0.07	$3.15(3)\times10^{-4}$
	0.11	$3.18(2)\times10^{-4}$
	0.13	$3.20(2)\times10^{-4}$
25.0	0.005	$3.5(2)\times10^{-4}$
	0.01	$3.8(1)\times10^{-4}$
	0.015	$7.5(2)\times10^{-4}$
	0.02	$8.2(1)\times10^{-4}$
	0.025	$8.4(1)\times10^{-4}$
	0.03	$8.5(2)\times10^{-4}$
	0.05	$9.18(7)\times10^{-4}$
	0.07	$1.00(1)\times10^{-3}$
	0.11	$1.07(7)\times10^{-3}$
	0.13	$1.10(10)\times10^{-3}$
34.0	0.005	$8.2(1)\times10^{-4}$
	0.01	$1.33(2)\times10^{-3}$
	0.015	$1.65(3)\times10^{-3}$
	0.02	$1.81(4)\times10^{-3}$
	0.025	$1.85(4)\times10^{-3}$
	0.03	$1.93(5)\times10^{-4}$
	0.05	$2.33(3)\times10^{-3}$
	0.07	$2.47(3)\times10^{-3}$
	0.11	$2.58(2)\times10^{-3}$
	0.13	$2.60(3)\times10^{-3}$

Table 8.26 Fig. 6.16 (Par.6.5.3)

Temperature and $[CH_3I]$ dependence of the pseudo-first-order rate constant for the formation of $[Rh(dmavk)(I)(COCH_3)(PPh_3)]$ in acetonitrile.

Temperature (°C)	$[CH_3I]$	k_{obsd}
16.8	0.005	$1.55(2)\times10^{-2}$
	0.01	$2.17(1)\times10^{-2}$
	0.015	$2.478(5)\times10^{-2}$
	0.02	$2.504(3)\times10^{-2}$
	0.025	$2.496(3)\times10^{-2}$
	0.03	$2.543(5)\times10^{-2}$
	0.05	$2.607(4)\times10^{-2}$
	0.07	$2.630(4)\times10^{-2}$
	0.11	$2.649(2)\times10^{-2}$
25.0	0.005	$3.87(3)\times10^{-2}$
	0.01	$5.19(3)\times10^{-2}$
	0.015	$5.19(2)\times10^{-2}$
	0.02	$6.14(1)\times10^{-2}$
	0.025	$6.180(9)\times10^{-2}$
	0.03	$6.58(2)\times10^{-2}$
	0.05	$6.801(8)\times10^{-2}$
	0.07	$6.759(7)\times10^{-2}$
	0.13	$6.849(8)\times10^{-2}$
34.0	0.005	$1.05(1)\times10^{-1}$
	0.01	$1.53(2)\times10^{-1}$
	0.015	$1.96(2)\times10^{-1}$
	0.02	$2.11(2)\times10^{-1}$
	0.025	$2.21(2)\times10^{-1}$
	0.03	$2.07(4)\times10^{-1}$
	0.07	$2.24(2)\times10^{-1}$
	0.11	$2.23(2)\times10^{-1}$
	0.13	$2.24(3)\times10^{-1}$

Table 8.27 Fig. 6.17 (Par.6.5.3)

Temperature and [CH_3I] dependence of the pseudo-first-order rate constant for the formation of [$Rh(tavk)(I)(COCH_3)(PPh_3)$] in chloroform.

Temperature (°C)	[CH_3I]	k_{obsd}
16.3	0.05	$2.67(4)\times10^{-4}$
	0.1	$3.68(10)\times10^{-4}$
	0.15	$5.2(1)\times10^{-4}$
	0.2	$6.1(2)\times10^{-4}$
	0.25	$6.6(1)\times10^{-4}$
	0.3	$7.0(2)\times10^{-4}$
	0.4	$8.6(2)\times10^{-4}$
	0.5	$9.2(2)\times10^{-4}$
	0.7	$1.01(2)\times10^{-3}$
25.2	0.05	$4.5(2)\times10^{-4}$
	0.1	$7.3(3)\times10^{-4}$
	0.15	$9.1(3)\times10^{-4}$
	0.2	$1.03(3)\times10^{-3}$
	0.25	$1.08(4)\times10^{-3}$
	0.3	$1.19(4)\times10^{-3}$
	0.4	$1.38(3)\times10^{-3}$
	0.5	$1.49(3)\times10^{-3}$
	0.7	$1.64(3)\times10^{-3}$
35.0	0.05	$7.55(6)\times10^{-4}$
	0.1	$1.40(5)\times10^{-3}$
	0.15	$2.00(2)\times10^{-3}$
	0.2	$2.51(5)\times10^{-3}$
	0.25	$3.04(5)\times10^{-3}$
	0.3	$3.63(6)\times10^{-3}$
	0.4	$4.39(9)\times10^{-3}$
	0.5	$4.9(1)\times10^{-3}$
	0.7	$5.8(1)\times10^{-3}$

Abstract

The aim of this study was to determine the mechanism for the reaction between iodomethane and complexes of the type [Rh(N,O-BID)(CO)(XR_3)]; N,O-BID = mono anionic bidentate ligands of the general formula: (i) dimethylaminovinylketone; dmavk (ii) methyltrifluoroaminovinylketone; tavk; X= As or P, R = phenyl and substituted phenyls, PPh_3, $AsPh_3$, P(*p*-Cl-Ph)$_3$ or P(p-OMe-Ph)$_3$. Determination of the mechanism was achieved utilizing X-ray crystallography, reaction kinetics and ^{31}P-NMR.

[Rh(dmavk)(CO)(PPh_3)] crystallizes in the orthorombic crystal system with space group $Pca2_1$ and final R value of 2.04 %. [Rh(dmavk)(CO)($AsPh_3$)] and [Rh(dmavk)(I)(CH_3)(CO)(PPh_3)] crystallize in the triclinic crystal system with space group PI. The final R value for each was 3.88 and 4.77 % respectively. [Rh(dmavk)(I)($COCH_3$)(PPh_3)] crystallizes in the monoclinic crystal system with space group $P2_1/c$ and a final R value of 6.72. In the case of the mono carbonyl complexes, i.e., for [Rh(dmavk)(CO)(PPh_3)] and [Rh(dmavk)(CO)($AsPh_3$)], the P/As atom is *trans* to the nitrogen atom of the N,O-BID ligand. The Rh-As bond is significantly longer than the Rh-P bond (2.3834(6) and 2.2751(13) Å respectively). The successful isolation and X-ray crystallographic characterization of the starting complex, [Rh(dmavk)(CO)(PPh_3)], and its oxidative addition products for the reaction between and iodomethane, i.e., [Rh(dmavk)(I)(CH_3)(CO)(PPh_3)] and [Rh(dmavk)(I)($COCH_3$)(PPh_3)] was for the first time accomplished in this laborotary. The *trans*-(N-Rh-P) configuration for the oxidative addition products is also retained from the same configuration present in the starting complex.

^{31}P-NMR studies showed that for the [Rh(L,L-BID)(CO)(PPh_3)] complexes: L,L'-BID = O,O-BID: tfaa, trop, cupf, acac, tta; O,S-BID: pbtu, hpt, anmeth, sacac; N,S-BID: cacsm, hacsm; N,O-BID: dmavk, ox, pic a fair correlation between ^{1}J(PRh) and the Rh-P bond

distance exists in these complexes; a decrease in Rh-P bond distance results in an increase in $^1J(PRh)$.

The [Rh(N,O-BID)(CO)(XR_3)] complexes undergo oxidative addition by iodomethane, forming the Rh(III)-alkyl species *via* an equilibrium step, followed by the formation of the Rh(III)-acyl species according to the following reaction:

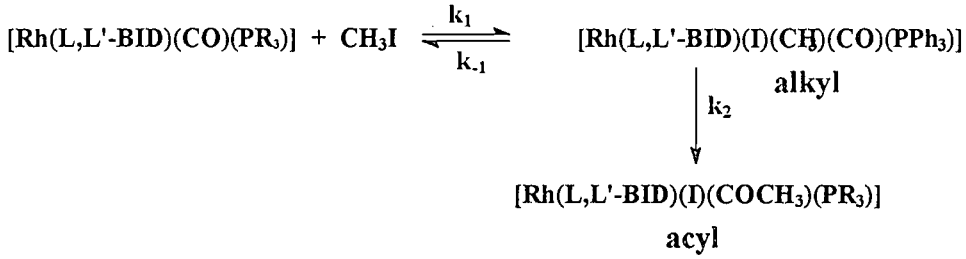

A significant solvent effect was observed for the oxidative addition reaction between iodomethane and [Rh(dmavk)(CO)(PPh_3)]. At 25 °C, this reaction proceeds 8 times faster in the highly polar solvent acetonitrile ($k_1 = 89(6)x10^2\ M^{-1}s^{-1}$) compared to the least polar solvent chloroform ($k_1 = 11.4(4)x10^2\ M^{-1}s^{-1}$). The activation parameters ($\Delta H^{\#}$ and $\Delta S^{\#}$) were determined from the temperature dependence of k_1 in acetone. Large negative $\Delta S^{\#}$ values ($\Delta S^{\#} = -139(40)\ J\ K^{-1}\ mol^{-1}$) and typical $\Delta H^{\#}$ values ($\Delta H^{\#} = 35(4)\ kJ\ mol^{-1}$) were obtained. Considering these experimental results, the formation of a linear, polar transition state with subsequent formation of an ion-pair intermediate is postulated. The rate constant of the oxidative addition was increased by both electronic and steric manipulation. The electronic manipulation was achieved by firstly the introduction of electron/donating substituents (CH_3 in place of CF_3) on the bidentate ligand, resulting in a four fold increase in magnitude for the rate of oxidative addition; and secondly by the interchanging triphenyl phosphine and its derivatives [PPh_3 *vs.* P(*p*-Cl-Ph)$_3$ *vs.* P(*p*-OMe-Ph)$_3$]. The formation rate of the Rh(III)-acyl species was found to be relative independent of the variation in nucleophilic character of the metal center. Steric manipulation was achieved by interchanging PPh_3 with $AsPh_3$. Replacing the PPh_3 ligand by $AsPh_3$ leads to an increase in the rate of oxidative addition and a decrease in the

rate of reductive elimination, resulting in an increase in the equilibrium constant for this step. A significant (*ca.* one order of magnitude) decrease in CO-insertion was observed from PPh_3 to $AsPh_3$ ($12.0(6)x10^{-4}$ compared to $1.32(2)x10^{-4}$ s^{-1}).

An increase in the K_1 values (i.e. thermodynamic stability of the Rh(III)-alkyl species) were observed by increasing the nucleophilic character on the Rh center and by decreasing the steric demand on the metal center.

The introduction of these N,O-BID ligands to the Rh(I) center in these complexes resulted in at least a *ca.* 4 fold activation in the oxidative addition rate as compared to the known O,O-BID ligand systems (i.e. acac, ox, etc.)

Opsomming

Die doel van hierdie studie was om die meganisme vir die reaksie tussen jodometaan en komplekse van die tipe [Rh(N,O-BID)(CO)(XR_3)] te bepaal; N,O-BID = mono anioniese bidentate ligande van die algemene formule: (i) dimetielaminovinielketoon; dmavk, (ii) metieltrifluoroaminovinielketoon; tavk; X = As of P, R = feniel en gefunksionaliseerde feniele, PPh_3, $AsPh_3$, P(*p*-Cl-Ph)$_3$ of P(p-OMe-Ph)$_3$. Die bepaling van die meganisme is gedoen deur gebruik te maak van X-straal kristallografie, reaksiekinetika en ^{31}P-KMR.

Die volgende uitgangstowwe is kristallografies gekarakteriseer: [Rh(dmavk)(CO)(PPh_3)] kristalliseer in 'n ortorombiese kristalstelsel met ruimtegroep $Pca2_1$ en finale R-waarde van 2.04 %. [Rh(dmavk)(CO)($AsPh_3$)] en [Rh(dmavk)(I)(CH_3)(CO)(PPh_3)] kristalliseer in trikliniense kristalstelsels met ruimtegroep PI. Die finale R-waarde van bogenoemde komplekse was onderskeidelik 3.88 en 4.77 %. [Rh(dmavk)(I)($COCH_3$)(PPh_3)] kristalliseer in 'n monokliniese kristalstelsel met ruimtegroep $P2_1/c$ en 'n finale R-waarde van 6.72 %. In die geval van monokarbonielkomplekse, soos bv. [Rh(dmavk)(CO)(PPh_3)] en [Rh(dmavk)(CO)($AsPh_3$)], koördineer die P/As atoom *trans* t.o.v. die stikstofatoom van die N,O-BID ligand. Die Rh-As bindingslengte is aansienlik langer as dié van Rh-P (2.3834(6) en 2.2751(13) Å onderskeidelik). Die suksesvolle isolasie en X-straalkristallografiese karakterisering van die uitgangstof, [Rh(dmavk)(CO)(PPh_3)], en sy oksidatiewe addisie produkte vir die reaksie tussen jodometaan, t.w., [Rh(dmavk)(I)(CH_3)(CO)(PPh_3)] en Rh(dmavk)(I)($COCH_3$)(PPh_3)], is vir die eerste keer in hierdie laboratorium gedoen. In beide die uitgangstof en die oksidatiewe addisieprodukte word die *trans*-(N-Rh-P) konfigurasie behou.

^{31}P-KMR studies van die [Rh(L,L-BID)(CO)(PPh_3)] komplekse: L,L'-BID = O,O-BID: tfaa, trop, cupf, acac, tta; O,S-BID: pbtu, hpt, anmeth, sacac; N,S-BID: cacsm, hacsm;

N,O-BID: dmavk, ox, pic het aangetoon dat 'n redelike korrelasie tussen $^1J(PRh)$ en die Rh-P bindingsafstand, met 'n variasie in $^1J(PRh)$ bestaan.

Die bereide [Rh(N,O-BID)(CO)(XR_3)] komplekse ondergaan oksidatiewe addisie van jodometaan wat tot die vorming van die Rh(III)-alkielspesie lei (*via* 'n ewewigstap), gevolg deur die vorming van die Rh(III)-asiel kompleks, volgens die volgende reaksieskema.

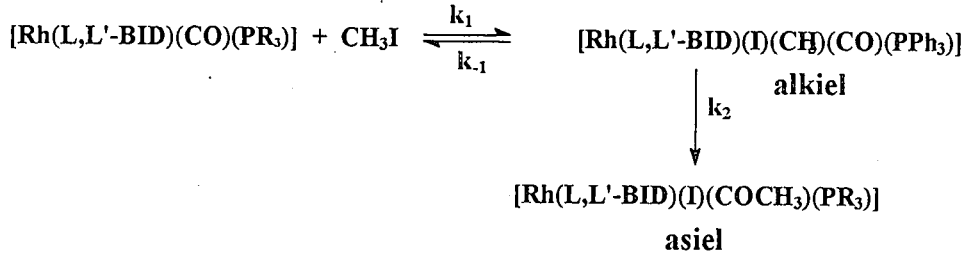

'n Beduidende oplosmiddelafhanklikheid ten opsigte van die oksidatiewe addisie reaksietempo tussen jodometaan en [Rh(dmavk)(CO)(PPh_3)] is waargeneem. Die reaksie verloop 8 keer vinniger in die mees polêre oplosmiddel asetonitriel ($k_1 = 89(6)x10^2\ M^{-1}s^{-1}$) in vergelyking met die mins polêre oplosmiddel chloroform ($k_1 = 11.4(4)x10^2\ M^{-1}s^{-1}$) by 25 °C. Konvensionele aktiveringsparameters van k_1 ($\Delta H^{\#}$ en $\Delta S^{\#}$) is vanaf die temperatuurafhanklikheid in asetoon bepaal. Groot negatiewe $\Delta S^{\#}$-waardes ($\Delta S^{\#}$ = -139(40) $J\ K^{-1}\ mol^{-1}$) en tipiese $\Delta H^{\#}$-waarde ($\Delta H^{\#}$ = 35(4) $kJ\ mol^{-1}$) is verkry. 'n Lineêre, polêre oorgangstoestand, gevolg deur die vorming van 'n ioonpaar-intermediêr, is op grond van bogenoemde resultate as intieme meganisme vir die oksidatiewe addisie reaksie gepostuleer. Manipulasie van die tempokonstante vir die oksidatiewe addisiestap is vermag deur beide elektroniese en steriese variasie. Die elektroniese manipulasie is eerstens gedoen deur die implimentering van elektron donerende substituente (CH_3 i.p.v. CF_3) op die bidentate ligand, wat tot 'n viervoudtoename in grootte van die tempo van oksidatiewe addisie gelei het; en tweedens deur trifenielfosfien te vervang met sy afgeleides [PPh_3 *vs.* P(*p*-Cl-Ph)$_3$ *vs.* P(*p*-OMe-Ph)$_3$]. Steriese manipulasie is gedoen deur PPh_3 te vervang met $AsPh_3$, en dit het gelei tot 'n toename in die tempo van oksidatiewe addisie en 'n afname in die tempo van reduktiewe eliminasie, wat 'n toename in

ewewigskonstante (K_1) tot gevolg gehad het. 'n Betekenisvolle toename in CO-insersie is waargeneem vir PPh_3 in vergelyking met $AsPh_3$ ($12.0(6)x10^{-4}$ en $1.32(2)x10^{-4}$ s^{-1} onderskeidelik).

Die implimentering van hierdie N,O-BID ligande in die [Rh(N,O-BID)(CO)(PPh_3)]-komplekse bring ten minste 'n viervoud grootte aktivering van die die Rh(I) sentra, soos waargeneem in die oksidatiewe addisietempo, in vergelyking met bekende ligandsisteme (d.i. acac, ox, ens.) mee.